INVESTIGATION OF HEAT TRANSFER WITH FILM COOLING TO A FLAT PLATE IN A SHOCK TUBE

THESIS

Scott A. Jurgelewicz
Captain, USAF

AFIT/GAE/ENY/89D-17

DEPARTMENT OF THE AIR FORCE
AIR UNIVERSITY
AIR FORCE INSTITUTE OF TECHNOLOGY
Wright-Patterson Air Force Base, Ohio

AFIT/GAE/ENY/89D-17

INVESTIGATION OF HEAT TRANSFER WITH FILM COOLING TO A FLAT PLATE IN A SHOCK TUBE

THESIS

Presented to the Faculty of the School of Engineering

of the Air Force Institute of Technology

Air University

In Partial Fulfillment of the

Requirements for the Degree of

Master of Science in Aeronautical Engineering

Scott A. Jurgelewicz, B.S.

Captain, USAF

December 1989

Approved for public release; distribution unlimited

Acknowledgements

An individual cannot complete a project of this magnitude without the help of many others. To my advisor, Dr. William C. Elrod, I would like to extend my sincere gratitude. His unlimited patience, understanding, and own brand of humor made this a true learning experience. Dr. James E. Hitchcock deserves many thanks for providing expert advice, and patiently answering countless questions. To Lt. Col. Paul I. King, for providing instrumentation expertise, and for teaching me to question all my results, I am also deeply indebted. Many thanks to the staff of the A.F.I.T. fabrication shop, for promptly manufacturing all the hardware required of this project. To the Laboratory Staff: Mr. Nicholas Yardich; Mr. Jay Anderson; Mr. Dan Rioux; Mr. Tim Major; Mr. Mark Deroux; and Mr Andy Pitts, I am truly grateful. Your constant help and support on never-ending hardware problems will always be remembered. I also wish to thank the computer consultants and operators I badgered many a late night. But the greatest thanks of all go to my lovely wife Jan, for enduring my time at A.F.I.T. with love, patience, and understanding. Last, and certainly not least, I wish to thank my daughters, Sarah, and Jennifer for giving up much their time with "Dad".

Scott A. Jurgelewicz

Table of Contents

List of Figures

List of Tables

List of Symbols

Symbol	Description	Units
c	Sonic Velocity	m/s
c_f'	Coefficient of Friction	
C_p	Constant Pressure Specific Heat	kcal/kg-K
D	Diameter of the Film Cooling Holes	m
h	Heat Transfer Coefficient	$kcal/m^2$-s-K
$\overline{h}$	Average Spanwise Heat Heat Transfer Coefficient	$kcal/m^2$-s-K
Hg	Mercury	
I	Current	Amperes
k	Ratio of Specific Heats, Thermal Conductivity	kcal/m-s-K
kcal	Kilocalories	
m	Meters	
M	Blowing Ratio ($\rho_c U_c/\rho_2 U_2$), Range Variable	
M_s	Mach Number of the Shock	
Nu	Nusselt Number (hx/k)	
P	Pressure	in. Hg
Pr	Prandtl Number ($C_p\mu/k$)	
psig	Pounds per Square Inch, Gauge	lb/in^2
q	Heat Flux	$kcal/m^2$-s
r	Recovery Factor	
R	Resistance	Ohms
Re	Reynolds Number (Ux/ν)	

Symbol	Description	Units
s	Steady Region in the Boundary Layer, Seconds	
sq	Square	
St	Stanton Number ($h/\rho UC_p$)	
t	time	s
T	Temperature	°C or °K
T_a	Averaged Temperature	°K
Tu	Free stream Turbulence Intensity	
u	Unsteady Region in the Boundary Layer, Velocity Fluctuations About the Mean	m/s
U	Velocity	m/s
V	Voltage	Volts
x	Axial position,	m
	Downstream Distance From Film Cooling Holes,	m
	Distance From Face of Heat Flux Gage	m

Subscripts

act	Actual
avg	Averaged
aw	Adiabatic Wall
c	Coolant
i	Summation Variable at ith time interval
j	Summation Variable at jth time interval
M	Number of Finite Element Divisions
N	Number of Finite Element Divisions
o	Uncooled Case, Background Tu Level

Symbol	Description	Units
s	Shock	
t	Time Dependent	
T	Thermal Boundary Layer	
u	Velocity Boundary Layer	
w	Wall	
x	Local	
1	Ambient	
2	Region 2	
4	Driver Property	
∞	Freestream	

Superscripts

*	Reference Condition	
α	Dimensionless Variable	
λ	Dimensionless Variable	

Greek Letters

α	Dimensionless Variable	
β	Dimensionless Variable	
δ	Boundary Layer Thickness	m
Δ	Change in	
λ	Dimensionless Variable	
θ_w	Temperature Difference	$^\circ$K
ρ	Density	kg/m^3
τ	Dummy Integration Variable	
ξ	Unheated starting Length	m

ABSTRACT

The heat transfer occurring through turbulent boundary layers in modern gas turbines is not well understood. The heat transferred to a flat plate through a turbulent boundary layer presents many similarities without the complex flow patterns. The gas used in this study was air. The flow behind a passing shock wave in a shock tube was used to simulate the high temperature ratio flows found in gas turbines. Highly responsive heat flux gages were used to measure the temperature history of a flat plate exposed to the flow. High speed digital recorders were used to sample and store the information. Heat transfer rates were determined from the temperature history using a computer program and a quadrature method. The temperature history was numerically averaged to filter out noise effects before it was used to calculate the heat flux. It was found that low shock Mach numbers produced measured heat flux rates that were predictable by theory. At higher Mach numbers the rounded leading edge of the plate produced reflections that increased the measured heat flux as the Mach number increased; but theory, dependent on incident shock Mach number, underpredicted these actual values.

Film cooling flows were then studied under the same

cont'd

flow conditions. Comparisons were made to correlations based on the ratio of heat transfer coefficients. The governing flow parameter was confirmed to be the blowing ratio. Ratios of heat transfer coefficients with blowing ratios of approximately two to three produced the best agreement with correlations.

The effects of free stream turbulence on the heat flux with film cooling were also briefly studied. The ratios of the measured Stanton numbers were used as a correlating parameter. The results agreed with existing turbulence models. But not enough data was available to determine the governing flow parameter here.

INVESTIGATION OF HEAT TRANSFER WITH FILM COOLING TO A FLAT PLATE IN A SHOCK TUBE

I. Introduction

Gas turbine designers are constantly attempting to increase turbine performance and efficiency. One way to accomplish this goal is to increase the turbine inlet operating temperature. However, to accommodate higher turbine temperatures, and maintain component life, an understanding of the actual heat transfer process that occurs in the turbine is needed. Because of this need, the effect of many factors on rates of heat transfer have been investigated experimentally.

Turbine cascade flow geometry can complicate heat transfer measurements, while flat plate flow geometry reduces the complication. This allows a better understanding of the basic heat transfer mechanisms involved, and can be applied to future turbine blade research. The use of a shock tube to generate high temperature flows provides several advantages over other

methods. Large scale models are relatively expensive to operate, while shock tubes are relatively inexpensive and simple. Large and small scale models in wind tunnels can reach a steady state thermal equilibrium, which makes heat transfer difficult to measure and interpret (Dunn, 1977:1). Shock tubes provide a means of eliminating the establishment of thermal equilibrium due to their very short run times and the relatively high heat dissipation rates available in their metal walls. Even though shock tubes have very short run times, the use of highly responsive heat flux gages allow transient effects to be properly sampled and recorded.

Background

The shock tube has been in use for almost 100 years, but its application as a research tool was not recognized until the 1940's (Glass, 1958:1-3). However, the lack of instrumentation capable of responding to flow properties that occur within milliseconds slowed initial development. Once acceptable instrumentation became available, shock tubes found wide acceptance in the study of chemical kinetics, dissociation and ionization, aerodynamics, and heat transfer (Gaydon, 1963:3-8). Many handbooks provide an abundant source of experimentally verified heat transfer

correlations for steady flow (Kakaç and others, 1987). But experimentally verified heat transfer correlations for unsteady flow conditions, such as those that occur in a shock tube, are not as numerous.

Published literature contains the results of many studies that have been conducted in an attempt to expand available information on the heat transfer occurring in shock tubes. The extension of these results to previously verified steady state correlations provide design engineers with useful information and guidelines. Felderman investigated the passage of a shock wave over a semi-infinite flat plate in a shock tube, and produced curves which gave the dimensionless time, α, required for the flow behind a shock to reach a steady state (Felderman, 1968). Davies and Bernstein studied heat transfer and transition to turbulent flow in the shock induced boundary layer, and found that for $\alpha = x / U_{\infty}t < 0.3$, the flow is substantially steady (Davies and Bernstein, 1969). In this relation the nondimensional alpha is calculated with x as the distance from the leading edge, U_{∞} is the velocity of the free stream, and t is the time elapsed since the shock passed the leading edge. Dunn and Stoddard used thin-film heat-flux gages to measure local hot spots on airfoils, and obtained "spatially resolved heat-transfer rates on gas turbine components" (Dunn and Stoddard, 1977:2-3, 15-18). Dillon and Nagamatsu measured the heat transferred to a

shock tube wall from the flow behind a shock wave. Their results showed an excellent agreement with laminar and turbulent boundary layer theory (Dillon and Nagamatsu, 1984). Smith studied the transient boundary layer and heat transfer to a sharp leading edge flat plate (Smith, 1986). Novak used the same plate in his studies on heat transfer (Novak, 1987). However, the sharp leading edge of the plate used in the studies of Smith and Novak was in fact a wedge at an angle of attack, relative to the flow, which caused boundary layer separation and influenced the results. This study employed a flat plate, with a rounded leading edge, to eliminate these effects. Smith and Novak also relied on a microcomputer software digitizing process which reduced the number of data points available by a factor of 15. The reduced availability was a tradeoff between large computation times with full data sets; and relatively small computation times with data subsets. The latter choice also allowed more data sets to be processed in a given time. For this study a generic computer program was developed to provide a means of accurately reducing the data on any computer, and eliminate the need for machine specific software. The program was run on a large main frame computer to further minimize computation time.

The first well known study on film cooling used a heated secondary flow, and was applied to a film-heating problem, the de-icing of airplane wings (Goldstein,

1971:343). Jones and Shultz examined cooling flow effects over a flat plate in a shock tube (Jones and Shultz, 1971). The cooling flows used in their study were initiated using a secondary diaphragm and reservoir sequenced to the primary shock . Goldstein provides a compilation of film cooling studies, with correlations from experimental studies conducted on many geometries and flow conditions (Goldstein, 1971). This study examines the effects of a cooling flow, consisting of pressurized air, on the flow induced behind a moving shock, and the heat transfer occurring through the resulting boundary layer.

Free-stream turbulence effects on rates of heat transfer are also well documented in the literature. Schlichting states that the local Nusselt number can be increased by increasing the free-stream turbulence intensity (Schlichting, 1979:315). Simonich and Bradshaw found that grid generated free-stream turbulence increased heat transfer by about five percent for every one percent increase in longitudinal turbulence intensity (Simonich and Bradshaw, 1978:671). Blair found that the Reynolds analogy factor $2\ St\ /\ c_f$, increased slightly more than one percent for each one percent increase in the grid generated free-stream turbulence level (Blair, 1981:41). This study takes advantage of a concurrent study of free-stream turbulence effects on heat transfer conducted by Rockwell. The use of the results of Rockwell's study will be limited

to using the measured background free stream turbulence and the measured free stream turbulence available with a turbulence generator. (Rockwell, 1989).

Objectives and Scope

In this experimental investigation of the rate of heat transfer from a relatively high temperature gas, to a cold flat plate, the gas was air. The high temperature gas was in the flow induced behind a shock wave passing down a shock tube. The specific objectives were:

1. Develop a Fortran program to numerically reduce the raw voltage data into equivalent heat transfer units.

2. For a flat plate with a rounded leading edge, determine heat transfer rates without film cooling. Then obtain the same information, under identical flow conditions, with film cooling.

3. Examine the influence of free-stream turbulence on heat transfer rates with and without film cooling.

The flows considered in this study are not identical to the flows found in a gas turbine, nor are they intended to be. The flow in a turbine is a mixture of combustion gases, not air. The total temperatures and pressures considered in this study are not as high as those found in a typical turbine, but the ratio of flow temperatures to

plate temperatures is similar. The heat transfer rates were determined at four locations along the center of the flat plate, for a range of temperature ratios. All of the reduced data are compared to previous experimental and theoretical results for flows with and without film cooling and free stream turbulence.

II. Theory

The Shock Tube

Shock tubes provide a simple and inexpensive means of generating the high temperature ratio flows needed in this study. Figure 1(a) shows a simple shock tube consisting of two sections, a high pressure side, and a low pressure side separated by a diaphragm. When the diaphragm is ruptured a shock wave forms and propagates into the driven section of the shock tube. Assuming a calorically perfect gas, the Mach number of the shock wave, M_s, is implicitly determined using the relation (Chapman and Walker, 1971:137-142) :

$$\frac{P_4}{P_1} = \left(\frac{k-1}{k+1}\right)\left(\frac{2k}{k-1}M_s^2 - 1\right)\left(1 - \frac{\left(\frac{k-1}{k+1}\right)\left(M_s^2 - 1\right)}{M_s}\right)^{\left(\frac{-2k}{k-1}\right)} \qquad (1)$$

P_4 is the absolute pressure of the driver gas, P_1 is the absolute pressure of the driven section, and k is the ratio of specific heats. The gas in regions 1 and 4 is initially at rest. Figure 1(b) shows that as the diaphragm is ruptured, a series of pressure waves move into a gas of increasing sonic speed, and quickly coalesce to form a moving shock wave. Figure 1(b) portrays this series of

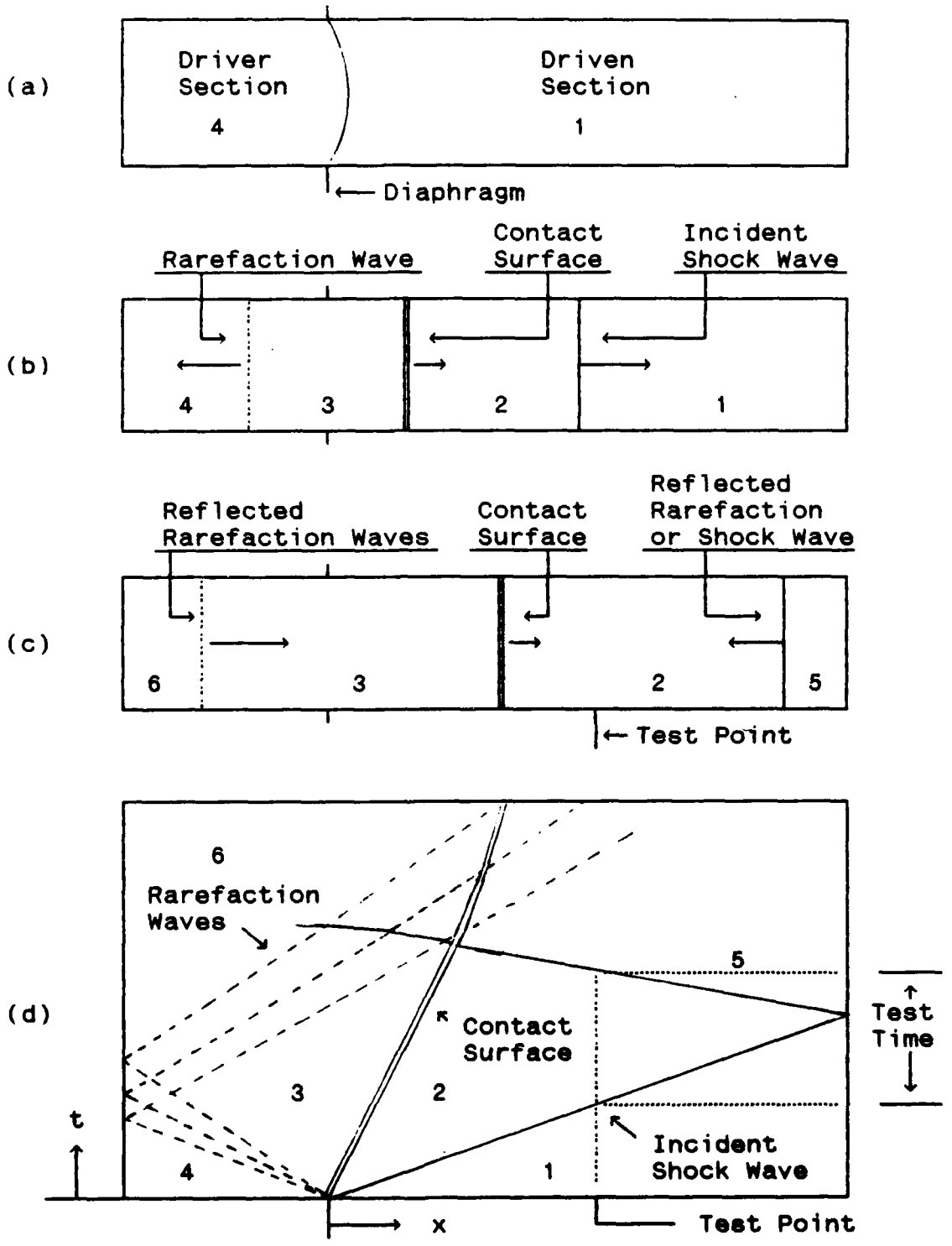

Figure 1 : Shock Tube Wave Behavior (Shapiro, 1987:1007)

events: it also indicates other processes occurring in the shock tube. At the same instant the shock wave forms, a rarefaction wave is formed and propagates into the driver section at local sonic velocity. The contact surface that propagates into the driven section moves with the same velocity imparted to the flow by the passing shock, and separates two distinct regions. Regions 2 and 3 are at the same pressure and experience the same velocity, but they are not at the same temperature. The temperature discontinuity is a result of region 3 achieving its pressure through an isentropic expansion, while region 2 is formed through a non-isentropic shock interaction (Shapiro, 1987).

The flow conditions found in region 2 are the concern of this study, and only occur for several milliseconds. Figure 1(c) shows that if data gathering is to occur under the flow conditions in region 2, the data can only be taken after the incident shock wave passes the test point, and before the next disturbance is reflected back over the test point. Depending on certain factors, either the shock wave reflected from the driven end, the rarefaction waves reflected from the driver end, or the contact surface may arrive at the test point first, any one of these disturbances will change the flow conditions in region 2. Figure 1(d) graphically illustrates one way to determine the test time, and account for the various disturbances.

For the details of the various methods of studying shock tube wave phenomenon, the reader is referred to any one of a number of texts dealing with compressible gas dynamics (Shapiro, 1987). The normal shock relations govern the temperature and pressure ranges available in this study, so both properties will increase as the Mach number increases.

The static pressure ratio across a normal shock is given by (Shapiro, 1987:1002),

$$\frac{P_2}{P_1} = 1 + \frac{2k}{k + 1} (M_s^2 - 1) \qquad (2)$$

the static temperature ratio across a normal shock by,

$$\frac{T_2}{T_1} = \left(\frac{2k}{k + 1} M_s^2 - \frac{k - 1}{k + 1} \right) \left(\frac{k - 1}{k + 1} + \frac{2}{(k + 1) M_s^2} \right) \qquad (3)$$

and the flow velocity in region 2 can be determined using,

$$U_2 = c_2 \left(\frac{M_s^2 + \frac{2}{k - 1}}{\frac{2k}{k - 1} M_s^2 - 1} \right) \qquad (4)$$

Where c_2 is the sonic velocity in region 2, and U_2 is the velocity of the flow in region 2 (Zucrow, 1976:342). Since the properties of the initial state in region 1 are known, the flow properties behind the shock in region 2 are easily determined.

The Boundary Layer

Actual flow behavior always departs from theoretical flow predictions to a certain extent, chiefly because of viscous interactions. The flow considered here is no exception. As the incident shock wave passes over the flat plate and shock tube walls, a very thin boundary layer develops. This very thin layer is where the static temperature transitions from its high free stream value T_2, to the surface temperature T_w. The flow velocity also changes from its free stream value U_2, to zero at the surface of the plate in this thin layer. Figure 2 illustrates the nature of this boundary layer after it encounters the flat plate, with great exaggeration.

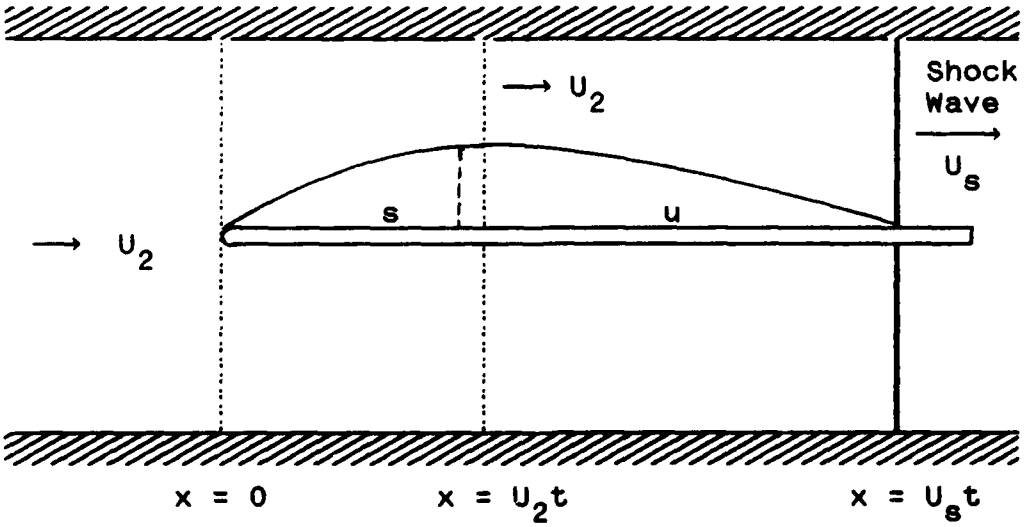

Figure 2 : The Boundary Layer on a Flat Plate After a Shock Wave Has Passed the Leading Edge (Mirels, 1956:52-53; Schlichting, 1987:440).

As the shock passes over the plate, an unsteady boundary layer is formed, denoted by u in Figure 2. The point of initiation of this unsteady boundary layer moves with the shock. The location of the point of initiation of the unsteady boundary layer is given by $x = U_s t$, Where x is the distance from the leading edge, U_s is the shock velocity, and t is the time elapsed since the shock passed the leading edge. Schlichting states that the transient nature of this unsteady boundary layer is similar to an impulsively started flat wall, but slightly thicker (Schlichting, 1987:441). At any fixed point on the surface of the plate a transition occurs from the flow conditions which characterize the transient boundary layer, to those of a steady-state boundary layer which develops from the leading edge. The criterion for this transition was previously mentioned as the nondimensional time, α, required for the boundary layer to reach a steady state (Davies and Bernstein, [illegible]). Denoted by s in Figure 2, the steady-state layer is formed by viscous effects and propagates out into the free stream, normal to the surface of the plate just as the transient layer does. This disturbance to the flow starts at the leading edge just as the shock passes, and is carried downstream with the free stream velocity U_2. This means that for $x > U_2 t$, the flow is not yet aware of the presence of the leading edge, and the steady-state boundary layer can only exist for $x \leq$

U_2t . The steady-state boundary layer does not end right at $x = U_2t$, due to interactions that occur between the downstream influence of the leading edge, and the upstream formation of the unsteady boundary layer. So the actual length of the fully-developed steady-state boundary layer along the plate will always be somewhat less than the maximum length of $x = U_2t$ (Schlichting, 1987:439-445; Shapiro, 1987, 907-1159). The boundary layers of interest in this study are the thermal and velocity boundary layers. For $Pr < 1$, the thicker of the two is the thermal boundary layer. Shapiro relates the two boundary layer thicknesses in a turbulent boundary layer with $\delta_u / \delta_T = (Pr / r)^{1/2}$, where δ_u , and δ_T are the velocity and thermal boundary-layer thicknesses, respectively. Pr is the Prandtl number of the flow, and r is the recovery factor (Shapiro, 1987:1120)

Mirels solved the Equations that govern the flow in the transient region (Mirels, 1956), while Blasius determined the governing Equations for the case of the steady boundary layer (Blasius, 1908). The theory they established has been built upon quite heavily, providing the design engineer with insight when considering specific flow behaviors.

Heat Transfer Through the Boundary Layer

Since even the flat plate geometry studied here is not without the flow complications set up by boundary layers, theoretical prediction of the heat transfer to the plate surface is complex. However, the comparison of theoretical predictions to the measured heat transfer data will, hopefully, provide an indication of how theoretical predictions should be treated in the future. The Equations to be developed in this Chapter can be used with Equations (2), (3), and (4) to predict theoretical heat transfer rates. For this study however, the observed values for P_1, P_4 , T_1 , and the Mach number are used in the theoretical Equations for comparison to the measured data.

The problem of determining the heat transfer, q, to the surface of the plate is solved using Newton's law of cooling,

$$q = h_x (T_{aw} - T_w) \tag{5}$$

where h_x is the local heat transfer coefficient, T_{aw} is the adiabatic wall temperature, and T_w is the temperature of the flat plate. A positive heat transfer occurs when $T_{aw} > T_w$. If a constant property flow of perfect gas is assumed, the adiabatic wall temperature can be written as (Mirels, 1956:23),

$$T_{aw} = T_2 + r \frac{U_2^2}{2C_p} \quad (6)$$

where r, the temperature recovery factor, is well approximated by $\sqrt[3]{Pr}$ for turbulent flow (Mirels, 1956:23; Kakaç et al, 1987:2-32) and C_p is the constant pressure specific heat.

The local Nusselt number is given by,

$$Nu_x = \frac{h_x x}{k} \quad (7)$$

where x is the distance from the leading edge, and k is the thermal conductivity of the fluid. For the steady turbulent boundary layer (Kakaç et al, 1987:14-24), on an isothermal surface at any instant in time,

$$Nu_x = 0.0287 Re^{4/5} Pr^{3/5} \quad (8)$$

where the Reynolds number is given by,

$$Re = \frac{U_2 x}{\upsilon} \quad (9)$$

the Prandtl number by,

$$Pr = \frac{C_p \mu}{k} \quad (10)$$

υ is the kinematic viscosity of the fluid, and ρ its density. According to Kakaç, "Eckert made the remarkable observation that if the specific heat can be treated as a constant, and all the fluid properties are evaluated at an

appropriate reference temperature T^*, the low-speed constant-property correlating Equations for Nu can be used for air for Mach numbers up to 20, the errors being less than a few percent" (Kakaç et al, 1987:2-48). The Eckert reference temperature is given by,

$$T^* = 0.5(T_w + T_2) + 0.22(T_{aw} - T_2) \qquad (11)$$

Equations (5 - 11) constitute the theoretical heat transfer solution for steady turbulent flow, and were used for comparison to the experimental results, with all fluid properties evaluated at T^*. The solution for the case of steady laminar flow was not mentioned here because it is not used in the comparisons of this study. For details on the steady-state laminar solution the reader is referred to a text such as Kays and Crawford (Kays and Crawford, 1980:147).

The solution for the case of unsteady theoretical heat transfer ($x > U_2 t$) is attributed to the theory of Mirels (Mirels, 1956), where the leading edge effects are neglected and the problem is treated as an infinite flat plate. According to Mirels, when the Prandtl number of the gas flow is close to one, approximations to his exact solution can be made.

For high speed, compressible flows of an ideal gas, with constant specific heat C_p, the adiabatic wall

temperature is (Schlichting, 1987:442),

$$T_{aw} = T_2\left(1 + r\frac{k+1}{2}M_2^2\right) \tag{12}$$

where the recovery factor for this flow condition is different than the value used in the steady case. Mirels approximates the recovery factor by (Mirels, 1956:14),

$$r = Pr^{\alpha} \tag{13}$$

with (Schlichting, 1987:442),

$$\alpha = 0.39 - \frac{0.02}{1 - (U_2 / U_s)} \tag{14}$$

For the solution of the laminar unsteady boundary layer Schlichting's approximations to the Nusselt number, and other variables used are (Schlichting, 1987:442-443),

$$Nu_x = \frac{1}{2} c_f' \, Re_t Pr^{\lambda} \tag{15}$$

where c_f' is the local skin-friction coefficient and is approximated by,

$$c_f' = \frac{1.128}{Re_t^{1/2}}\left(1 - \beta\frac{U_2}{U_s}\right) \tag{16}$$

with $\beta = 0.346$. The local, unsteady Reynolds number is approximated as,

$$Re_t = \frac{tU_2^2}{\upsilon_w} \tag{17}$$

where t is the time elapsed since the shock passed locally,

and υ_w is the kinematic viscosity evaluated at the wall temperature. The value of the exponent λ in Equation (15) is found from the relation (Schlichting, 1987:443),

$$\lambda = 0.35 + \frac{0.15}{1 - (U_2 / U_s)} \qquad (18)$$

Equations (12 - 18) were used to find the theoretical heat transfer rate in the unsteady laminar region that immediately follows shock passage, with all fluid properties evaluated at the plate surface temperature, T_w.

The theoretical unsteady turbulent solution was obtained by substituting the unsteady Reynolds number of Equation (17) into Equation (8) for the local Nusselt number. However, all the fluid properties were evaluated at the surface temperature of the plate, T_w (Novak, 1987:16; Smith, 1986:17). After the Nusselt number was computed the rest of the calculations proceeded just as all the other heat transfer computations, Equation (7) was solved for the local heat transfer coefficient h_x , then Equation (5) was used to determine the heat flux, q.

It should be noted that the development of these Equations assumes that the plate surface temperature is constant with x. Mirels found that the wall remains within 10 percent of its original value for $M_s < 100$ (Mirels, 1956:25).

Heat Transfer with Film Cooling. The main objective of film cooling is to inject a cooling secondary flow into a hot boundary layer, to form a protective film. Film cooling is not intended to protect just the surface at the point of injection, but is intended to be a protective layer for the entire region downstream of the injection point. Because a high temperature flow environment can severely shorten component life, film cooling can decrease the surface temperature, and maintain component life. However, in film cooling there are considerable differences in geometry, operation, and objectives (Goldstein, 1971:322). So for this study, only simple cases are considered.

The analysis of flows in which film cooling is used are generally not easy, but simple analyses exist, and are well correlated by experimental results. In many cases film cooling produces a turbulent boundary layer, and this study assumes that this is always the case (Kakaç et al, 1987:2-48).

The governing heat transfer equation for film cooling is Equation (5), but for the film cooling case the adiabatic wall temperature is different.

For film cooled heat transfer, Ammari found that the ratio of the heat transfer coefficients is well-correlated by (Ammari, 1989:8),

$$\frac{\bar{h}}{h_o} = 1.0 + 0.555 \exp\{ -0.14(x/ D)M^{-1/2}\} \qquad (19)$$

where; $\bar{h}$ is the average span wise heat transfer coefficient, h_o the heat transfer coefficient for the uncooled case, x the downstream distance from the point of coolant injection, D the cooling hole diameter, and M the blowing ratio parameter given by,

$$M = \frac{\rho_c U_c}{\rho_2 U_2} \qquad (20)$$

Ammari states that Equation (15) provides an excellent correlation within the range of $0.5 < M < 1.5$, and $1.5 < x/ D < 25$, where the coolant is injected normal to the plate. To simplify calculations it was assumed that the flow at the cooling hole exit was choked.

The theoretical solutions provided by Equations (5-18) were also used to compare to the measured heat transfer data with film cooling. But the real comparison of interest here is between Equations (19-20), and the measured values of the heat transfer.

Heat Transfer with Free Stream Turbulence. Free stream turbulence is defined here as the ratio of velocity fluctuation about a mean value, which implies at least two dimensional flow, to the mean flow velocity, or,

$$Tu = \frac{\overline{(u_2^2)}^{1/2}}{U_2} \qquad (21)$$

were $\overline{(u_2^2)}^{1/2}$ is the velocity fluctuation in the x direction, so only longitudinal effects are accounted for.

In contrast to film cooling, free-stream turbulence serves to increase the rate of heat transfer, and reduce film cooling effectiveness. Free stream eddies become entrained in the boundary layer, making it highly three dimensional. This increases the rate of heat transfer by transitioning laminar flows to turbulent flows, and increases the diffusivity of flows that are already turbulent. (Schlichting, 1987). Many studies have been conducted to determine the relationship between the level of free-stream turbulence, and its influence on the rate of heat transfer. In fact, some early studies on free-stream turbulence effects on the rate of heat transfer are in disagreement (Simonich and Bradshaw, 1978:672).

As was stated earlier, the intent here is not to study free-stream turbulence effects in detail, but to use the information made available by Rockwell (Rockwell, 1989). This information is in the form of the measured background turbulence level of the shock tube facility, used in both studies, and the measured turbulence level when free-stream turbulence is generated in the flow. These measurements are used to guage the changes in heat transfer brought about by different values of Tu.

Blair found that his measured values for the turbulent Stanton number were within ± 2 percent of theoretical

predictions, and that there was even less error for the laminar case (Blair, 1983:38).

Simonich and Bradshaw found that the ratio of the Stanton numbers,

$$\frac{St}{St_o} = 1 + A\frac{\overline{(u_2^2)}^{1/2}}{U_2} \qquad (22)$$

could be determined from the Reynolds analogy (Simonich and Bradshaw, 1978:671). They also stated that the coefficient A is uncertain to at least ± 25 percent, and is numerically about five for the turbulence range of their study, 0 < Tu < 7.5 percent (Simonich and Bradshaw, 1978:671).

Heat Transfer Measurements

A direct measurement of the heat being transferred from the hot gas behind the shock to the plate is not possible. However, the use of fast response thin film heat flux gages makes the measurement of the plate surface temperature history relatively simple, if it is assumed that the gage substrate and plate temperature are equal. The thin film gage senses the instantaneous surface temperature of the gage substrate, which is measured by recording the calibrated voltage output of the thin film gage. This temperature history can then be used to determine the heat transfer rate to the plate, as seen by the gage.

The heat flux gages used in this study consisted of a thin platinum film, formed by vapor deposition on an insulating substrate of Pyrex 7740 (Medtherm, 1985). The heat transfer model considers the gage substrate a semi-infinite solid, as shown in Figure 3.

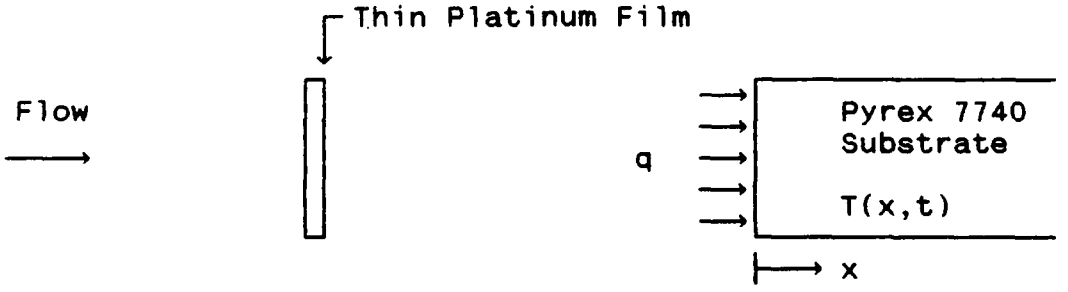

Figure 3 : Heat Transfer Model for Thin Film Gage Substrate

The Pyrex substrate has well known thermal properties which remain essentially constant over small temperature ranges (Bogdan, 1967:5). If substrate properties are assumed to remain constant, the heat transfer Equation can be written as (Bogdan, 1967:2-3; Kendall, 1966:2),

$$\frac{\partial T(x,t)}{\partial t} = \frac{k}{\rho C_p} \frac{\partial^2 T(x,t)}{\partial x^2} \qquad (23)$$

where
q = heat flux to the Pyrex 7740
k = thermal conductivity of the Pyrex 7740
ρ = density of the Pyrex 7740
C_p = specific heat of the Pyrex 7740
T = temperature of the Pyrex 7740
t = time
x = distance from the face of the gage

and the boundary conditions are,

$$T(x,0) = 0 \quad , \quad \text{for } x > 0$$

$$q(0,t) = -k \frac{\partial T(0,t)}{\partial x} \quad , \quad \text{for } t > 0$$

$$T(x,t) = 0 \quad , \quad \text{for } x \rightarrow \infty \text{ and } t > 0$$

The solution to this Equation is obtained by imposing Duhamel's superposition integral method for the case of an unsteady surface temperature, on a semi-infinite solid. For details the reader is referred to any one of a number of good texts on conduction heat transfer (Arpaci, 1966:307). Hitchcock used this method to obtain the solution (Hitchcock, 1985:2.1),

$$q(0,t) = \frac{1}{2}\left(\frac{\rho C_p k}{\pi}\right)^{1/2}\left[\frac{\theta_w(t)}{t^{1/2}} + \frac{1}{2}\int_0^t \frac{[\theta_w(t) - \theta_w(\tau)]}{(t-\tau)^{3/2}}\, d\tau\right] \quad (24)$$

where $\theta_w = T_w - T_i$, T_w is the surface temperature for the time in question, T_i is the initial plate temperature, and τ is a dummy integration variable.

Two common methods are available for the solution of Equation (24). The first involves the use of an analog circuit network which converts sensor inputs directly into the heat transfer rate, several sources detail the design and operation of these circuits (Bogdan, 1967:6-14, 18-22; Schmitz, 1963; Skinner, 1960). The second method is a finite differencing scheme to approximate Equation (24), and is the method used in this study. Cook and Felderman

developed an approximation to this solution using sensor voltages instead of temperatures for the independent variable (Cook and Felderman, 1966:561). Hitchcock also approximated Equation (24) using the same numerical technique applied by Cook and Felderman to obtain an expression for q, at any time τ_N, as (Hitchcock, 1985:5),

$$q(\tau_N) = 2\left(\frac{\rho C_p k}{\pi}\right)^{1/2}\left[\frac{\theta_w(\tau_o)}{2\tau_N^{1/2}} + \sum_{i=1}^{N}\frac{\theta_w(\tau_i) - \theta_w(\tau_{i-1})}{(\tau_N - \tau_i)^{1/2} + (\tau_N - \tau_{i-1})^{1/2}}\right] \quad (25)$$

where τ_o denotes conditions at $t = 0$, and τ_i at $t = t_i$. The accuracy of Equation (25) is constrained by the size of the discrete intervals into which the temperature history is divided. Since, in this study, the sensor output is sampled at a high rate and every sample point is used to calculate a value for q, the error associated with the interval size is minimized. It should be noted that if this expression is used in a computer program, additional round-off errors due to machine floating-point arithmetic will influence the results.

Since the change in gage temperature is generally less than five degrees Celsius for this study, the term

$$\left(\frac{\rho C_p k}{\pi}\right)$$

in Equation (25) can be considered a constant based upon

studies conducted by Bogdan (Bogdan, 1967).

All the data runs in this study used Equation (25) to evaluate the measured heat flux occurring at the surface of the plate, regardless of the presence of film cooling, or free-stream turbulence. As a result, the measured heat transfer coefficient is given by,

$$h = \frac{q}{T_{aw} - T_w} \tag{26}$$

This is then used to find the measured Stanton number,

$$St = \frac{h}{\rho_2 U_2 C_p} \tag{27}$$

and the measured Nusselt number,

$$Nu = \frac{hx}{k} \tag{28}$$

Equations (25-28) thus provided a means to compare the measured heat transfer to theoretical predictions. They also provided a consistent basis for calculation of uncooled, film cooled, and free stream turbulence heat transfer parameters.

III. Experimental Apparatus

Hardware

The facilities and equipment used in this study are essentially the same used by Novak, and Smith (Novak, 1987; Smith, 1986). The main differences are the use of a rounded leading edge flat plate, complete with film cooling holes, and the use of heat flux gages with a higher sensitivity. A turbulence generator was also installed between the last two sections of the shock tube.

Shock Tube. The primary tool for this study was the low speed shock tube at AFIT. This tube has a 4 inch by 8 inch internal cross-section, a driver section 4 feet long, a 16 foot driven section, and a dump tank attached to the end of the driven section. The test section is the last four feet of the driven section, just before the dump tank, and contains the flat plate. Figure 4 shows a layout of the shock tube as it was used in the study. The driver and driven sections were separated by a Mylar diaphragm, available in thicknesses of 0.001, 0.002, 0.005, and 0.007 inches. Only the 0.002, and 0.005 inch diaphragms were used in this study, as will be discussed later. The driver section is mounted such that it is free to move in the

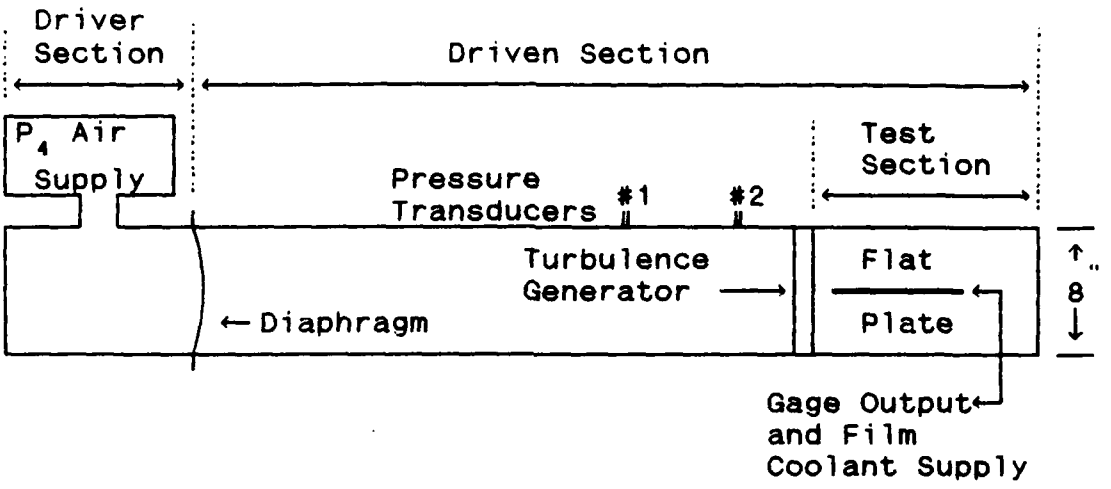

Figure 4 : Shock Tube Layout (Not to Scale)
(Note: Dump Tank not Shown)

horizontal plane to facilitate changing the diaphragm, and cleaning the shock tube. The driver and driven sections are locked together by a hydraulic latching mechanism. The air supply used to pressurize the driver section was ordinary compressed air at 100 psig. A calibrated pressure gauge was used to measure the driver pressure P_4 , as an aid in controlling the shock speed. The Mylar diaphragm was ruptured by a pneumatically operated plunger.

Instrumented Flat Plate. The instrumented flat plate was installed on the shock tube center line, as shown in Figure 4. The plate was 25.5 inches long, 4 inches wide, and 3/4 inch thick. The leading edge of the plate was rounded and located 12 feet, 2.5 inches from the Mylar diaphragm.

Film Cooling. The film cooling system consisted of a pressurized bottle of dry breathing air, at 2500 psig, with the output pressure controlled by a pressure regulator and an electrically actuated solenoid valve. Film cooling flow only occurred if the solenoid was pressurized from the bottle, and the switch was activated. The solenoid valve, located just outside the shock tube wall, was connected to the film cooling supply chamber in the plate as illustrated in Figure 5. The film cooling supply chamber imbedded in the plate consisted of

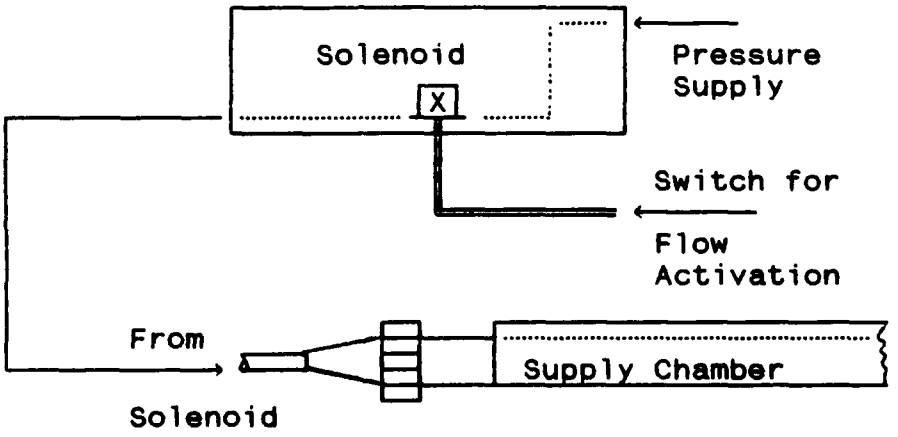

Figure 5 : Film Cooling Supply Arrangement

a 0.5 inch I.D. pipe, with a total length of 24.5 inches. The flat plate had a total of 41 film cooling holes, 0.039 inches (1 mm) in diameter, separated by two diameters center to center. The row of film cooling holes were centered on the plate, 2 inches from the leading edge. Figure 6 shows the cooling hole arrangement.

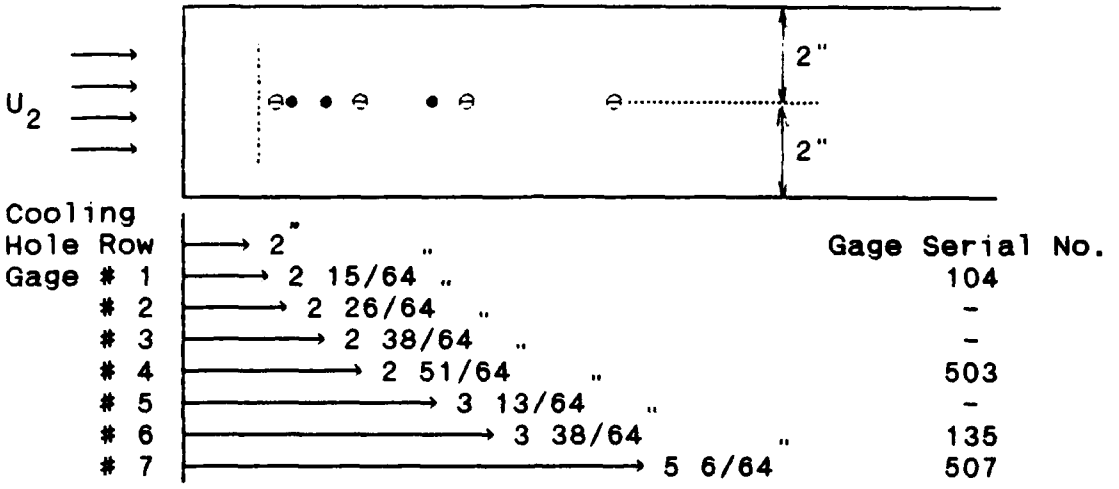

Figure 6 : Layout of Flat Plate (Not to Scale)

Turbulence Generator. Figure 4 shows the turbulence generator in relation to the shock tube layout. The turbulence generating system operates on the same principal as the film cooling system. A 100 psig compressed air supply is fed to a quick-action, 1/4 turn valve. When the valve is actuated, it allows the compressed air to flow to a manifold in the turbulence generator, Figure 7 illustrates this arrangement. The turbulence generator is 2 inches wide, and placed upstream of the test section, with its downstream side 0.5 inches from the leading edge of the flat plate. Figure 8 shows that the pressure supplied to the generator from the manifold is distributed internally. The internal distribution supplies air to holes that discharge into the free-stream, normal to the surface. The holes are drilled into interchangeable,

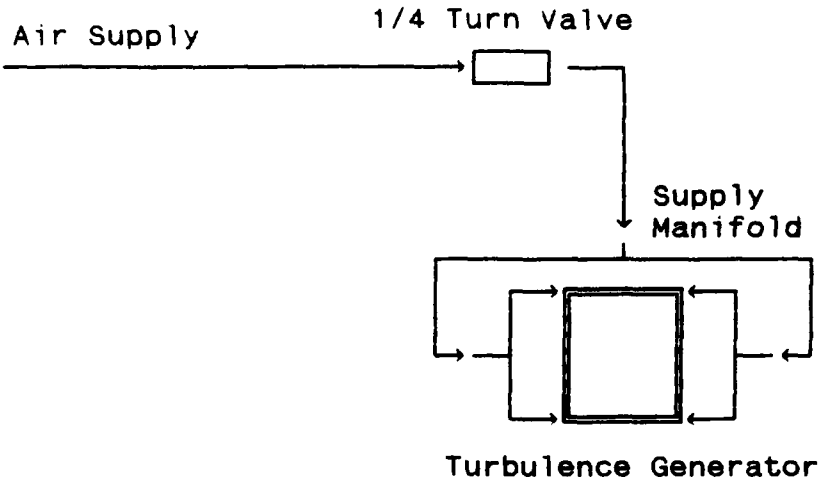

Figure 7 : Turbulence Generating System Schematic

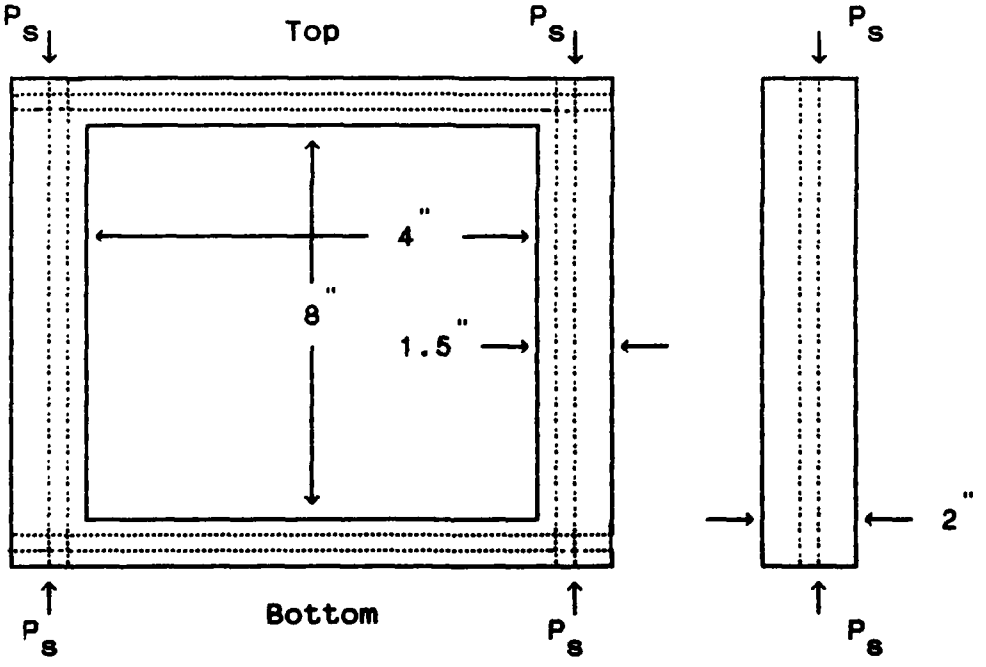

P_s = Supply Pressure

Figure 8 : Turbulence Generator Pressure Distribution
(Not to Scale)

threaded inserts that are provided in complete sets of 12, for 1/8, 3/16, and 1/4 inch hole diameters. There are four holes on each side face of the generator, symmetrically centered every two inches. The top and bottom faces have two holes each, also symmetrically centered every two inches. Only the 1/8 inch diameter inserts were tested.

Instrumentation

Waveform Recorder. The Data Lab DL1200 waveform recorder was used to digitally record the analog outputs of the all the instruments used in this study. The DL1200 is a 12 bit device, that simultaneously samples then records eight channels, by transforming the analog voltage inputs to digital values. Each channel was sampled at the maximum sampling rate available, one sample per channel every 2 microseconds. The DL1200 is able to store 4096 samples for each of the eight channels. At this sampling rate, the DL1200 can record 8.192 milliseconds worth of data. Since the available test time is typically 3 to 4 milliseconds, all the information made available in this time could be recorded The recorded data for each run were then downloaded from the DL1200 12 bit memory, to a Zenith 16 bit machine, and stored on diskette.

Heat Flux Gages. The gages used to measure the heat flux were Medtherm Corp. model PTF-100-1009 thin film resistance gages. Each gage was constructed of a platinum thin film mounted on a cylindrical Pyrex 7740 substrate, 0.218 inches in diameter. The 0.218 inches includes a stainless steel jacket 0.01 inches thick, each gage is as shown in Figure 9 (Medtherm, 1985).

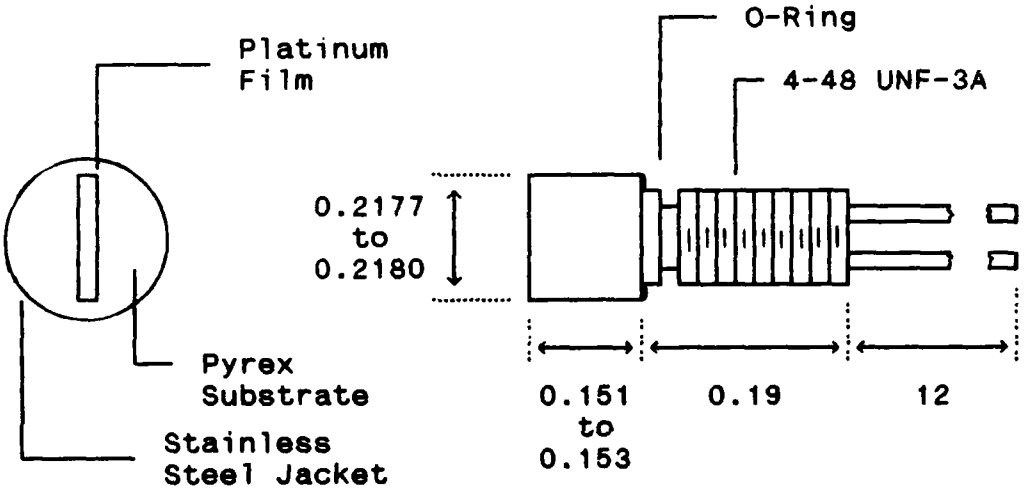

Figure 9 : Medtherm Heat Flux Gage
(All Dimensions in Inches)

The lead wires were 32 gauge, teflon-coated copper wires, 12 inches long. Gage sensitivity ranged from 0.0018 to 0.0027 Ohms / °C, without amplification. The flat plate provided seven flush-mount positions for these gages along the centerline of the plate. The centerline location prevented the boundary layer formed on the shock tube walls, two inches away, from influencing sensor readings.

The first gage was located 2 15/64 inches from the leading edge, or, 15/64 inches from the row of film cooling holes. The other gages were located along the centerline, as shown in Figure 6. Gage numbers 2, 3, and 5 were not used because they were inoperable, and are indicated by • in Figure 6. The data from gages 1, 4, 6, and 7 were available for all data runs, except a few runs when gage 1 or 7 became temporarily inoperable. The gages have a response time of 240 microseconds for 99.9 % of a step input. Before being recorded on the DL1200, the output of each gage was processed through a separate Wheatstone Bridge and amplifier circuit.

Wheatstone Bridge and Amplifier Circuitry. The resistance of the gages ranged from 77 to 110 Ohms at room temperature. As stated earlier, each gage was used as a resistance leg in a Wheatstone Bridge, so closely matched low-tolerance , ± 0.1 % , resistors were used in the other three legs of each bridge to aid in balancing the bridge. One leg utilized a 500 Ohm variable resistor in parallel with a precision resistor to balance the bridge, and maximize its sensitivity. Each Bridge circuit was incorporated into a Transamerica Instruments model PSC 8115 Bridge Supply Module. The constant bridge excitation voltage was set at 2.5 volts for each circuit, and a nominal 1000 Ohm resistor placed in series with the supply voltage of each bridge. The resistor limited the bridge

supply current to a nominal value of 2.5 milliamps, this arrangement kept the current well below the maximum gage current of 10 milliamps. Figure 10 illustrates a typical bridge circuit.

The small temperature changes encountered at the plate surface, less than 5 °C, changed the gage resistance by a very small amount. The small changes in resistance made the use of an amplifier circuit mandatory. The amplifier used for each circuit was a Transamerica Instruments Model 8015-1 High Gain Differential Amplifier. The combined bridge/amplifier circuit for each gage was calibrated to provide an output that ranged from 17.27 to 24.86 millivolts/ °F. The bridge/amplifier circuits for each gage were card mounted and installed in a Transamerica Instruments rack designed for these interchangeable modules. After the gage output signal was processed through these components it was recorded on the DL1200. Figure 11 shows a schematic of the data collection system for the heat flux gages.

Pressure Transducers. Two Endevco Model 8530A-100 pressure transducers were used in this experiment. The calibrated output of the pressure transducers was used for several reasons. The DL1200 required a trigger to start the data acquisition process; pressure transducer # 1 shown in Figure 4, provided this function. The use of the

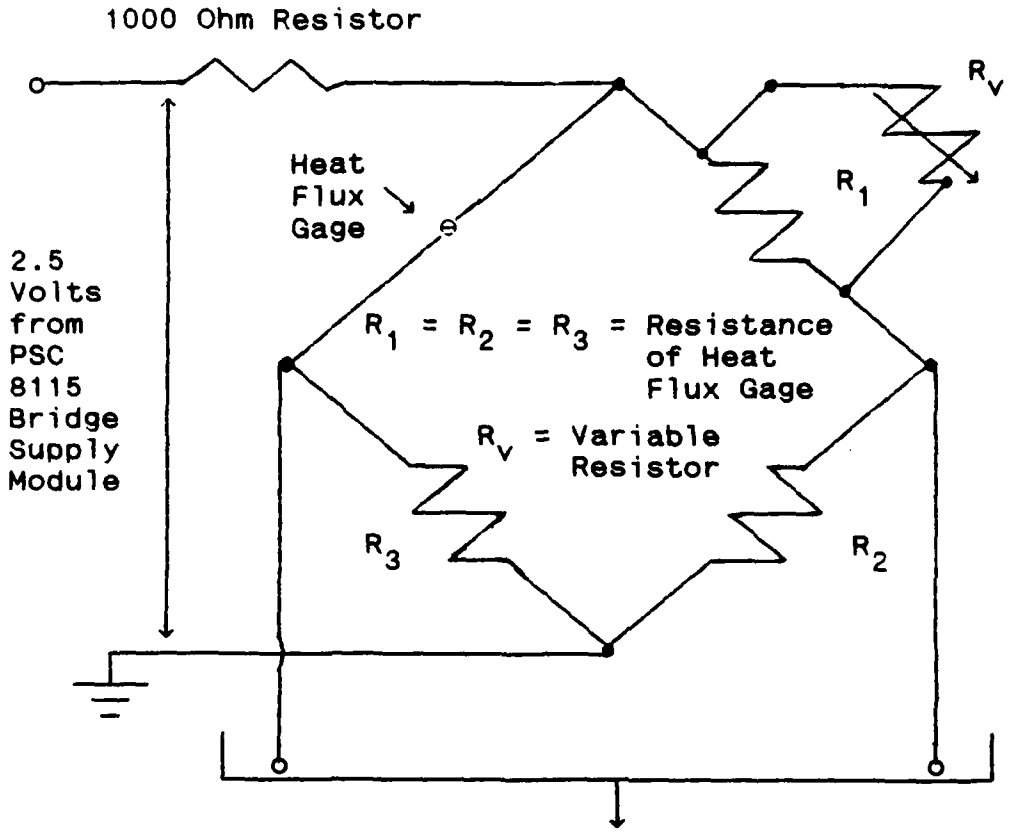

Figure 10 : Typical Wheatstone Bridge Circuit

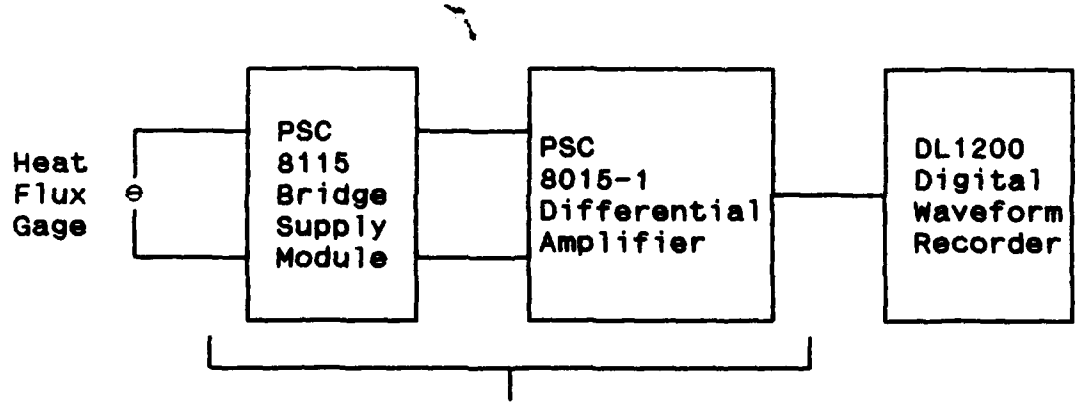

Figure 11 : Data Collection Schematic for Heat Flux Gages

pressure transducer as a trigger also allowed a 5 percent pre-delay in the data recording. That is, 5 percent of the DL1200 recorded data for each channel was allotted to sensor output that occurred before shock passage. This proved useful when film cooling data runs were made. Pressure transducer # 1 and # 2 were separated by 28 inches, this made the calculation of the shock speed simple. Pressure transducer # 2 was also located 16.5 inches from the leading edge of the flat plate. Both transducers were powered by a single Hewlett-Packard 10 Volt dc power supply, Model 6205. The output from each transducer was sent to a Neff Instruments Model 10 amplifier/filter unit. The amplification was set for a gain of 10, and the filter set at 20,000 Hertz for both transducers. Without the filters, the random line noise continually triggered the DL1200.

It should be noted here that the free-stream turbulence level measurements obtained from Rockwell were made using a single wire hot wire anemometer, for details on this instrumentation the reader is referred to his study (Rockwell, 1989).

IV. Experimental Procedures

Calibrations

All the instruments used to collect data were calibrated to reduce the errors found in the measurements, and to provide a level of confidence in the measurements. The heat transfer gages were connected to the circuitry described in Chapter III, and mounted loosely in the plate. The plate was then turned upside down allowing the gage to be calibrated to dangle out of its mounting hole. The power was applied to all the circuitry and allowed to warm up for five minutes, to reach operating temperature. Each amplifier circuit was then cycled through the internal zeroing routine pre-programmed into the modules, and the bridge/amplifier circuit was also internally balanced using a similar pre-programmed feature. The variable resistor placed in the bridge circuit, shown in Figure 10, was then used to externally balance the Wheatstone Bridge by observing the bridge/amplifier output. The voltmeter used for these measurements was zeroed, then used to measure the output of a dc power supply. This reading was then verified by another voltmeter processed in the same manner.

Bridge balancing was performed with the amplifier controls set at,

Gain	: 250
Filter	: 10 kHz
Operating Mode	: AMP D

These same levels were used for the calibration and for each data run. The voltmeter was left attached to the output for the rest of the procedure. The gage was then placed in a waterproof plastic bag, along with a J-type thermocouple. The J-type thermocouple was powered by an Omega Digicator which read the thermocouple output, referenced it to its internal ice point, and displayed a temperature output in degrees Fahrenheit. The digicator readings were verified by measuring several temperatures with another digicator, and a laboratory bulb-type thermometer. The plastic bag was then placed in a pot of tap water. A low tap water temperature was obtained by letting the tap water run until it reached its underground temperature of approximately 62°F. The bag was submersed in the water approximately three inches, allowing the gage face and thermocouple bead full contact with the bag surface exposed to the water, while the top of the bag was kept about 2 inches above the surface of the water. The pot was set on a thermal mixer, and a magnetic stirrer placed in the pot. The thermal mixer was then turned on to

slowly mix the water and eliminate local hot spots, then the heating element was turned on and placed at its middle position. Since the gage and thermocouple have different response times, they reached the same temperature at different times. This inherent error was minimized by slowly heating the water, while observing the voltage output of the bridge/amplifier circuit and the Digicator display. As soon as the Digicator display changed, a voltage reading was taken. This process was repeated 10 times for each gage calibrated. The resulting calibration curves were constructed by plotting a least squares curve fit through the data. The maximum error observed between the prediction and the data is 0.11 percent, and is attributed to observer response error since all the other predictions are below this value. Figure 12 shows the calibration curve containing the maximum error.

A brief summary of all calibrations made is included in Appendix A. The procedures used to calibrate the pressure transducers followed the same exacting standards used to calibrate the heat flux gages. The $\rho C_p k$ values used for the Pyrex 7740 gage substrate are also listed in Appendix A, along with the source of the $\rho C_p k$ values. It should be noted that the calibrated pressure transducers were used to verify the film cooling supply pressures.

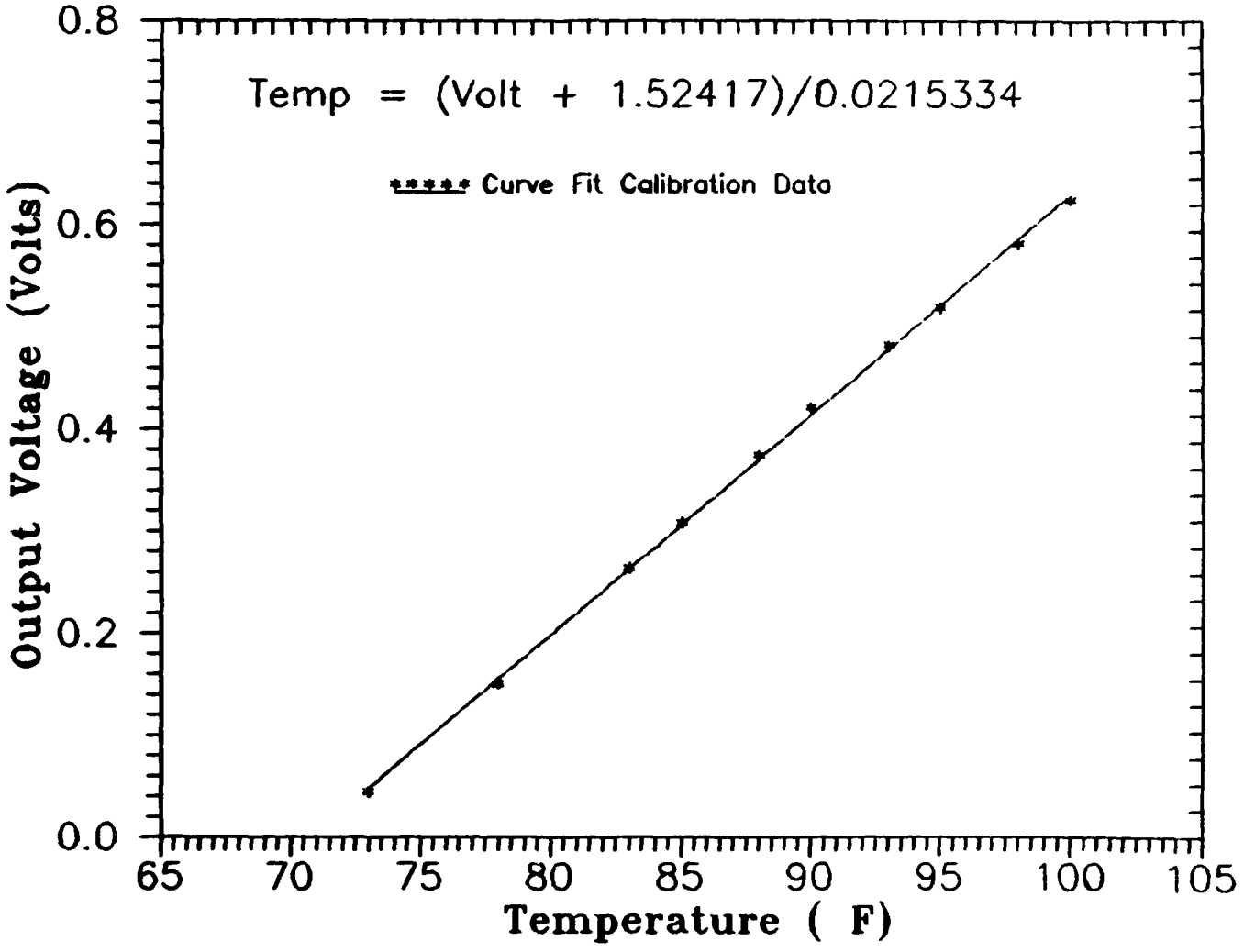

Figure 12 : Calibration Curve for Gage No. 1, S/N 104

Shock Generation

Since one is chiefly concerned with the comparison of heat transfer rates from different data runs, the repeatability of a certain shock speed is of primary importance. If two runs have the same shock speed, they will essentially have the same free stream flow conditions during the test time. For P_4 below 55 inches of mercury (gauge), a 0.002 inch diaphragm was used, and for P_4 above this pressure, a 0.005 inch Mylar diaphragm was used. This procedure produced a consistent stretching of the diaphragm, shown in Figure 1(a), and allowed the shock wavelets issuing from the ruptured diaphragm to form in the same manner.

To repeatedly produce a shock speed of a given strength required many factors to come together all at once. If the ambient conditions were not the same as they were when the original shock speed was observed, the driver pressure was varied accordingly. A shock speed that was within 0.5 percent of the original was considered acceptable. This method essentially produced the same heat transfer values, provided there were no flow anomalies occurring in the boundary layer. This procedure worked well until film cooling flow was initiated.

The initiation of the film cooling flow was made approximately one millisecond before the shock was

initiated, and was performed as consistently as possible. This allowed the pressurization of the film cooling supply chamber to the stagnation conditions cited in Chapter II.

Data Collection

All the data collected in this study were processed by the same collection and reduction system, arranged as shown in Figure 13. As stated in Chapter III, a Zenith 386 computer was used to download the recorded data from the DL1200. The software used to download the data was a Quickbasic program written by Tanis, and modified by Rockwell (Rockwell, 1989). This program converted the

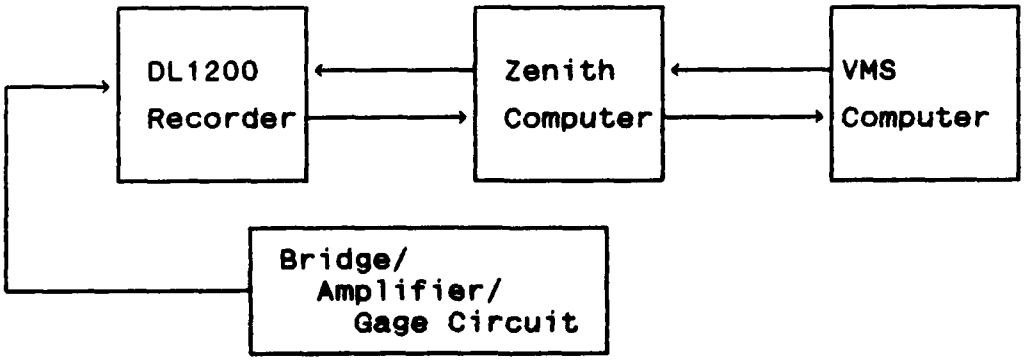

Figure 13 : Data Collection and Reduction Flowchart

data from the DL1200 12 bit architecture, to the Zenith 16 bit architecture, and stored the data in a nine column by 4096 row binary format, and named the data file

FILENAME.DTI. The program also provided options to convert the data to an ASCII format, and provided several other screen features.

As was done for the calibrations, sufficient time was allowed for the equipment to warm-up before the data collection process. The internal circuitry was then zeroed and balanced. Then the bridge was externally balanced in the same manner as the calibration procedure, to a nominal value of + 5 millivolts, which varied depending on the bridge being balanced. It was previously mentioned that gage current was limited to a nominal value of 2.5 milliamps. The reason for this limit is due to a tradeoff between the manufacturers recommendation of operating the gages at 1.0 milliamp, and the increased sensitivity available when the gages were operated at a higher current (Medtherm, 1985). However, even when the gages are operated at 2.5 milliamps, there was I^2R heating observed in the gage traces at ambient temperatures. Some of this observed fluctuation is attributed to electrical line noise, but how much is not known. The I^2R heating was discovered by observing that the bridges were balanced to a nominal + 5 millivolts, but quickly rose to a higher level, which was different for each gage. This level ranged from 10 to 50 millivolts depending on the gage, and was attributed to the differences in resistor matching in the individual bridge circuits, and the I^2R heating reaching

thermal equilibrium with its surroundings. Once the voltage levels reached these values, they remained relatively steady. The data reduction program compensated for this offset.

Data Reduction

After each data run was made, the data was converted into an ASCII format using the program mentioned above, and the shock speed was calculated. Figure 14 shows a typical voltage trace of a pressure transducer output for transducer # 1 and # 2. Figure 14 is typical in its depiction of the method used to calculate shock speed, but in other respects it is not typical. These reasons will be made clear in Chapter V. The points used to calculate the shock speed were the easily recognized "spikes" produced by the initial shock impact, indicated by a * in Figure 14. Since the two transducers were at a known distance from one another, the shock speed was easily calculated by observing the time difference between these two points. Then the sonic speed at the ambient temperature was used to calculate the shock Mach number. Shock speeds found in this manner produced consistent results from one data run to the next, and allowed the theoretical calculations, which are highly dependent on the Mach number, a proper

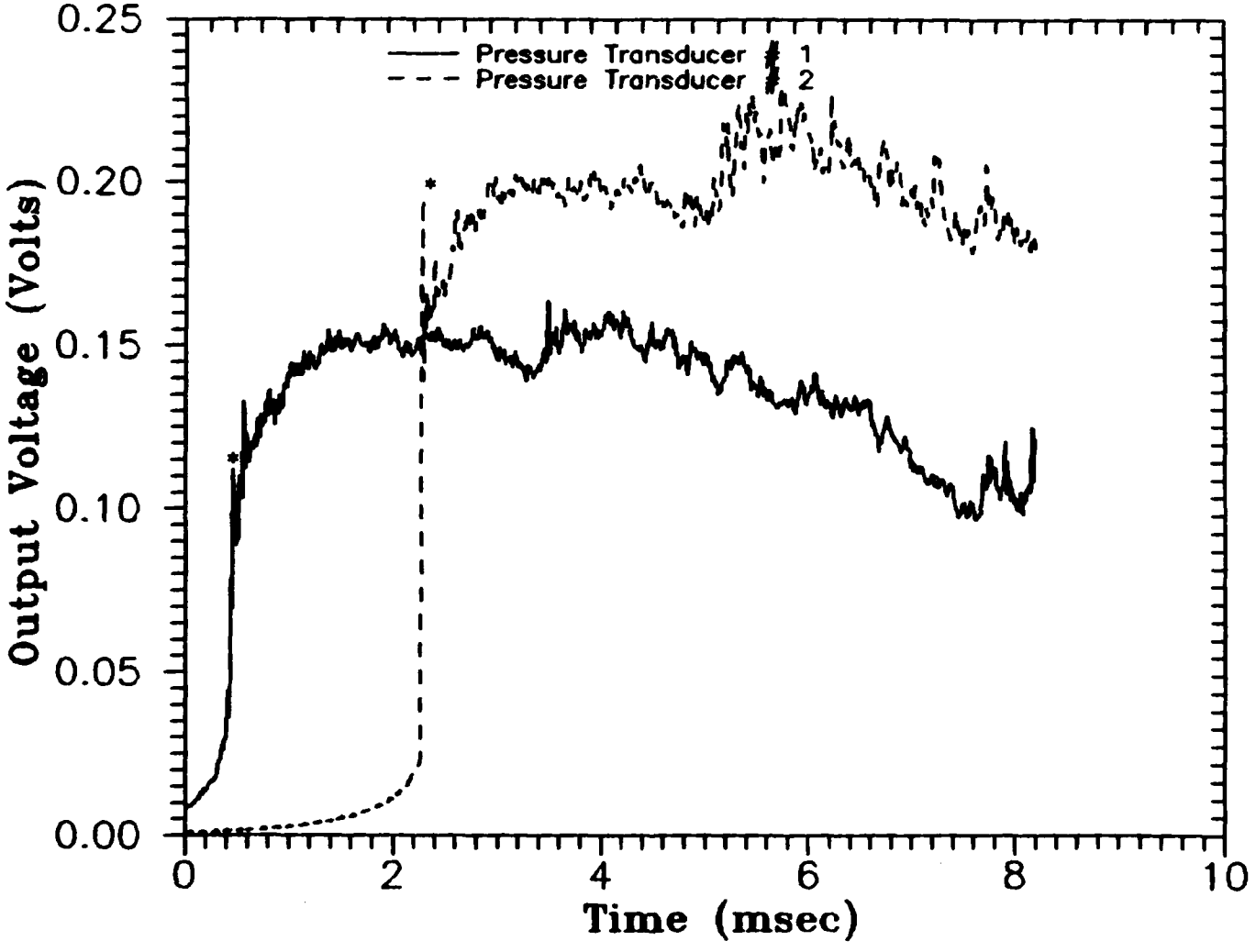

Figure 14, Typical Pressure Transducer Output (From Run C003)

comparison to the measured values

If a calculated shock speed for a film cooled data run produced a match with the corresponding shock speed for the uncooled case, the time of shock passage was found for each gage just as it was for the uncooled run. This was accomplished by loading the data file into a plotting program, such as Grapher, and then opening the file so the columns could be observed. Since the shock passage produced an abrupt rise in the trace from the previously quiescent level, the rise was easily distinguished when the columns of numbers were paged through. The time for shock passage between pressure transducers was determined in this manner for the shock speed calculations. Previous studies expressed a certain degree of difficulty in determining the time of shock passage due to background noise levels (Novak, 1987). However, the sensitivity of the gages used in this investigation made the passage point quite distinct except at very low Mach numbers. Previous studies also used various means of reducing the background noise found in the heat flux gage output, which consisted mainly of averaging methods (Novak, 1987; Smith, 1986). This investigation took a different tack.

The flow conditions measured in this study were those behind the incident shock, in region 2, as stated in Chapter 2. However, determining the time at which region 2 flow conditions changed from region 2 to those of region 5

was not always evident from the gage output trace. For this reason a graphical solution was used to determine the ending time (Shapiro, 1987:912-1027). By calculating the ending time for the lowest shock Mach number used, M = 1.16, and the highest, M = 1.32, the shock Mach numbers that fell in between these values were easily interpolated. At gage 7, this time range was from 3.06 to 3.5 milliseconds. Once the starting and ending times that defined region 2 flow conditions were determined, the actual data reduction process began. The data cutoff times were always approximately 3 milliseconds.

All actual heat transfer calculations took place in the computer program developed for this study, which is included in Appendix B. This program computed the theoretical heat transfer rates using Equations (5-18), then computed the actual heat transfer rate using Equation (25), for each gage location. It also determined the free stream Reynolds number, and the difference between the plate and free stream temperatures. This temperature difference was computed at set time intervals and used to find the mean temperature difference corresponding to the mean heat flux, for the solution of Equations (26-28). It output the Reynolds numbers of Equations (9) and (17) at set intervals. A comparison between the heat transfer obtained by this method, and previous studies (Novak, 1987, Smith, 1986), at the same Mach number, showed excellent

agreement. This method was also compared to the electrical analog method used by Rockwell and again showed excellent results for similar data inputs (Rockwell, 1989). At the heart of this program was a data averaging technique that averaged the temperatures calculated from the gage voltage inputs. The mean heat transfer rate was calculated for each gage, after steady flow was established, and used to calculate h, Nu, and St using Equations (26-28).

Data Averaging. In order to minimize the effects that the background noise levels might produce in the voltage to temperature to heat transfer calculations, a temperature averaging technique was employed to average the temperatures calculated from the gage voltage outputs. Figure 15 shows a typical gage voltage output trace with the random noise level readily evident at what should be a quiescent baseline level. The averaging process uses a moving average to determine the temperatures used in both the theoretical and the actual heat transfer calculations. The moving average temperature is given by,

$$T_{a_j} = \frac{1}{N} \sum_{i=-b}^{b} T_i \quad , \text{ for } b = (N - 1)/ 2, \text{ and } j = 1,\ldots,M \quad (29)$$

where T_{a_j} is the averaged temperature, M is the number of points to be averaged, N is an odd number which establishes the averaging bound, b, on either side of T_{a_j}. The value

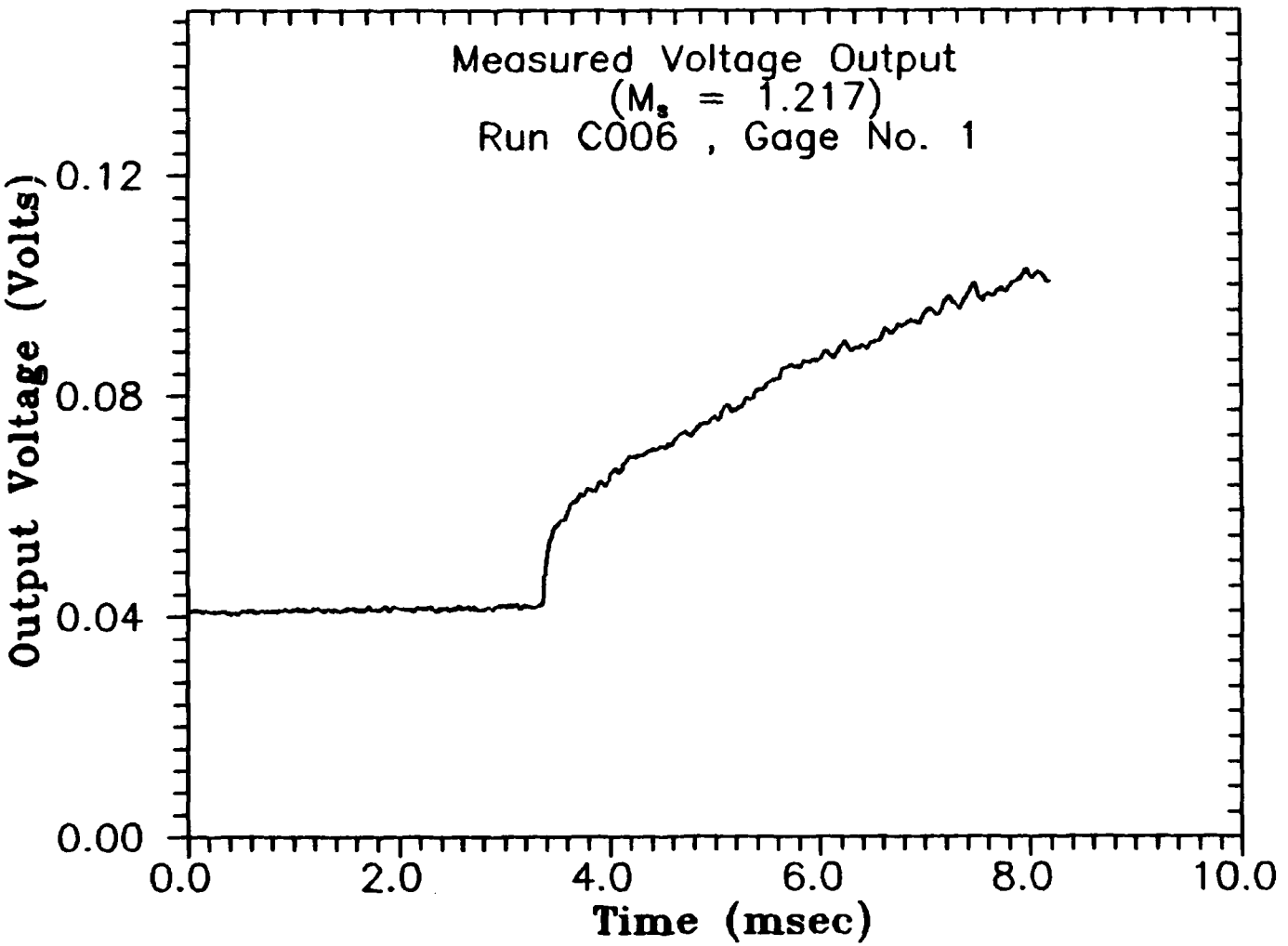

Figure 15 : Typical Gage Voltage Output

for N used in the program was 25, except at the time of shock passage. Here the initial value for T_{a_j} was set equal to the actual temperature, then the value of N was set equal to three to compute T_{a_j} at $j = 1$, then N was increased by two to calculate the next T_{a_j}, and so on until N reached 25. This process followed the actual temperature curve quite accurately; in fact, a full plot of the averaged and actual temperatures shows no difference between the two. To see the differences between the two curves the resolution must be increased. Figure 16 shows a comparison between the two curves in a highly magnified view. This Figure also shows that the averaging process does not follow peaks or troughs with steep gradients, as expected. Other numerical techniques are available to effectively "smooth" or filter the data and closely follow the peaks and troughs (King and Oldfield, 1985), but this method was chosen for its ease of use, and computational efficiency. The heat flux calculated using this averaging method followed the mean of the actual heat flux very well, but did not reproduce the magnitude of the peaks and troughs that the heat flux calculated using the actual temperatures did. This is as expected; because the averaging process reduces slope of the actual temperature plot, and the heat flux is proportional to the derivative of this slope, the slopes of the heat flux calculated using

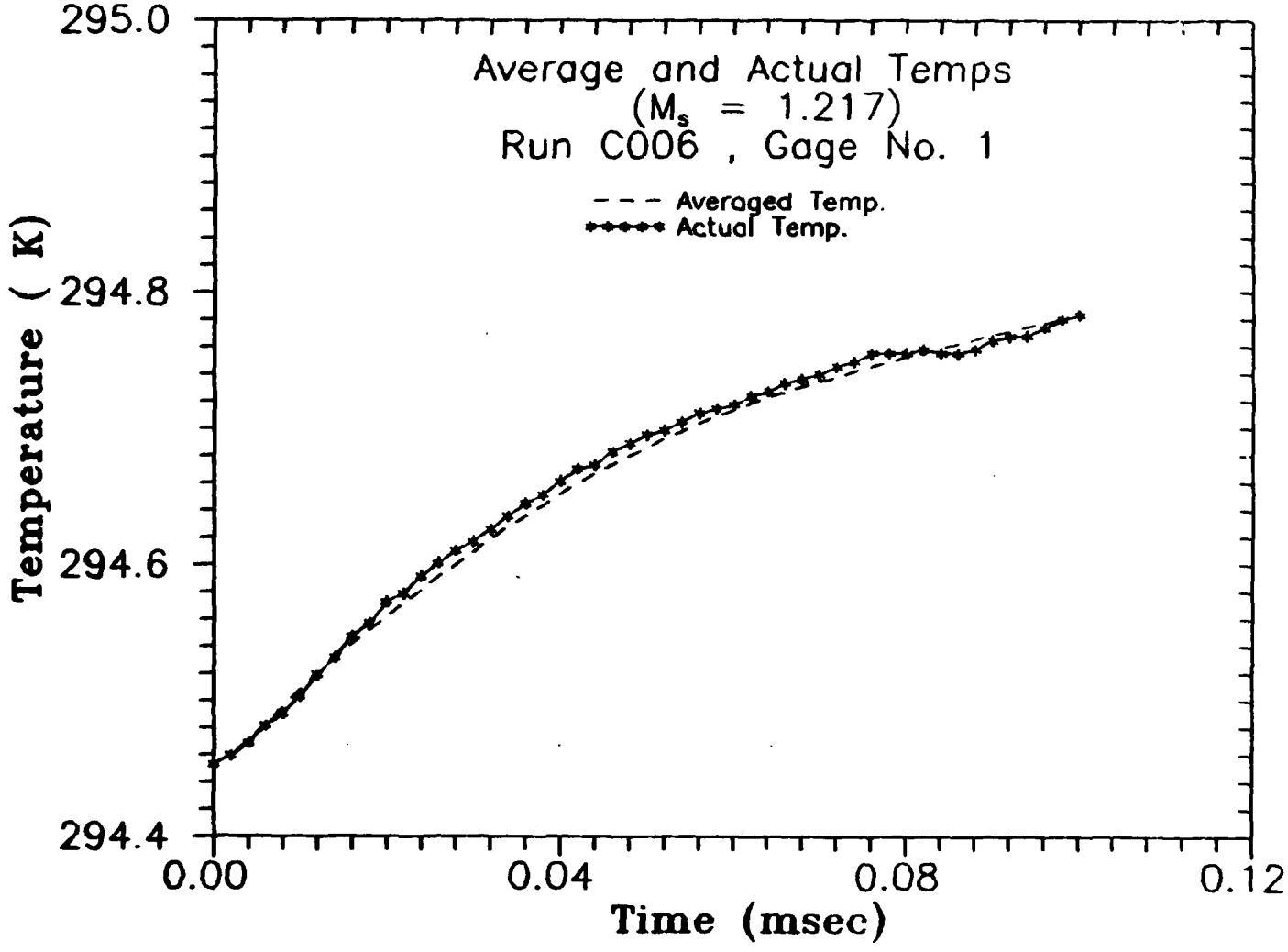

Figure 16 : Average vs Actual Temperatures

the averaged temperature will not be as steep as those calculated from the actual temperatures. Figure 17 compares the heat flux calculated by the temperature averaging process with the heat flux calculated using the actual temperatures, for the same data input file, and illustrates the differences in the slopes.

The film cooling holes were taped over to obtain data for the heat transfer without film cooling. Also, the turbulence measurements used here were made at a point in the free-stream two inches above the plate, and 3/4 of an inch forward of the film cooling holes. So the turbulence values used here do not account for the turbulence decay, but assume the level remains the same down the instrumented length of the plate.

It should also be noted that the film cooling supply lines were allowed to stabilize at room temperature for approximately five minutes. Assuming isentropic flow, this allowed the use of the room temperature T_1, as the stagnation temperature of the cooling hole exit, or $T_c = 0.8333T_1$. This simplifies the film cooling hole exit velocity calculation needed in Equation (20). The film cooling supply pressures used for the data runs in this investigation were run so the exit pressure was at least four times greater than the highest pressures expected in the flow, assuming the flow was choked only at the cooling hole exits.

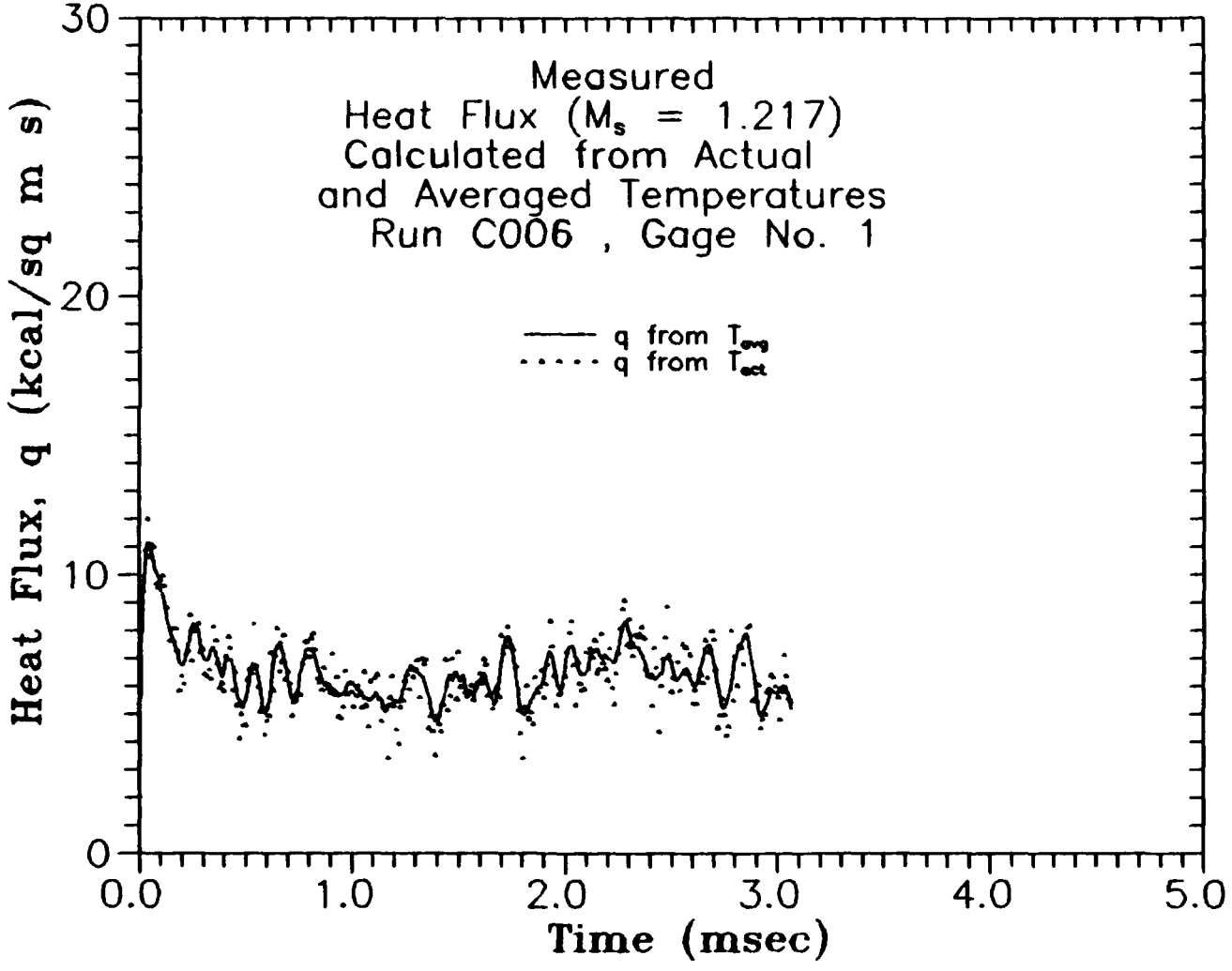

Figure 17 : q Calculated From Average and Actual Temperatures

V. Results and Discussion

Data runs were made to determine heat transfer rates at various film cooling flow rates, and one free-stream turbulence level. The experimental data collected were broken into a series of ten data sets, with a series naming convention to distinguish between them. Each series began with a letter designator, followed by three numbers which defined each particular data run. The extension .DAT was used on every data and program result file. To eliminate confusion between program result file names, the series convention name it was derived from preceded all result filenames. Table I lists the data series filename convention used, along with a brief description of the series contents. Figure 18 illustrates the manner in which

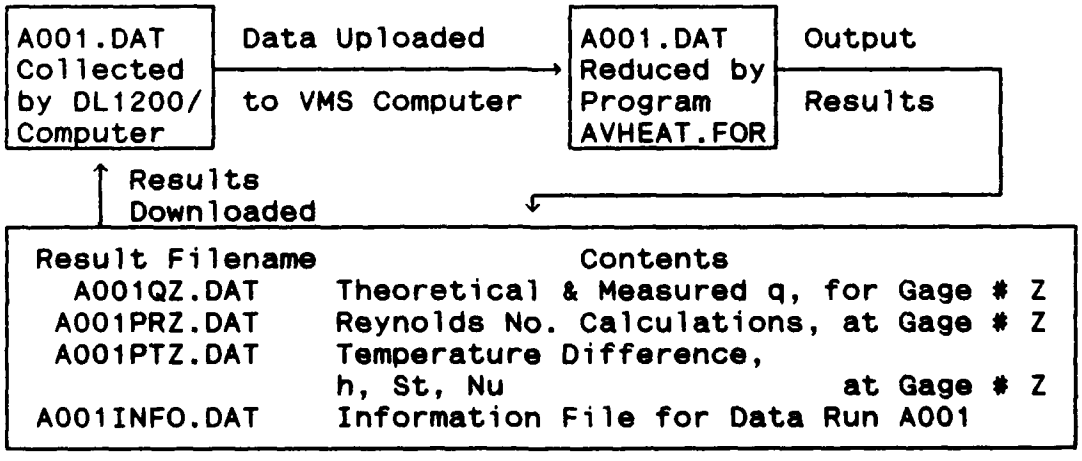

Figure 18 : Results Filename Flowchart

Table I

Data Filename Series Convention (xx = Series Number)

Data Series Prefix	Brief Description
A0xx	All test runs, to check equipment, programs, etc.
B0xx	Also test runs, used to test the accuracy of data reduction program.
C0xx	Heat flux data runs, without cooling, for comparisons.
D001 to D010	Film cooling run tests, at a supply pressure of 100 psig.
D011 to D019	Film cooling at 50 psig.
D020 to D041	Film cooling at 25 psig.
E0xx	Film cooling at 10 psig.
G0xx	Film cooling at 20 psig.
H0xx	Film cooling with a free stream turbulence of 12%.
J0xx	Verification runs.

the data reduction program names the files containing the results, using A001.DAT as an example.

Many of the data runs made produced results which were not used in the heat transfer comparisons, for various reasons. The reasons are explained throughout this Chapter. The test conditions for the data runs that were used in the heat transfer comparisons are summarized in Table II.

Heat Transfer

Each of the data runs listed in Table II, and many that are not in Table II, were processed by the data reduction program. The measured and theoretical heat transfer rates for each run were then plotted to obtain a visual representation of the local heat flux. Figure 19 shows one such plot. The time at which the shock passed the gage is referenced as zero.

Figure 19 is typical of all the low speed (low Mach number) results at gage number 1. The measured heat flux is characterized by an unsteady laminar flow, then quickly transitions to a steady turbulent flow. This is typical of the boundary layer transition depicted in Figure 2, as the unsteady region u, transitions to the steady region s.. The high rate of heat transfer for the initial laminar

portion is due to a theoretically instantaneous impulse in the surface temperature from the shock. This temperature gradient is theoretically infinite, but due to the extremely thin shock and limited gage response the heat flux is high, but not infinite. The high heat flux quickly reduces to a lower value until the transition to turbulent flow occurs.

Table II

Summary of Test Conditions

Data Run	P_1(in Hg)	P_4/P_1	T_1(C)	T_2(K)	U_2(m/s)	M_s(obs)
C004	29.20	2.85	21.0	324	85.8	1.161
C005	29.21	2.85	21.2	325	86.3	1.162
C006	29.20	3.19	21.3	335	113.0	1.217
C013	29.23	3.53	19.8	338	125.1	1.243
C015	29.23	3.88	20.0	343	136.4	1.267
C016	29.23	4.04	20.0	347	147.0	1.291
C017	29.21	4.38	20.2	351	157.0	1.312
D020	28.93	2.32	18.0	321	86.4	1.163
D024	28.86	2.84	17.6	331	111.7	1.215
D037	29.15	3.92	19.2	338	127.2	1.247
D038	29.15	4.05	19.1	341	135.7	1.266
D039	29.16	4.35	19.1	346	148.7	1.294
D040	29.18	4.37	19.1	347	148.9	1.294
D041	29.18	4.52	19.0	348	153.3	1.304
E001	29.19	4.60	19.1	352	160.1	1.319

Table II (continued)

Data Run	P_1(in Hg)	P_4/P_1	T_1(C)	T_2(K)	U_2(m/s)	M_s(obs)
E005	29.20	3.88	19.1	334	126.0	1.244
E007	29.36	2.36	19.0	323	86.9	1.164
E008	29.37	2.84	19.0	332	110.8	1.213
G001	29.37	2.88	19.0	332	111.0	1.213
G002	29.37	2.31	19.1	322	85.0	1.160
G004	29.38	4.00	19.2	341	134.1	1.262
G005	29.38	4.21	19.2	346	144.7	1.289
H001	29.40	4.40	20.2	349	152.5	1.302
H002	29.40	4.41	20.3	349	149.5	1.295
H003	29.40	4.40	20.3	349	151.0	1.298
H004	29.39	4.42	20.5	348	150.5	1.297
H005	29.40	4.41	20.5	350	153.5	1.304
J001	29.00	4.45	20.6	353	160.2	1.318
J002	29.00	4.46	20.5	353	159.0	1.316
J003	29.00	4.45	20.5	352	158.9	1.313
J004	29.00	4.45	20.5	352	159.1	1.314
J005	29.2	4.43	20.5	353	160.9	1.320

Once the flow departs the unsteady laminar region, it rapidly transitions to a steady turbulent flow condition. This observation is true for all the data runs graphed. After approximately 0.9 milliseconds a fully turbulent, and steady (relatively), flow condition is reached. Each plot

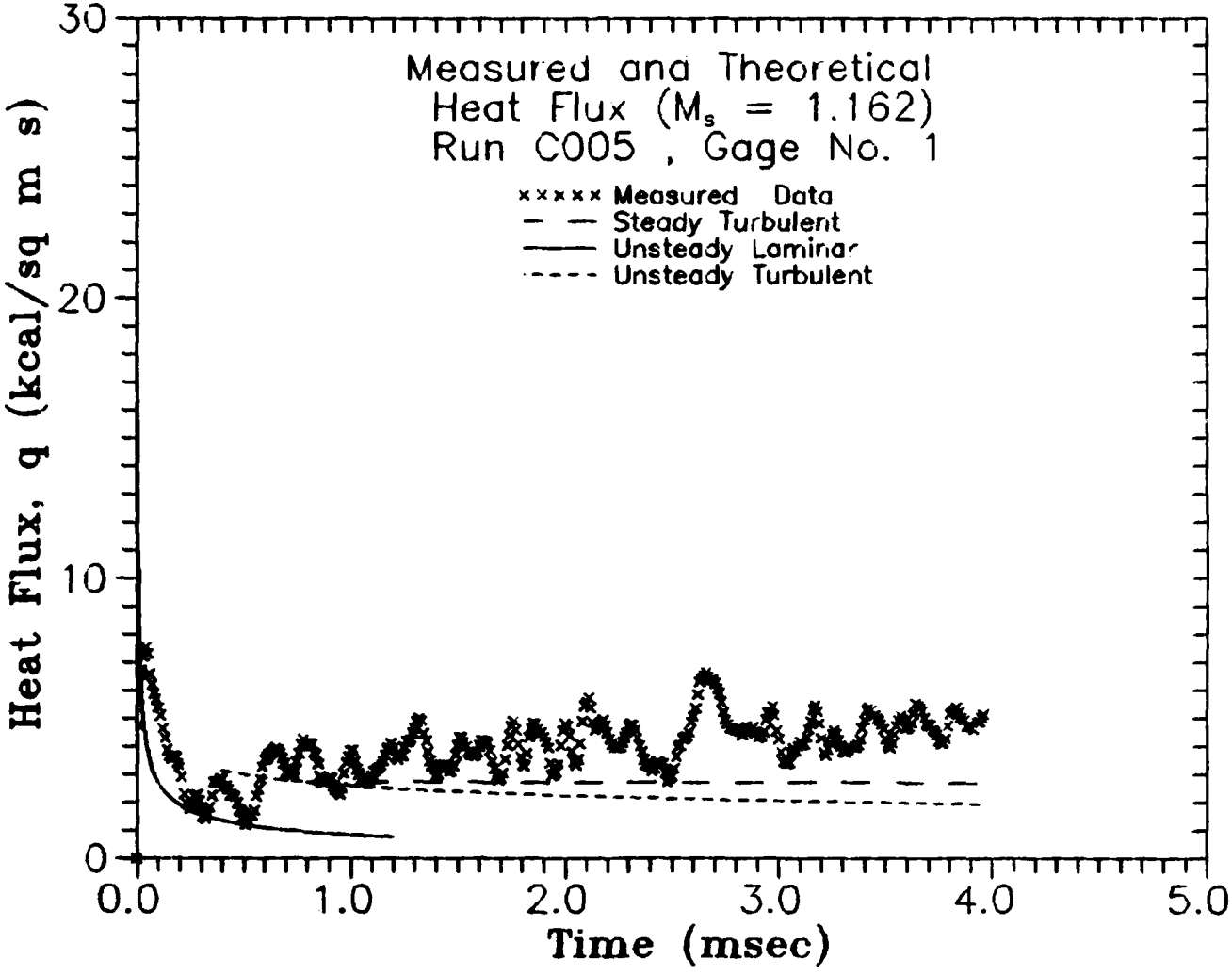

Figure 19 : Heat Transfer, Run C005-1

for q versus time (over 150 of these plots were made) showed a transition to steady turbulent flow no later than 0.9 milliseconds after shock passage. This occurred regardless of shock speed, and generally took less time as the distance from the leading edge increased. It is interesting to note that this corresponds to an α of approximately 4.53 for the low speed flows, and 2.81 for high speeds at gage number one.

The heat transfer plots for flows induced by the higher shock speeds do not show the same characteristics as the low speed plots. Figure 20 shows one such plot for M_s = 1.312. The significant deviation from the theoretical predictions is much greater than the plot of Figure 19. In Figure 19, after 0.9 milliseconds, the mean heat flux is approximately 20 percent greater than the theoretical predictions. In Figure 20 the same comparison shows a deviation of approximately 50 percent from the steady turbulent heat flux prediction. This suggests that something is amiss. Until the picture in Figure 21 was taken, it was thought that the difference was somehow due only to high free stream turbulence. Figure 21 contains a schlieren photograph of one of the causes of this anomaly. This observation is only probable because the entire surface of the plate was not visible through the optical glass portion of the shock tube. Only gage location number seven was visible through the glass, so a picture of the

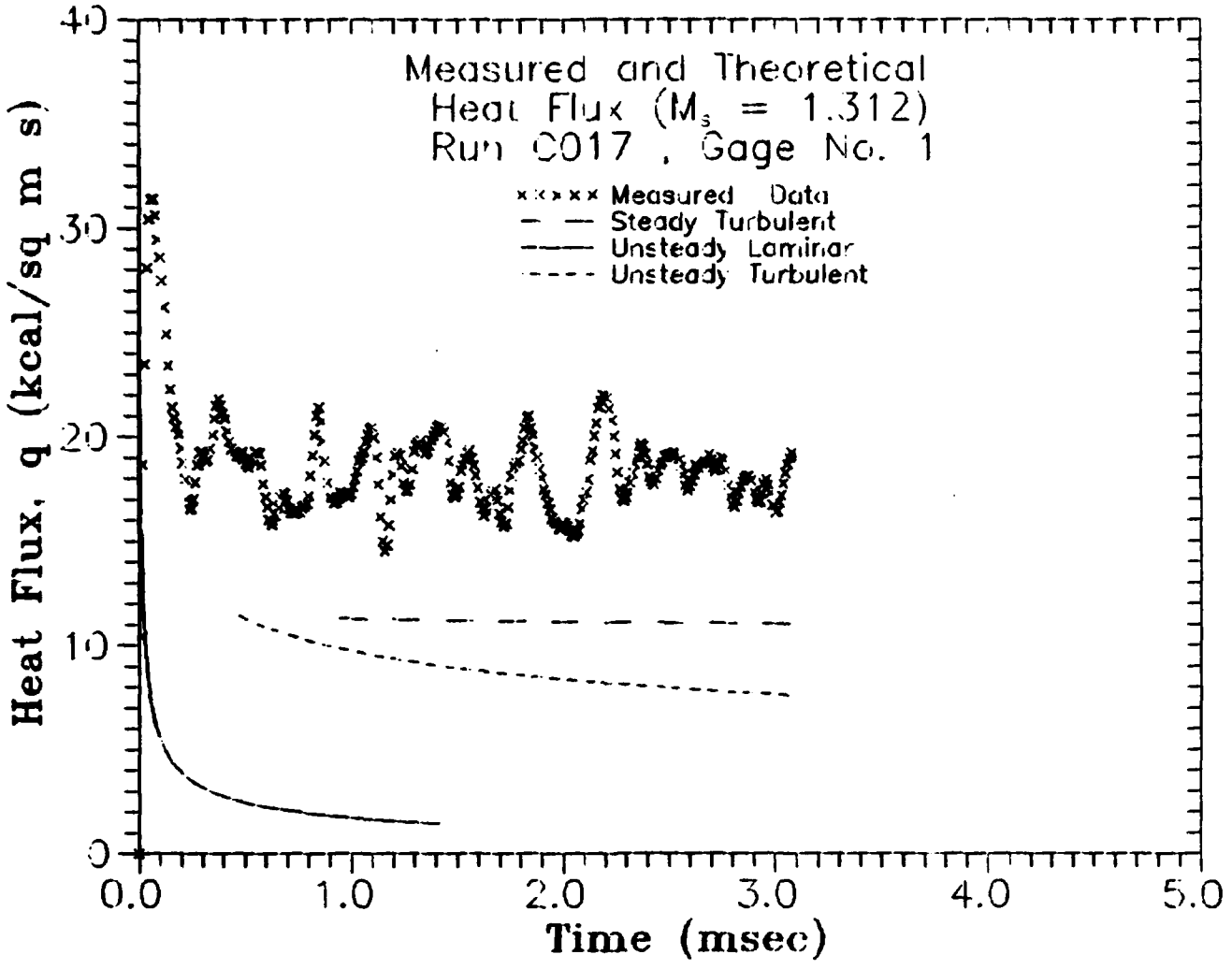

Figure 20 : Heat Transfer, Run C017-1

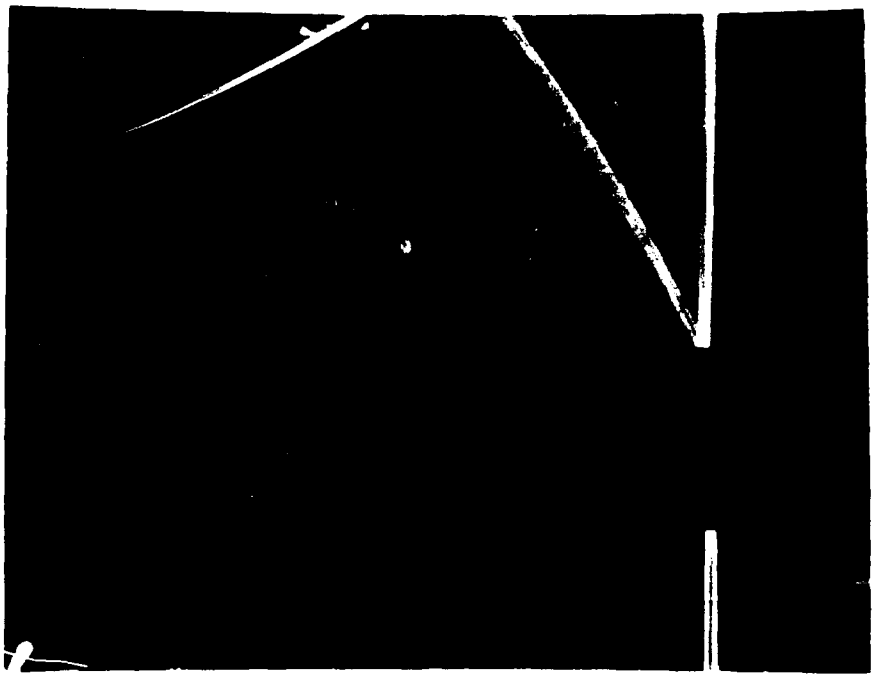

Figure 21 : Reflected Shock, P_4 = 100 in Hg, 3 msec from Pressure Transducer, or, at x = 49.6 inches

entire flow field was not possible. Figure 21 shows the incident shock approximately three inches downstream of gage number seven and a reflected shock in the upper left hand corner. The reflected shock is the object of concern. A reflected shock of the strength shown in the photo ($M_s \cong$ 1.3) could account for some of the difference between the theoretical and measured values of heat flux obtained in Figures 19 and 20, and it would significantly reduce the test time available in region 2. The slight curvature of the reflected shock, and its reduction in thickness from right to left, show that it is reflected from the rounded

leading edge of the plate. This observation was made by considering the interior of the shock tube, and the complete absence of any geometry other than right angles. A shock reflected from a rounded leading edge would exhibit these characteristics. As the reflection propagates out from the leading edge in the shape of an arc, its apex thins and loses some of its original strength. However, as the shock is reflected from the flat wall of the shock tube, the apex is reflected first, then the rest of the arc follows, to repeat the same process. This phenomenon is analogous to the way waves in still water reflect from a stationary surface. If an object is dropped into the water, waves radiate outward from the center of the disturbance, and lose their strength as the radius increases. However, if the waves are reflected by a flat stationary surface they reflect back with their original strength, minus any viscous dissipation encountered. Of course the reflected wave also loses strength as it radiates outward. It should be noted that this is a reproducible phenomenon.

With this taken into account, and the relatively high level of background free stream turbulence, 10 percent, the heat transfer results are not surprising. The increase in the heat flux between the plots of figures 19 and 20 is due to the increase in the Mach number of the incident shock, and the large background free stream turbulence. As the

Mach number increases the reflected shock strength increases, causing the temperature of the flow to increase. Since the theoretical equations are highly dependent on the Mach number of the incident shock, and cannot account for high free stream turbulence or reflected shocks, they do not accurately predict the actual heat flux under these conditions.

Several plots of the heat flux at various gage locations exhibited a sudden rise that was observed in previous studies that used this same facility (Novak, 1987; Smith, 1986). The rise generally produced an increase in the heat flux of approximately 200 to 500 percent, depending on the shock speed, within several tenths of a millisecond. The high background free stream turbulence cannot account for increases of this magnitude, but the reflected shocks could be causing these anomalies. Several examples are shown in Figures 22 through 26, each plot clearly shows the sudden rise in the heat flux.

Barring the observations of high turbulence levels, and reflected shocks, Equations (2-18) predicted the measured heat flux along the plate with good agreement, at low Mach numbers (therefore, low strength reflections) at all but gage location one. Since the accuracy of the predictions increased as the distance from the leading edge increased for all heat flux plots, regardless of shock Mach number, the decay of free stream turbulence as an

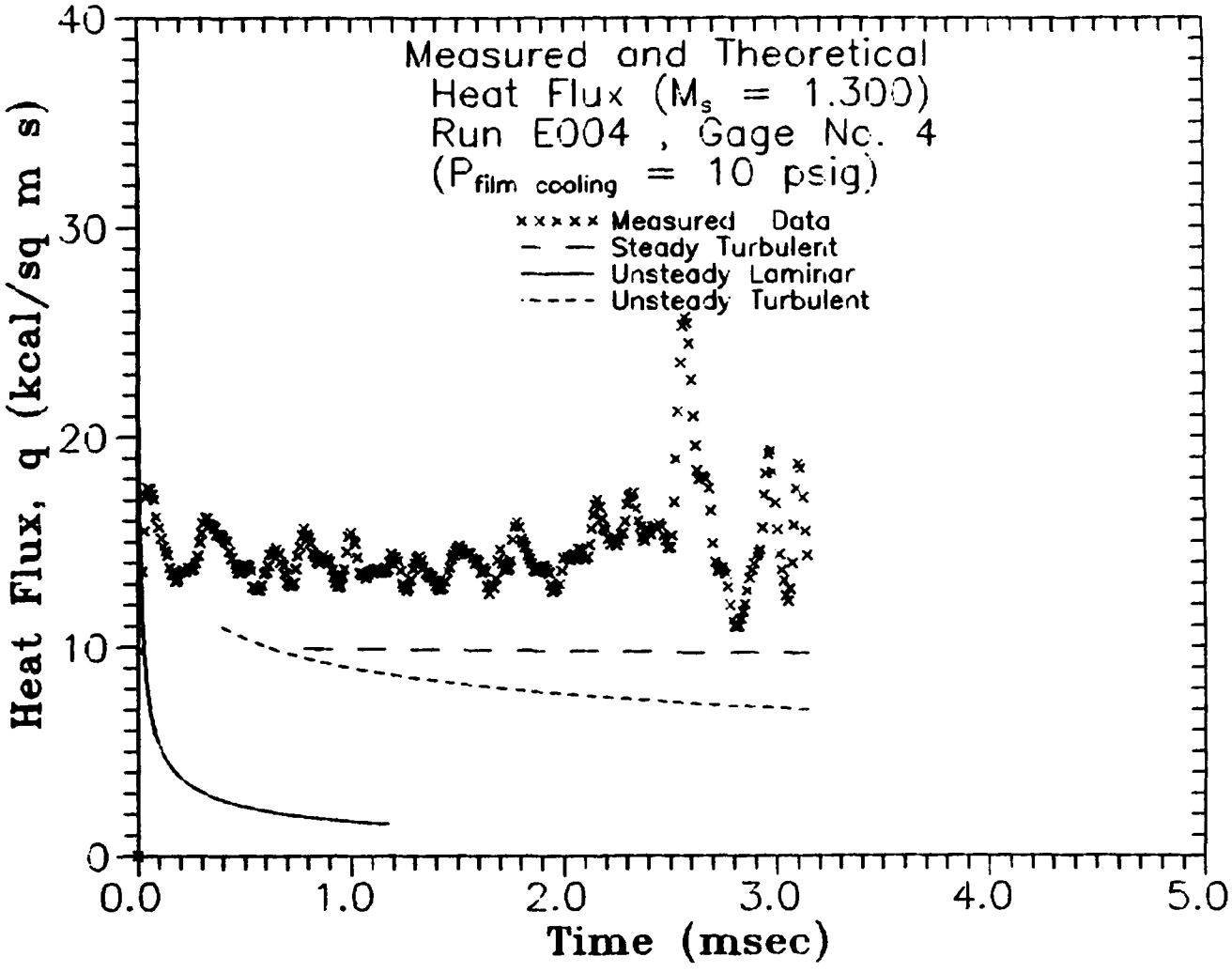

Figure 22 : Heat Transfer, Run E004-4

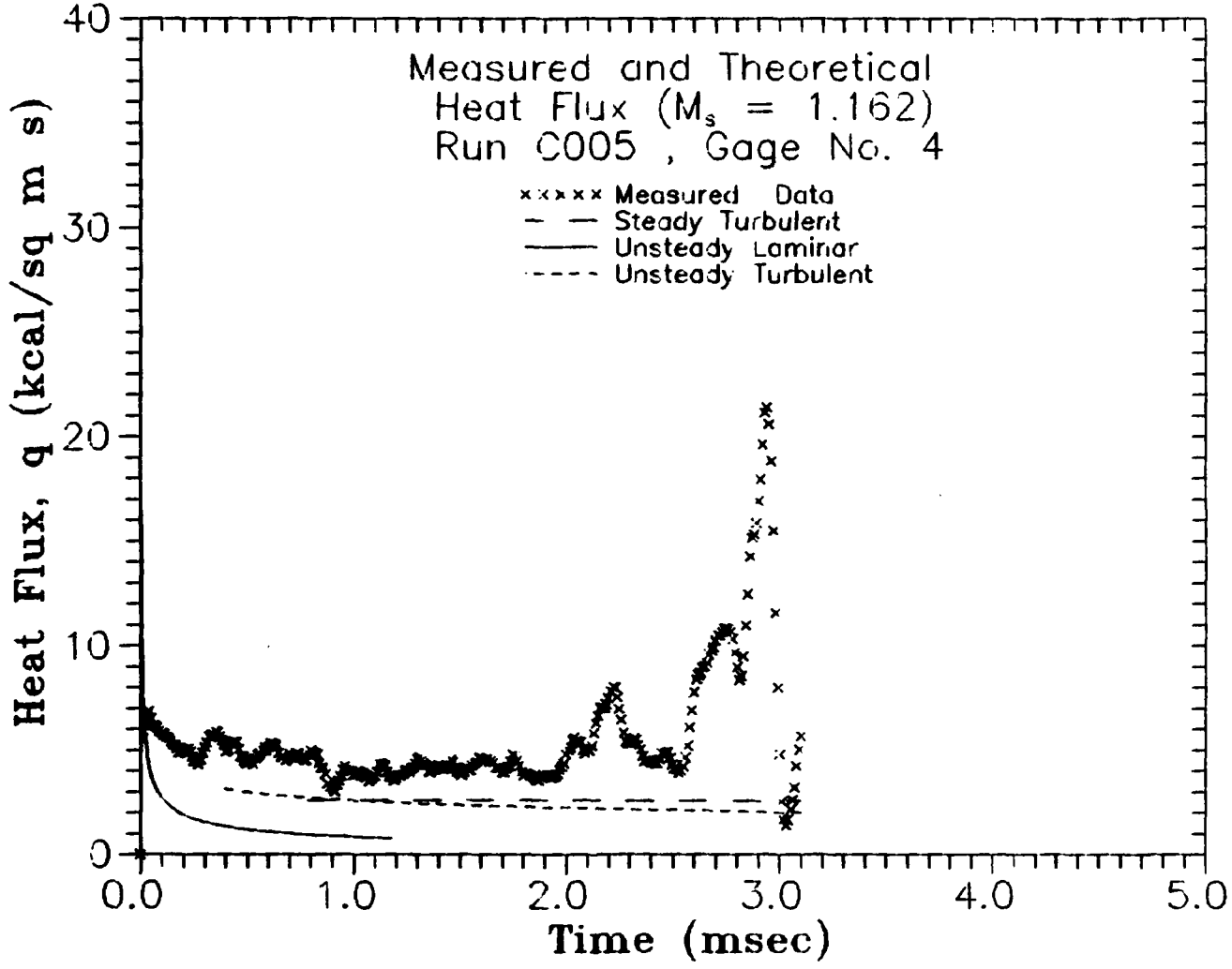

Figure 23 : Heat Transfer, Run C005-4

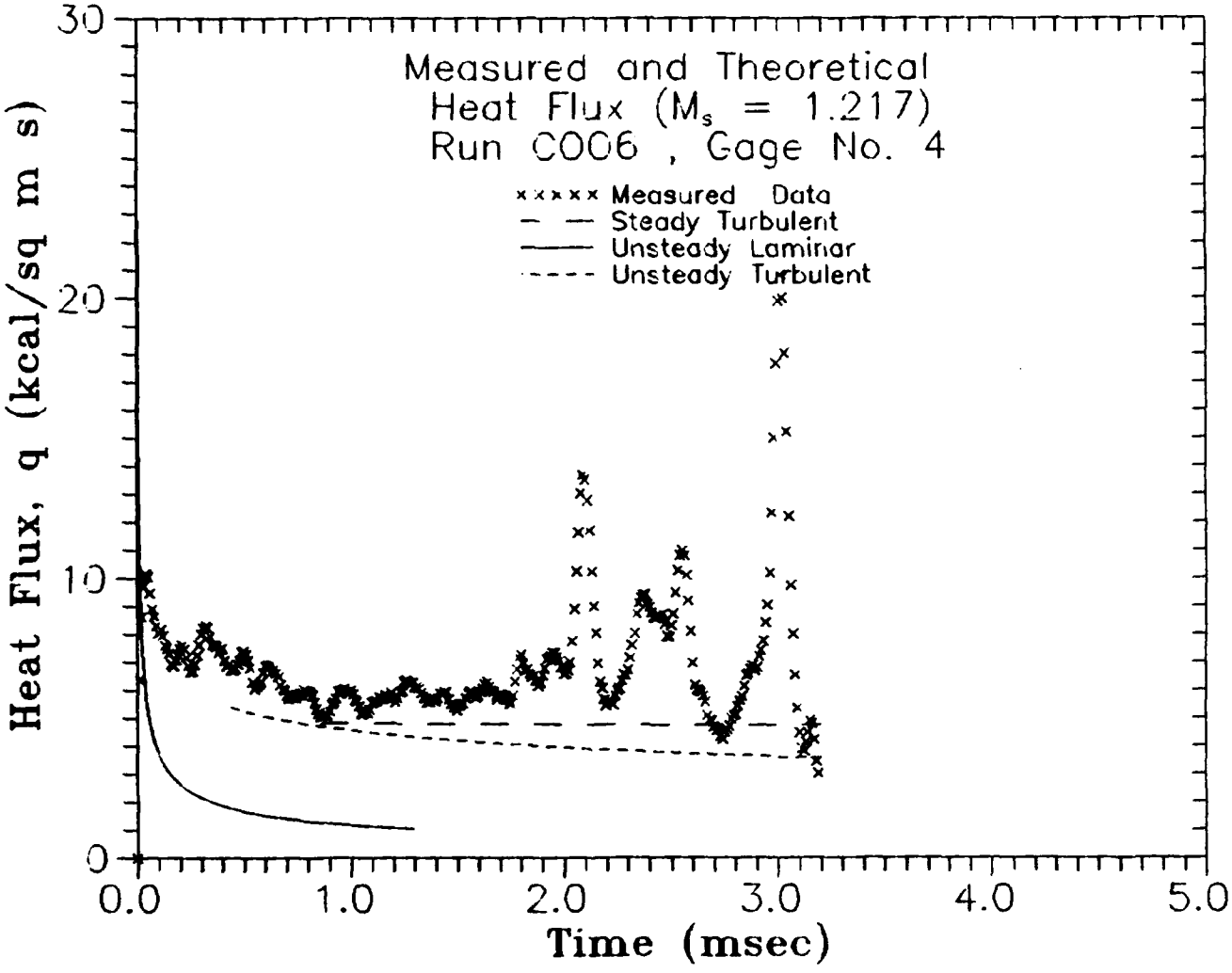

Figure 24 : Heat Transfer, Run C006-4

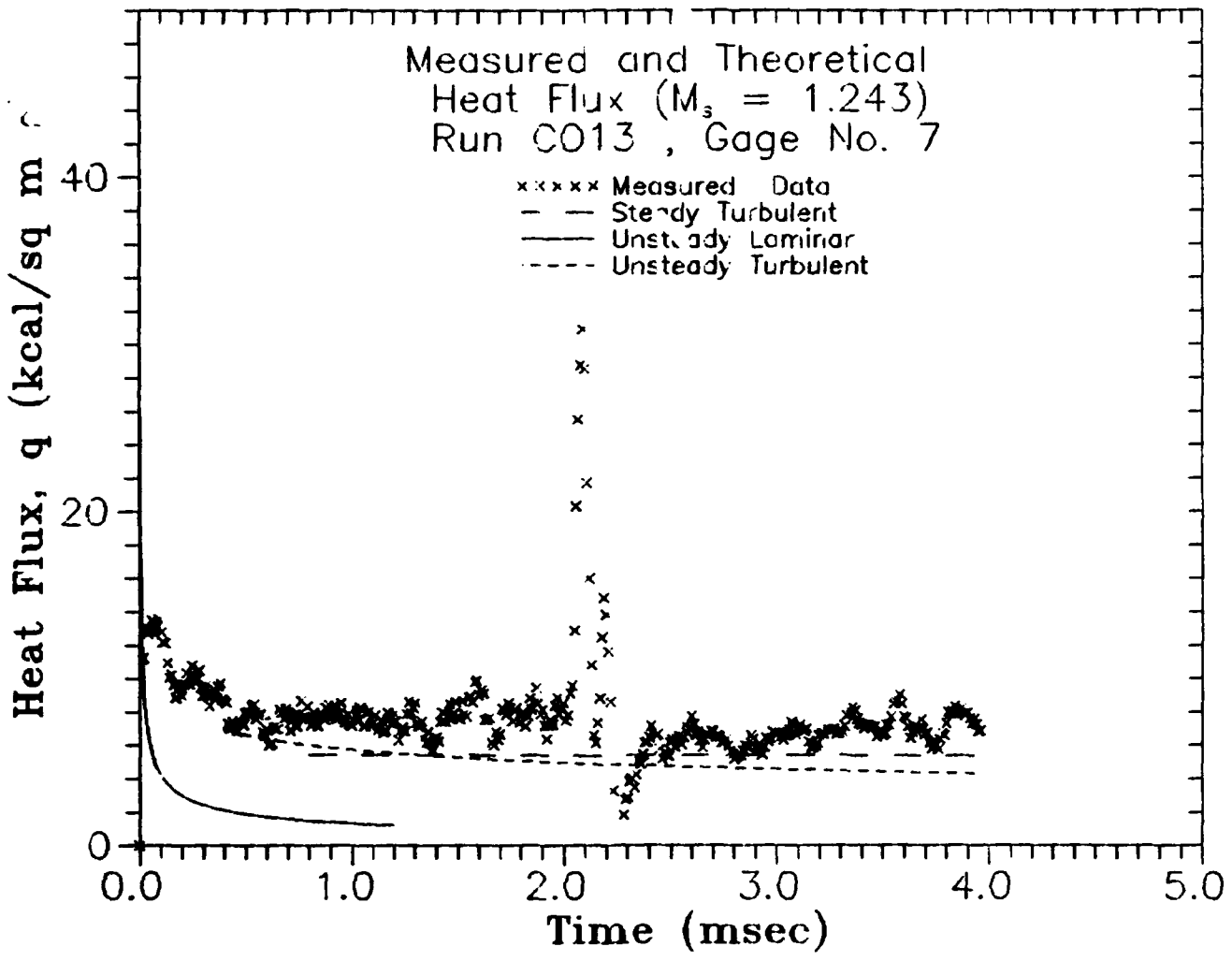

Figure 25 : Heat Transfer, Run C013-7

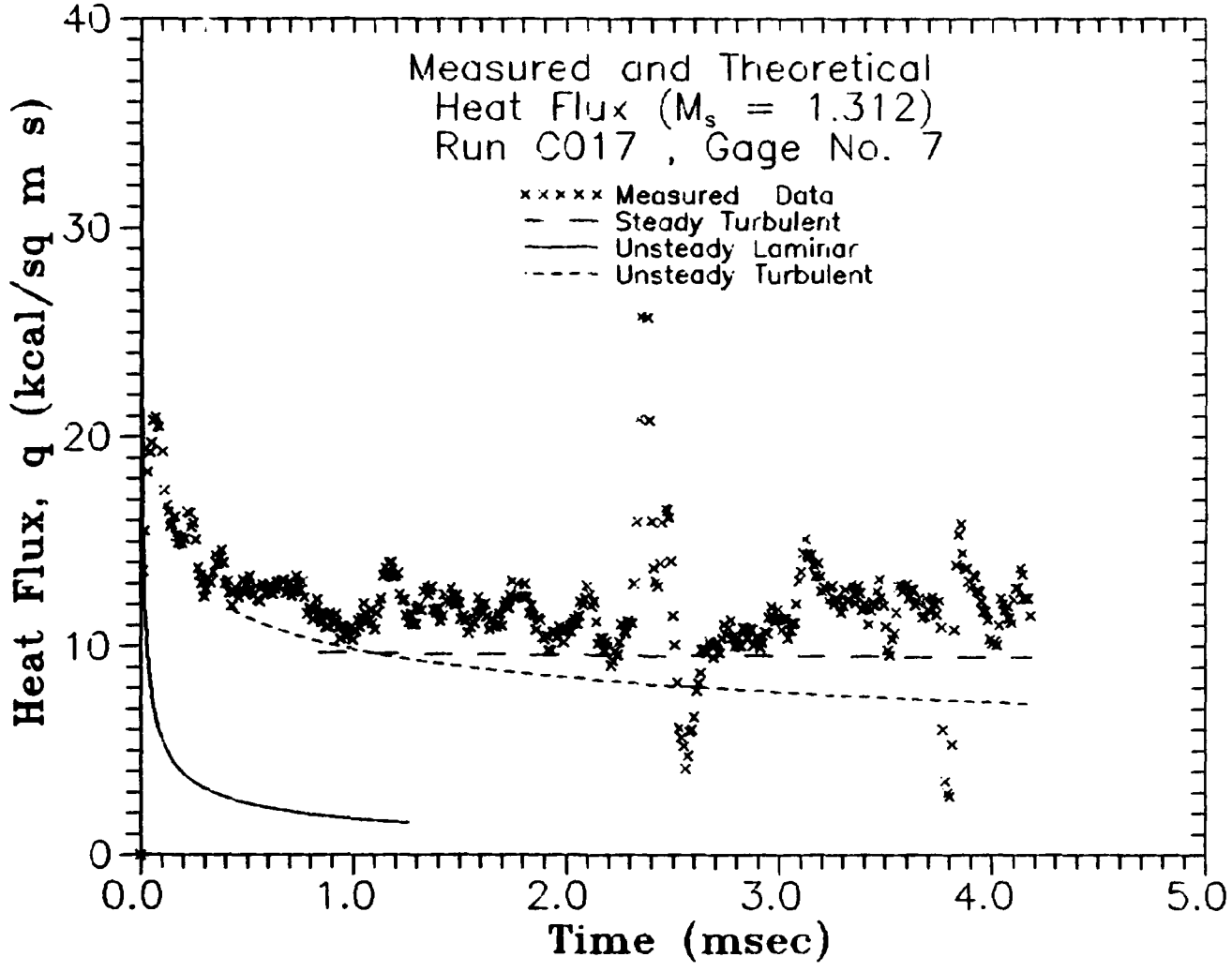

Figure 26 : Heat Transfer, Run C017-7

influential factor is indicated. The increasing inability of the theoretical equations to accurately predict the heat flux at gage location one as the shock Mach number increased confirms this. Other gage locations show a much better agreement, even at high Mach numbers, such as Figure 28. Figures 27, 28, and 29 show several examples of these plots for a range of Mach numbers and gage locations. They also illustrate the rapid onset of turbulent flow conditions immediately after the relatively high laminar heat flux associated with the shock passage has subsided. Only the plots of the heat flux at gage location one exhibited a laminar-to-turbulent transition, and this only occurred at low Mach numbers, as depicted in Figure 19,. Figures 27 to 29 show that this turbulent flow is indeed encountered almost immediately after the incident shock passes the gage location because they do not exhibit the typical laminar-to-turbulent transition of Figure 19. They also show that the unsteady turbulent solution can follow this rapid transition from the unsteady laminar heat flux to the steady turbulent heat flux quite well.

Before the results of the film cooling and free stream turbulence portions of this study are examined, one important point must be made. The calculation of the values for h, St, and Nu of equations (26-28) all depend on the calculated value of the heat flux, q. In order to provide a proper comparison between any two calculations of

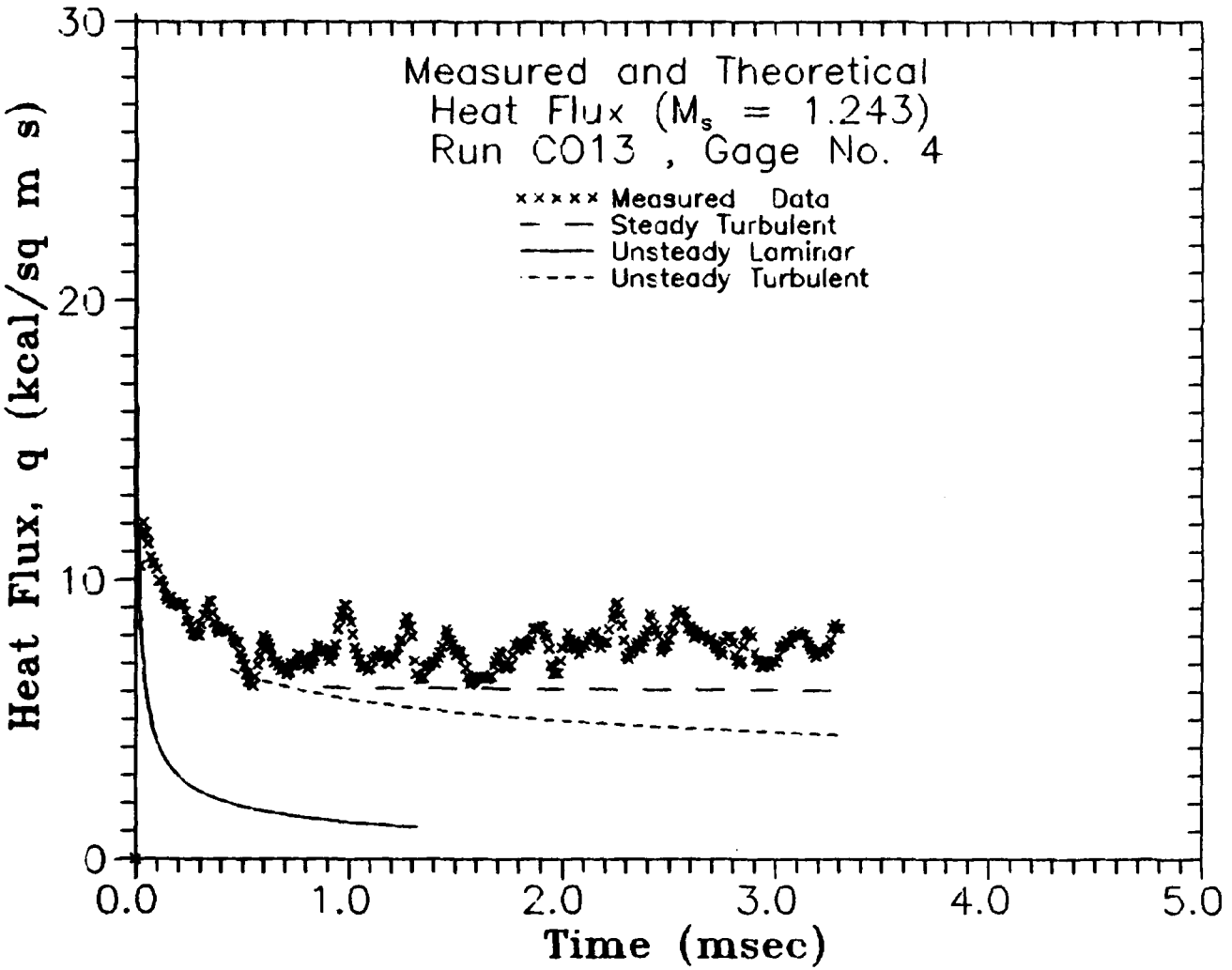

Figure 27 : Heat Transfer, Run C013-4

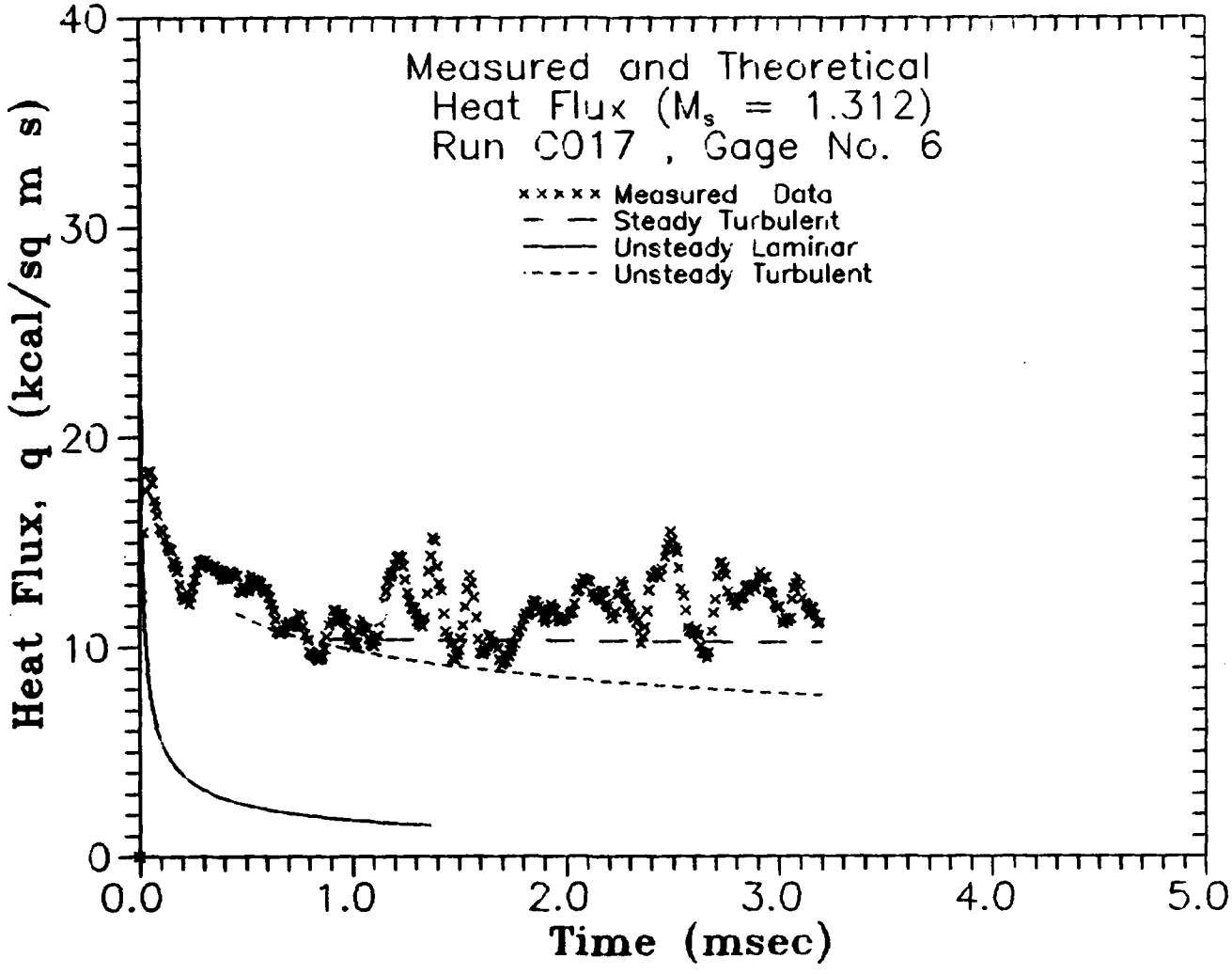

Figure 28 : Heat Transfer, Run C017-6

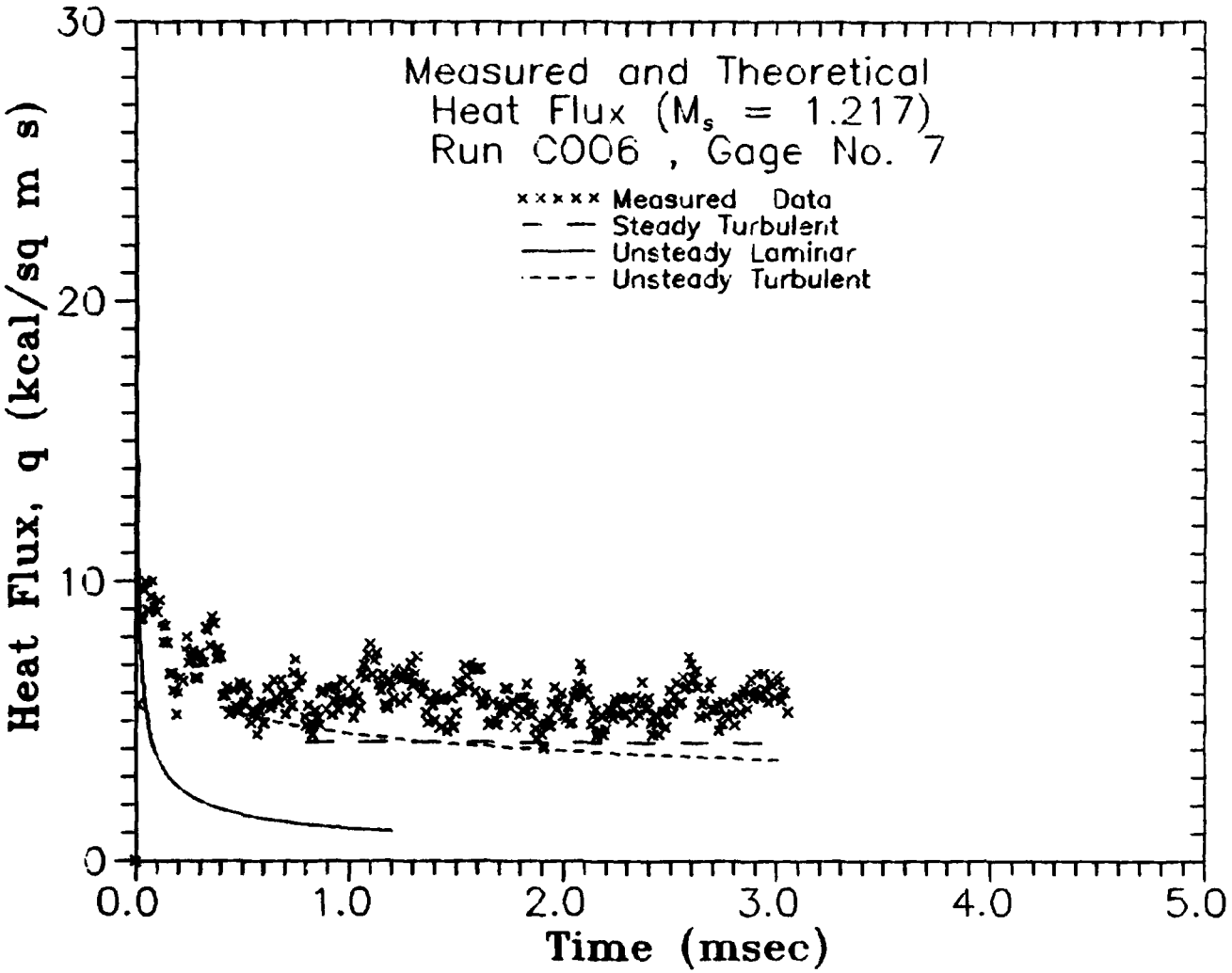

Figure 29 : Heat Transfer, Run C006-7

the heat flux, the mean value was used as the basis of comparison. By observing the plot of each heat flux calculation, the times at which each gage exhibited a steady flow pattern could be discerned. These times were used as the input to a program, RMS.FOR, which calculated the mean value for q from the results of the program AVHEAT.FOR. Again, all programs used in this investigation are included in Appendix B along with a brief description. The mean heat flux was then used as an input to another program, STANT.FOR, that calculated the values for h, St, and Nu based on the mean heat flux. This provided the same treatment for all data, and eliminated the unwanted influence of large heat flux gradients that Figures 22 through 26 portray.

Heat Transfer With Film Cooling

The use of the film cooling system to obtain useful results is not without its problems. If the film cooling flow is initiated after the shock passes, it may not become fully entrained in the boundary layer behind the shock, and may cause the boundary layer to lift-off the plate. If the film cooling flow does lift-off the boundary layer, the hot mainstream gases come in direct contact with the plate, and invalidate the film cooling process (Goldstein, 1971). On

the other hand, if the flow is initiated too early the ambient shock tube pressure, P_1, may be changed. This may result in changing the shock speed that is being duplicated in the data run.

To illustrate this point, the graph of Figure 14 is referred to. It was stated in Chapter II that the shock is formed by pressure wavelets moving out into a gas of increasing sonic speed, where they quickly coalesce to form a moving shock wave (Shapiro, 1987). But if the activation of the cooling flow is started too early, the resulting increase in the ambient pressure level may not allow the wavelets to coalesce at a uniform rate. They may instead coalesce at a different rate, and a single shock may not be formed before the test section. The pressure transducer plot of Figure 14 shows that the wavelets may not yet have formed into one coherent shock because there is more than one pressure "spike" visible on the plots for both transducers. The initial shock passage normally produces one spike which clearly indicates its passage over the pressure transducer. Also, the output of pressure transducer two seems to be affected by the shock reflections, mentioned previously, from five milliseconds until the end of the plot at 8.192 milliseconds. This observation eliminated many data runs from consideration in this portion of the study, and was guarded against by observing the plot of the pressure transducers for each

data run. Fortunately this only occurred at relatively low shock speeds. In Chapter IV it was mentioned that only certain size diaphragms were used in an attempt to consistently produce the same shock wave patterns. The size of the diaphragm, along with the way the diaphragm ruptures may also be connected with the manner in which the shock wave forms.

The blowing ratios used in this study are much higher than those typically used in film cooling studies. This is because the film cooling flow could not be properly initiated at low blowing rates due to the high pressure effects produced by the shock wave passing over the film cooling holes.

Various parameters were plotted against the ratio of the heat transfer coefficients for the film cooled versus uncooled case, in an attempt to determine their influence. Ammari's correlation of Equation (19) was also used for comparison to measured results (Ammari, 1989). The first attempt at correlating the results used the dimensionless downstream distance x/D, and the blowing ratio M, in the form used by Ammari,

$$(x/D)M^{-1/2} \qquad (30)$$

The plots of Figures 30 through 33 show the influence of the film cooling pressure supply on the measured heat transfer coefficient ratios by plotting the results

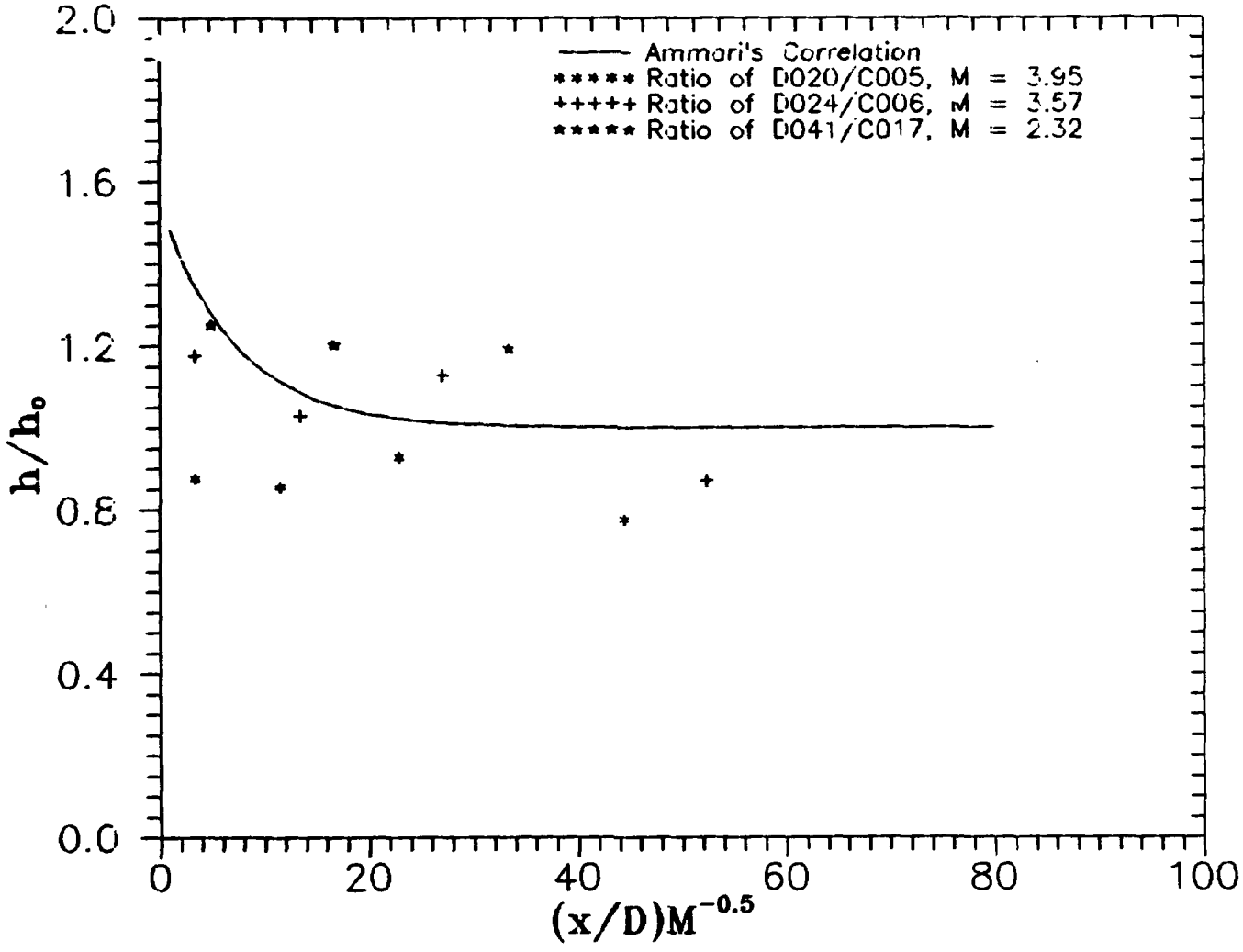

Figure 30 : Ratio of Heat Transfer Coefficients, D/C1

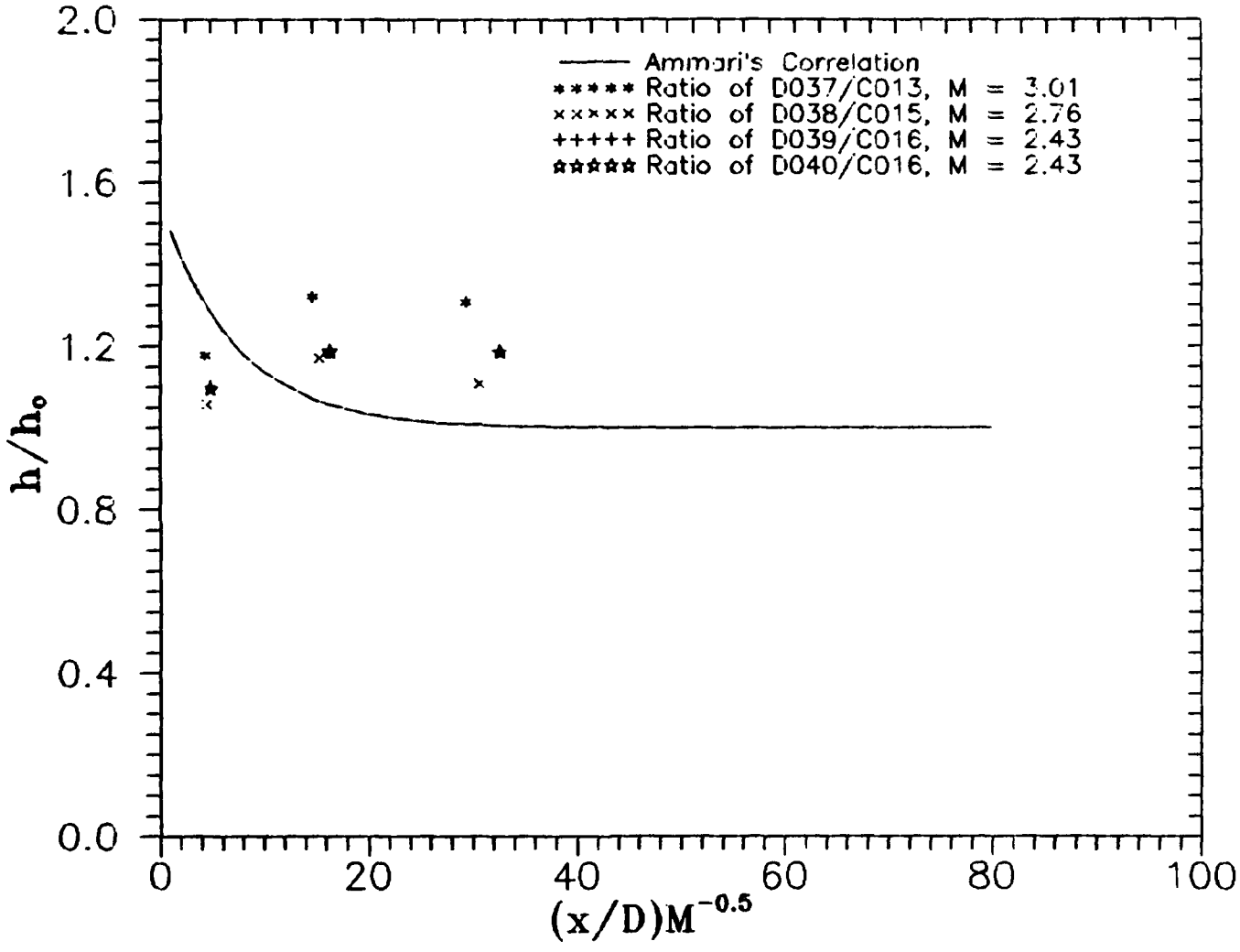

Figure 31 : Ratio of Heat Transfer Coefficients, D/C2

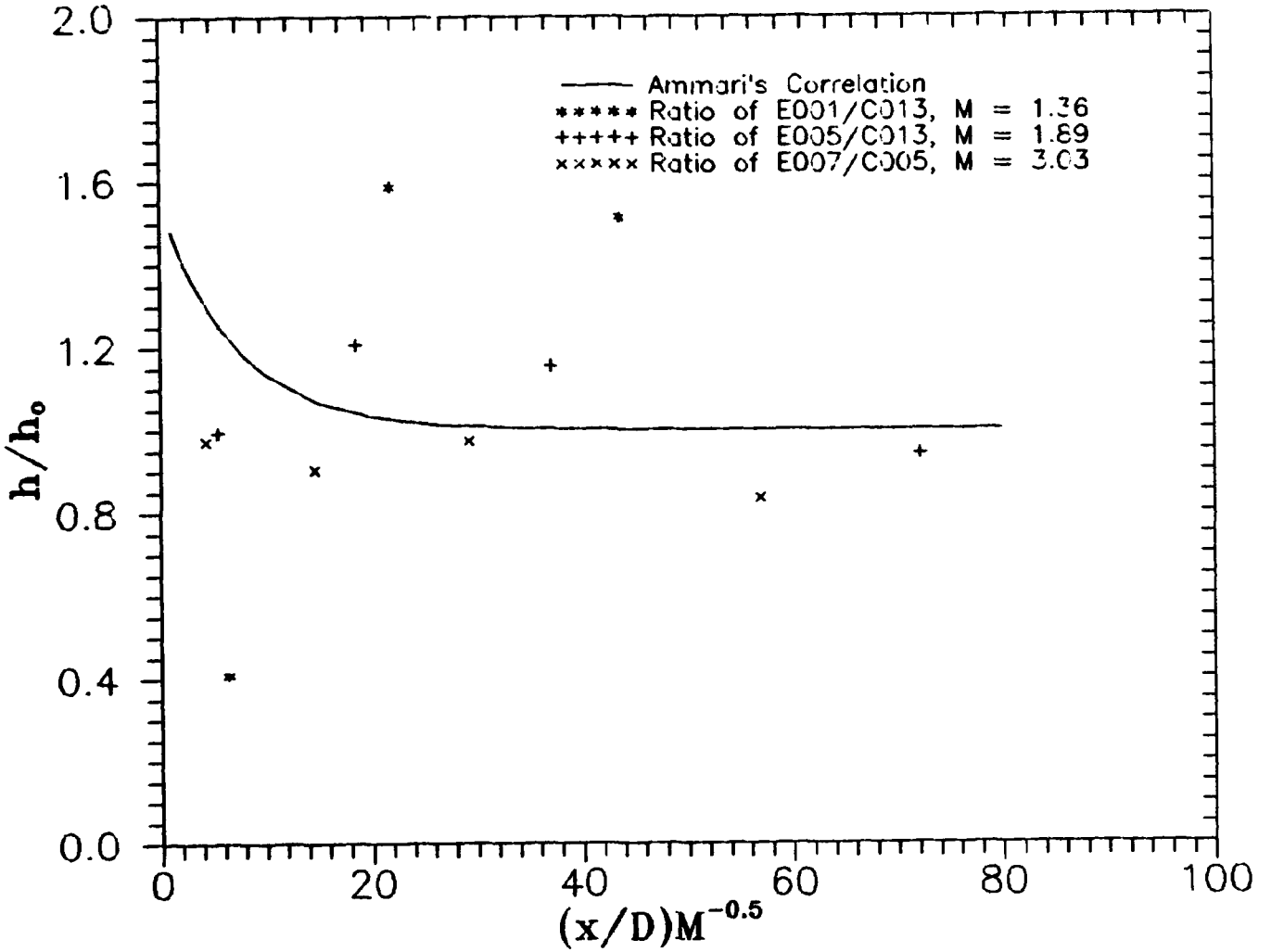

Figure 32 : Ratio of Heat Transfer Coefficients, E/C

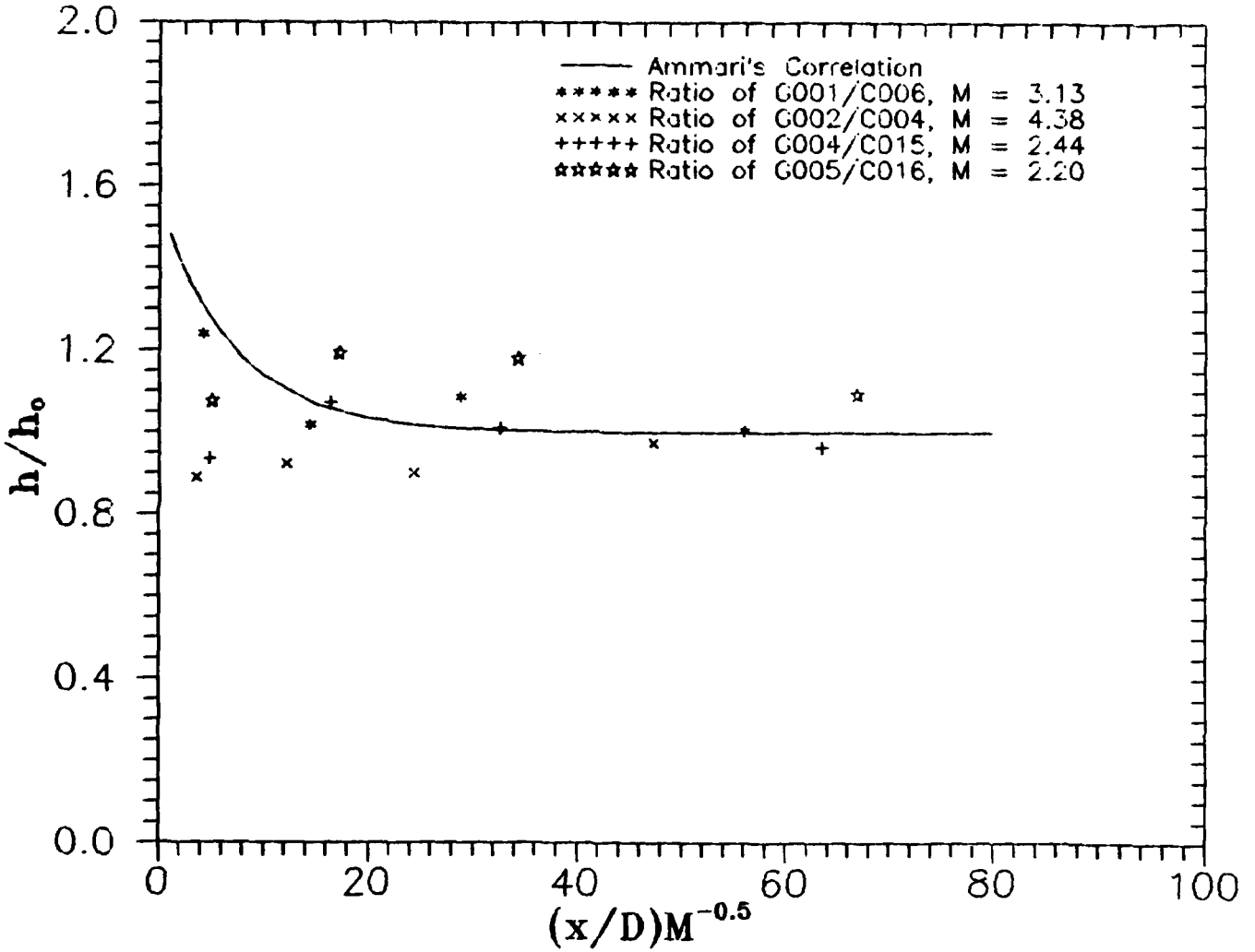

Figure 33 : Ratio of Heat Transfer Coefficients, G/C

obtained at different supply pressures. In Figures 30 and 31 the supply pressure is 25 psig, in Figure 32 it is at 10 psig, and in Figure 33 it is at 20 psig. Figure 32 shows considerable scatter, even though two of the data run comparisons have similar blowing parameters. The ratio of E007/C005 provides the closest approach to Equation 19, even though M is out of the range of Ammari's correlation. This suggests that the correlation can be extended. Figure 30 contains ratios of heat tranfer coefficients with a higher value of M, and shows that the higher values of M produce ratios greater than one, which confirms the reports of Goldstein (Goldstein, 1971). Figures 31 and 33 are contradictory; their comparisons contain a range of values for M but also exhibit the best overall comparison. This is especially true at the larger values of Equation (30). This suggested that perhaps the dimensionless downstream distance influenced the results, as well as M.

The comparisons of Figures 34 through 37 to Ammari's correlation extended well beyond Ammari's intended range of $x/D < 25$. Figure 34 clearly indicates no influence on the ratios of heat transfer coefficients for $x/D = 7.5$, as Figures 30 to 33 may have implied by plotting Equation (30) as the abscissa. Figure 35 does indicate a trend however, by showing that as the value of M increases, these ratios decrease. Figures 36 and 37 also indicate this trend, but show the data collapse towards one as the value of x/D and

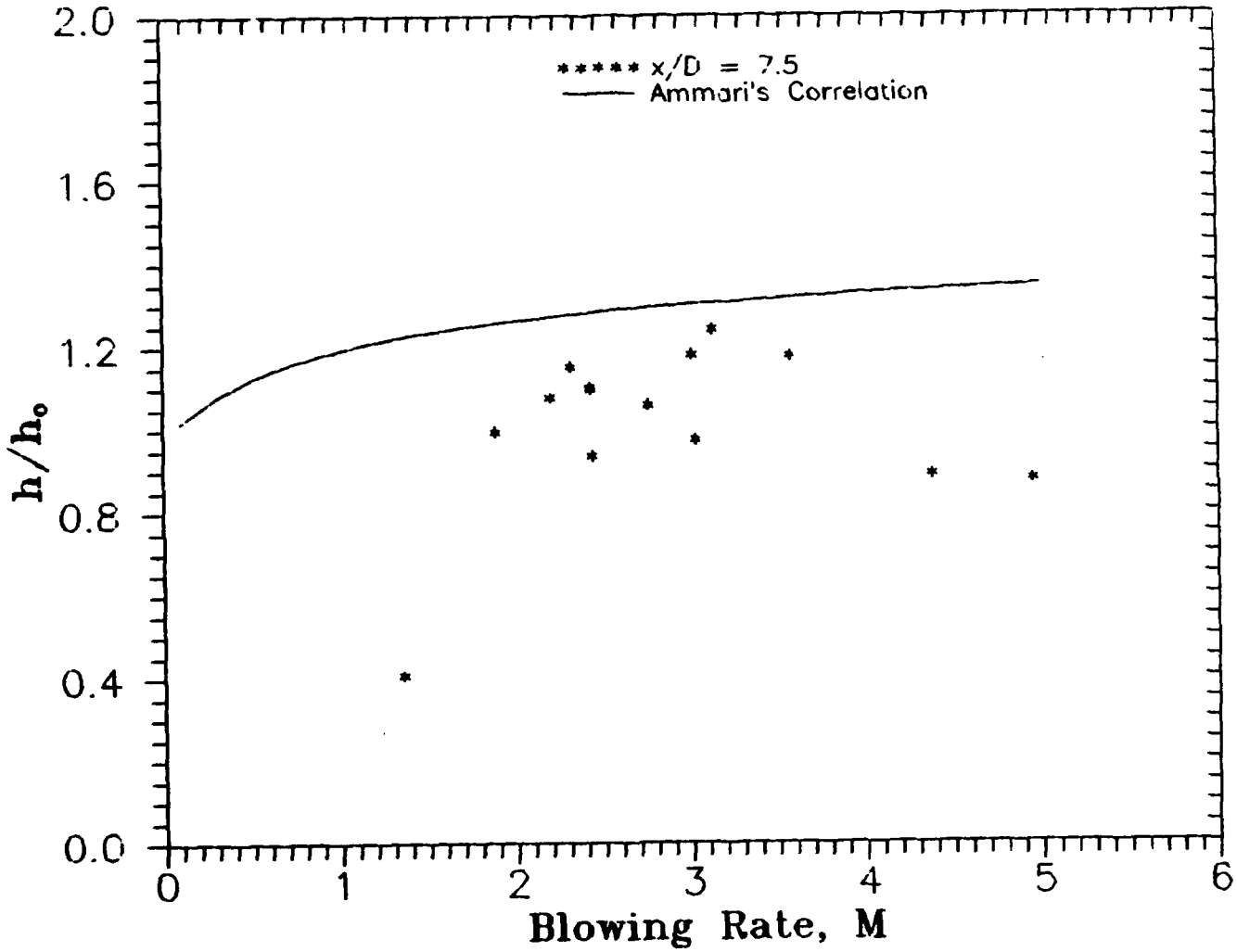

Figure 34 : Ratio of Heat Transfer Coefficients vs Blowing Rate, x/D=7.5

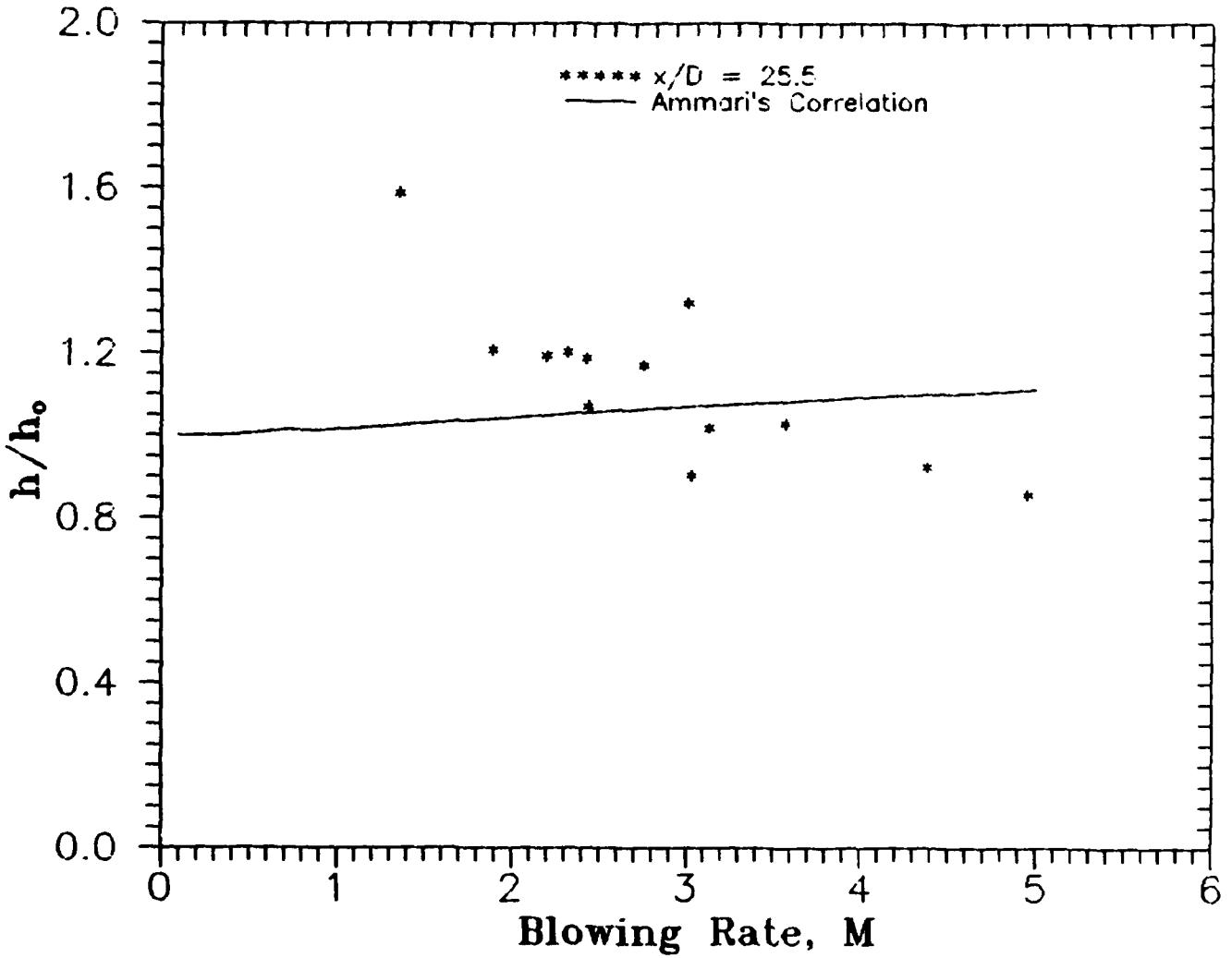

Figure 35 : Ratio of Heat Transfer Coefficients vs Blowing Rate, x/D=25.5

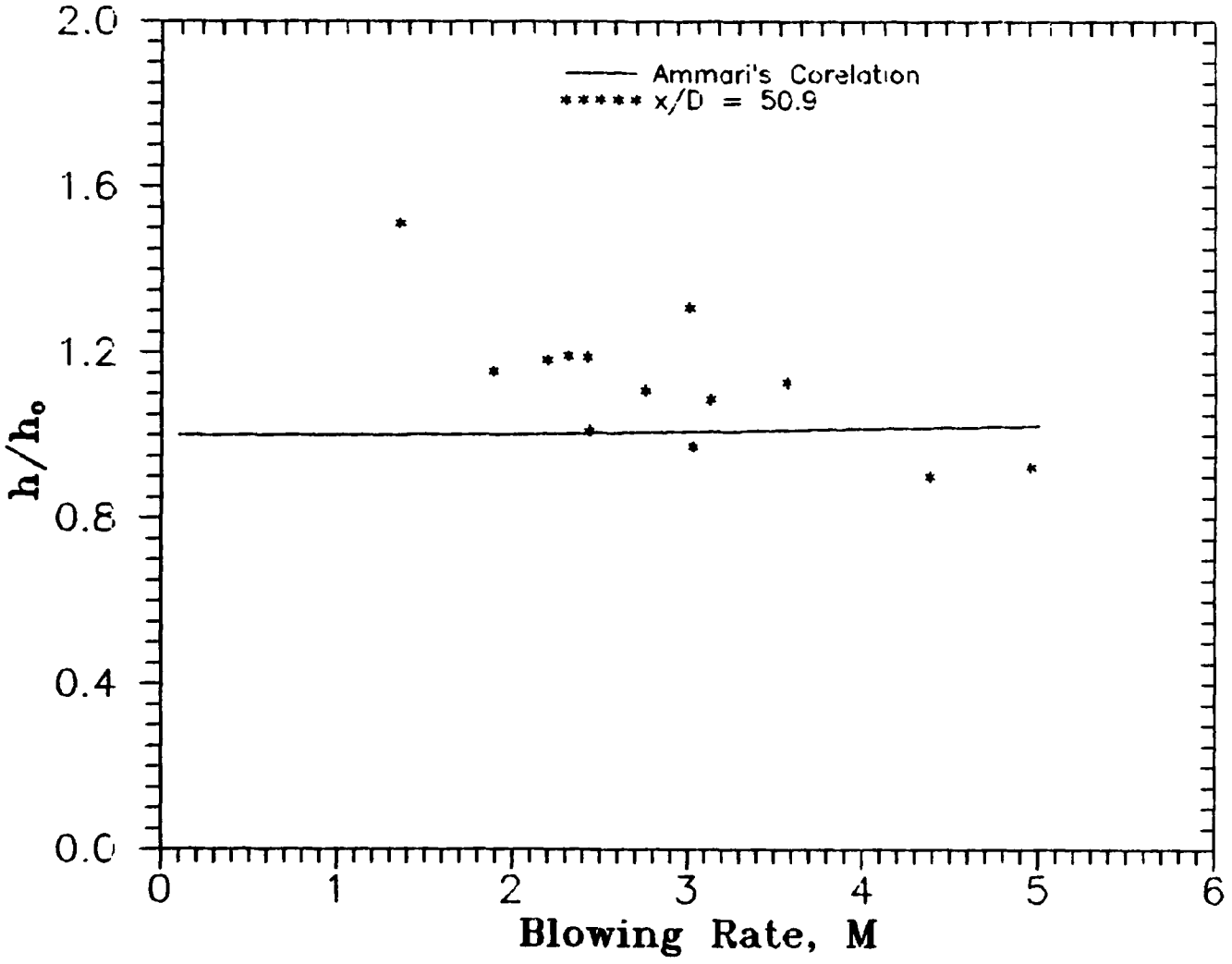

Figure 36 : Ratio of Heat Transfer Coefficients vs Blowing Rate, x/D=25.5

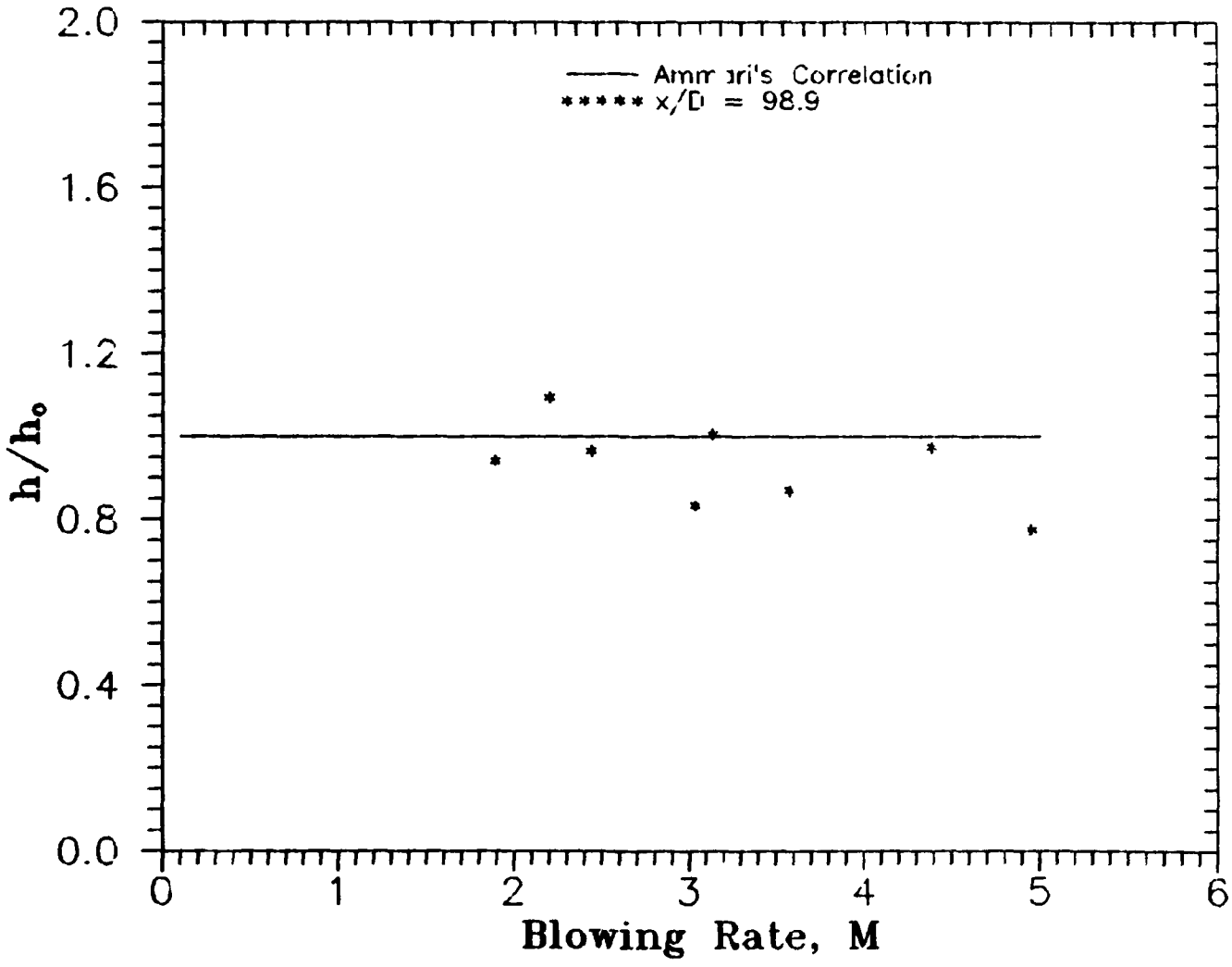

Figure 37 : Ratio of Heat Transfer Coefficients vs Blowing Rate, x/D=98.9

M increases. The trend in these graphs shows the influence of the blowing parameter M, on the effectiveness of film cooling. This confirms the findings of Ammari and Goldstein (Ammari, 1989; Goldstein, 1971).

The influence of M on the ratio of heat transfer coefficients was examined by plotting low, medium, and high values of M. Figures 38, 39, and 40 , respectively, show this influence. Figure 38 contains comparisons with values of M that are within Ammari's correlation, but are considerably scattered. This is contradictory to experimentally verified results that normal injection is most effective when $M \cong 1$ (Goldstein, 1971:343). The anomaly shown by this figure may be due to the influence of shock reflections, or differing turbulence levels. When the values for M in the range $2 < M < 3$ are plotted in Figure 39, the correlation of the blowing parameter on the ratios becomes clear. Even when Ammari's correlation is extended above $M = 3$ the influence of the blowing ratio is obvious, as Figure 40 indicates. Figure 41 was plotted to confirm previous observations that large values of M decreased the film cooling effectiveness (Goldstein, 1971:360).

These plots confirm previous results of many studies conducted on film cooling heat transfer, even though the range of available data is limited. Goldstein indicates that previous studies have shown that a single row of film

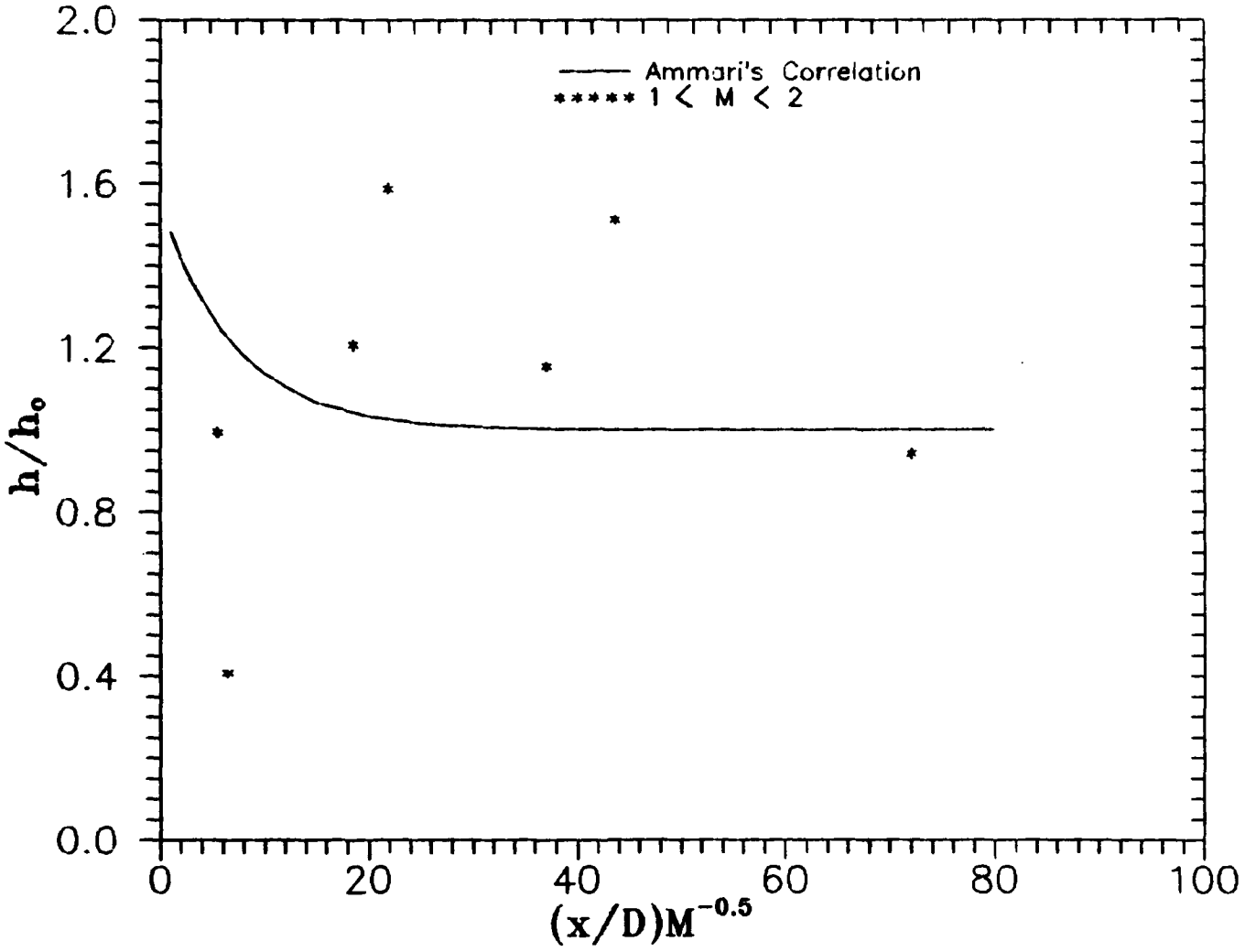

Figure 38 : Ratio of Heat Transfer Coefficients, Low M

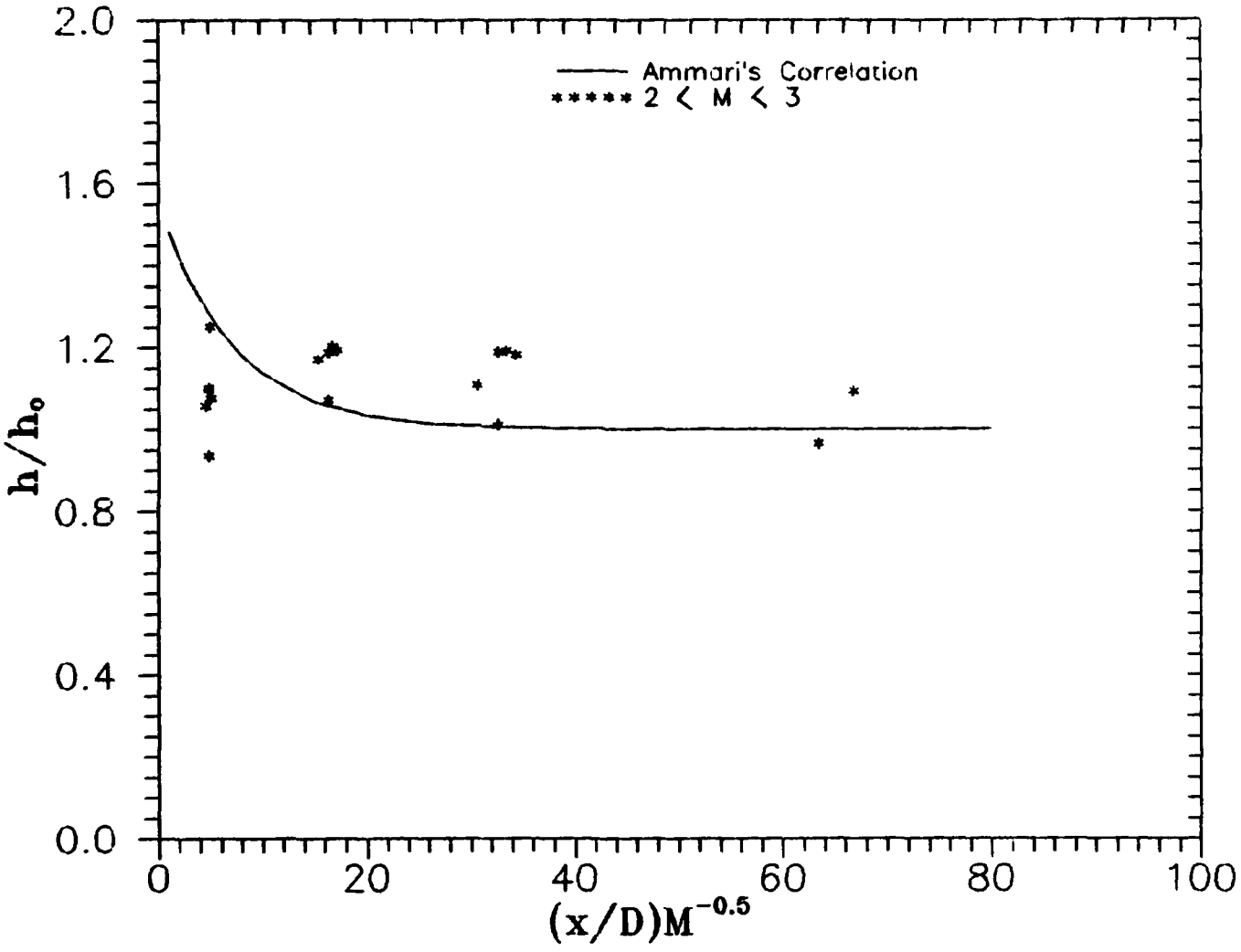

Figure 39 : Ratio of Heat Transfer Coefficients, Med M

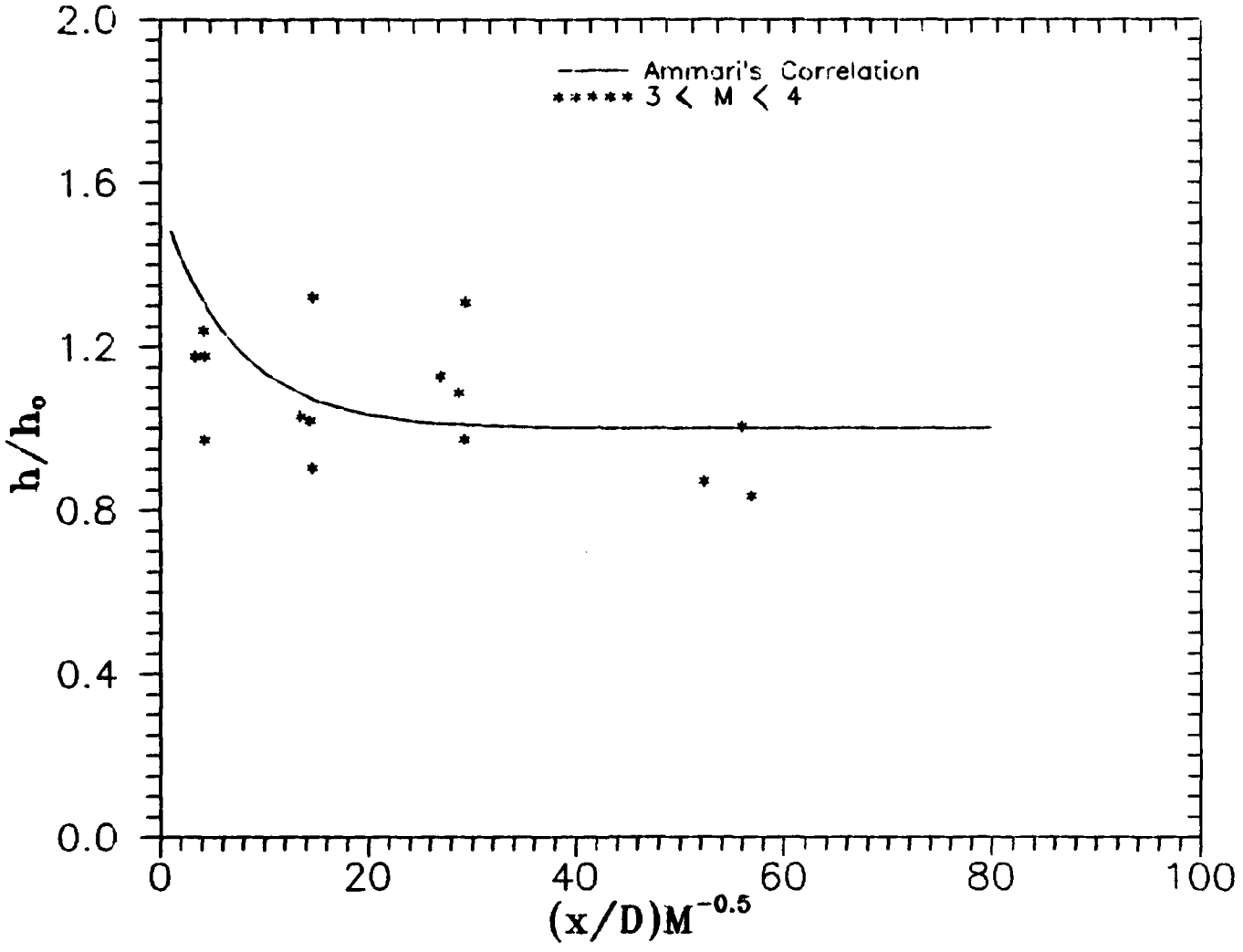

Figure 40 : Ratio of Heat Transfer Coefficients, High M

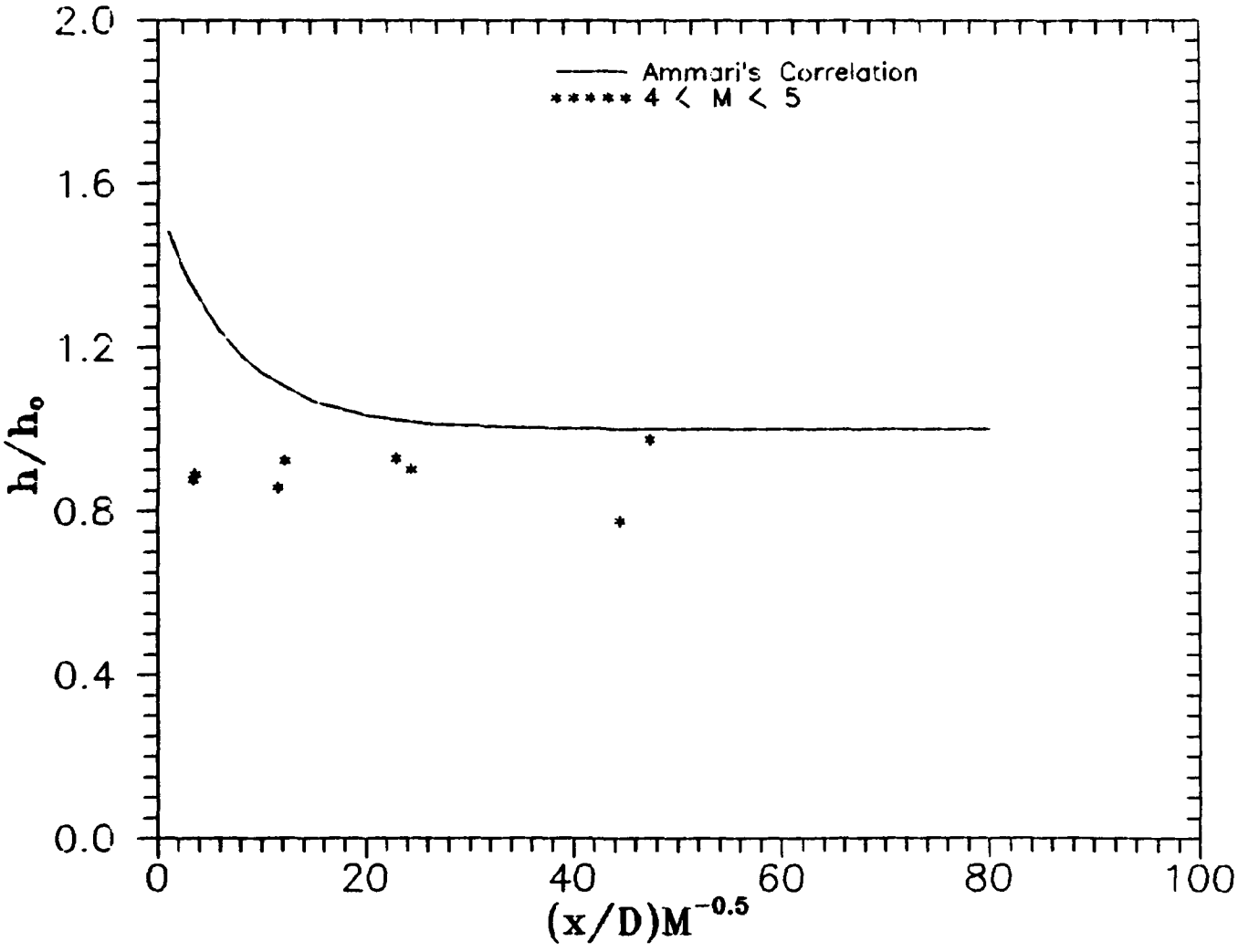

Figure 41 : Ratio of Heat Transfer Coefficients, M > 4

cooling holes tends to be very ineffective in film cooling except for the region immediately downstream of the central region of each hole (Goldstein, 1971:370).

The indications provided by the previous plots show that the correlating parameter is the blowing ratio, M. Figure 42 contains a plot of all the comparisons used here, along with a correlation based upon the results. In determining the correlation, the extraneous point at $h/h_o \cong 0.4$ was excluded. The results as obtained in this study, and as shown in Figure 42, correlate within ± 30 percent to the equation,

$$\frac{h}{h_o} = 1.443 - 0.3516 \ln(M) \qquad (33)$$

for $7.5 < (x/D) < 99$, and $1.36 < M < 4.95$.

Heat Transfer with Free Stream Turbulence

In this portion of the study the results are due, in part, to the experiments of Rockwell as noted earlier. Rockwell found that the background free stream turbulence level in the shock tube is approximately 10 percent. The approximation is because the methods used are only good to within ± 20 percent. He also found that when the driver pressure is brought up to 100 in Hg gage, and a 0.005 inch Mylar diaphragm is used, the turbulence generator will produce a 12 percent free stream turbulence level. This information was used to examine the influence of free

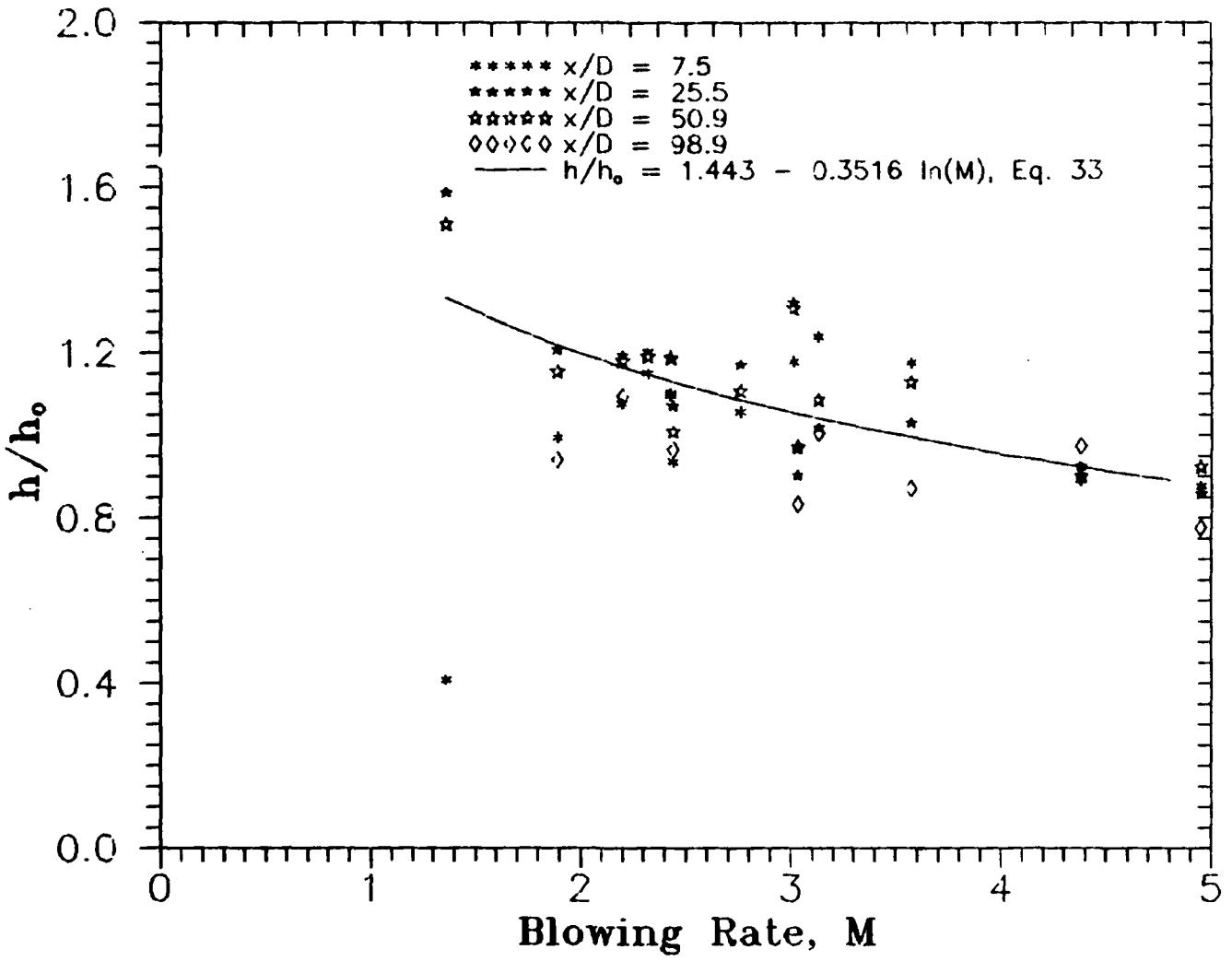

Figure 42 : Correlation of Ratio of Heat Transfer Coefficients vs M

stream turbulence levels on film cooling heat transfer.

The data run series used in this portion of the experiment was the H00x series, and only several data runs were made because there were not many successful runs made at driver pressures of this magnitude. However, useful results were obtained for several values of the film cooling supply pressure.

Equation (22) was the first relationship examined here, and it should be noted that this equation is based upon a Stanton number St_o, obtained at a nominal free stream turbulence level of 0.03 percent (Simonich and Bradshaw, 1978:671-672). The values used in the comparisons of this study have St_o measured at a nominal free stream turbulence level of 10 percent. So liberties are taken when this equation is used directly.

The plots of Figures 43 through 46 graphically illustrate the effect that an increase in the free stream turbulence level has on the rate of heat transfer with film cooling. Even though the ratio of the Stanton numbers, as plotted, are not at the true values of the abscissa Tu, or correctly plotted in relation to Equation (22), they do illustrate the tremendous increase that higher free stream turbulence produces. In all these figures the gage number is indicated on the plot. The effect of an increase in turbulence on the ratio of the Stanton numbers is to increase the Stanton number from its value St_o, by

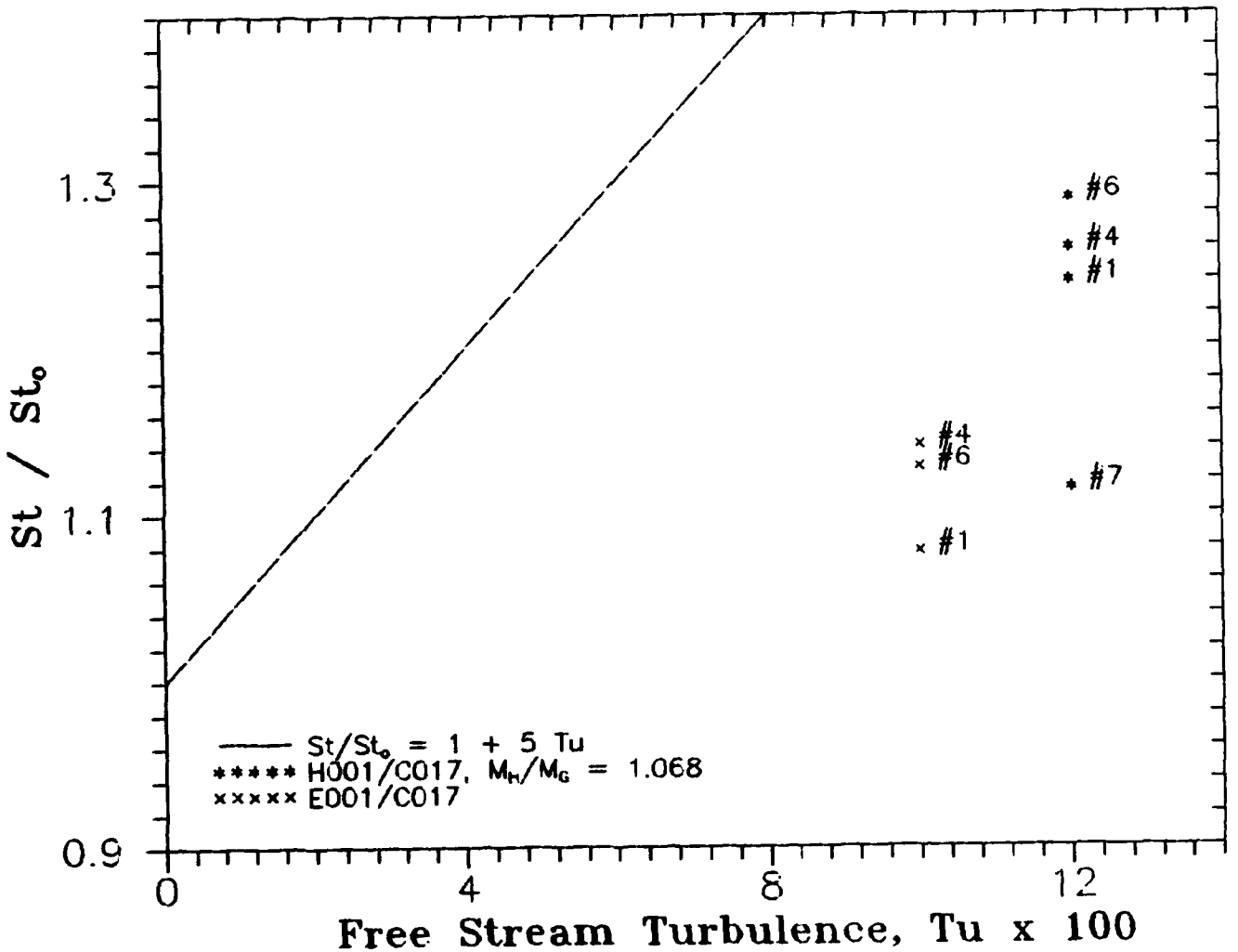

Figure 43 : Free Stream Turbulence Effects,H001

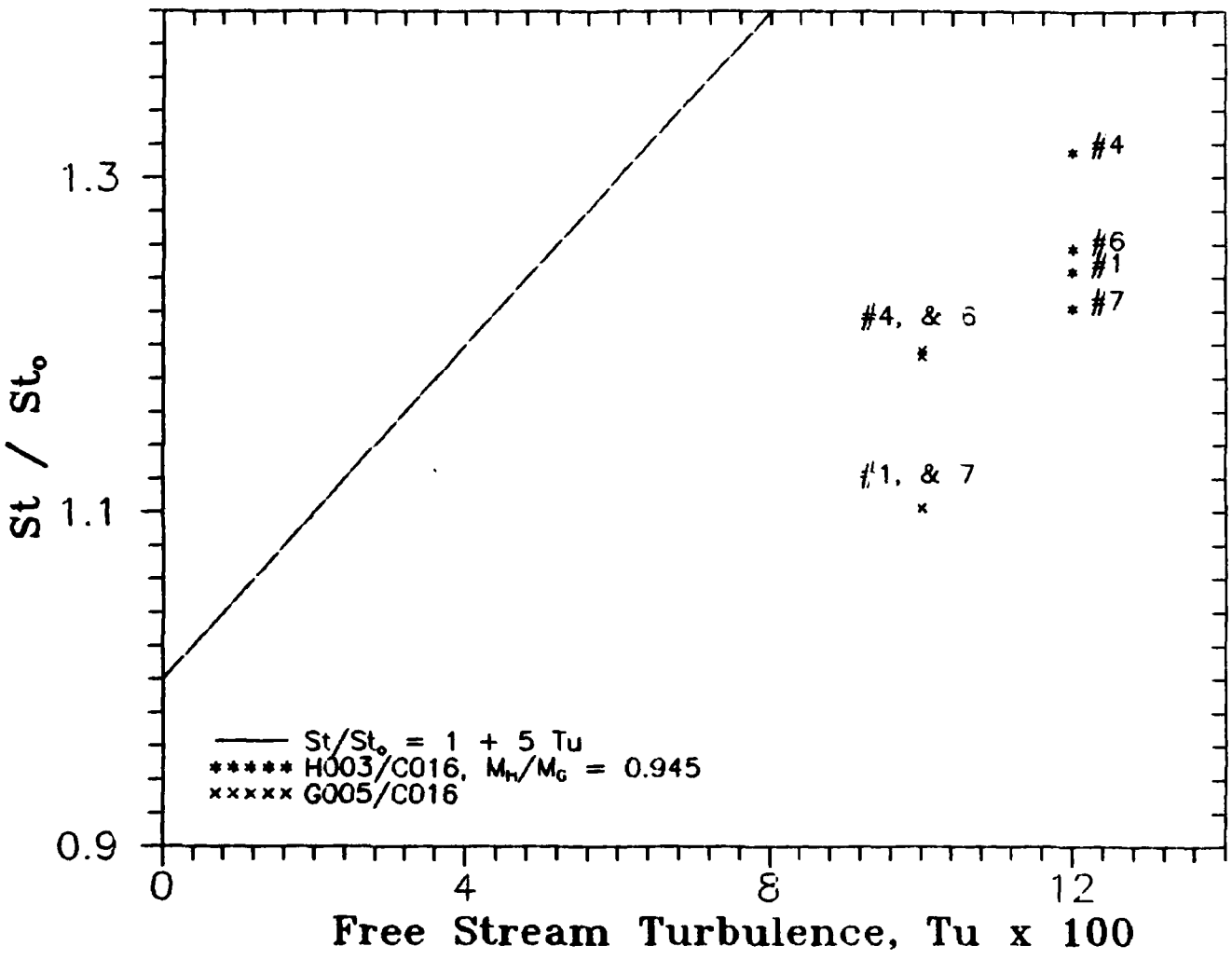

Figure 44 : Free Stream Turbulence Effects,H003

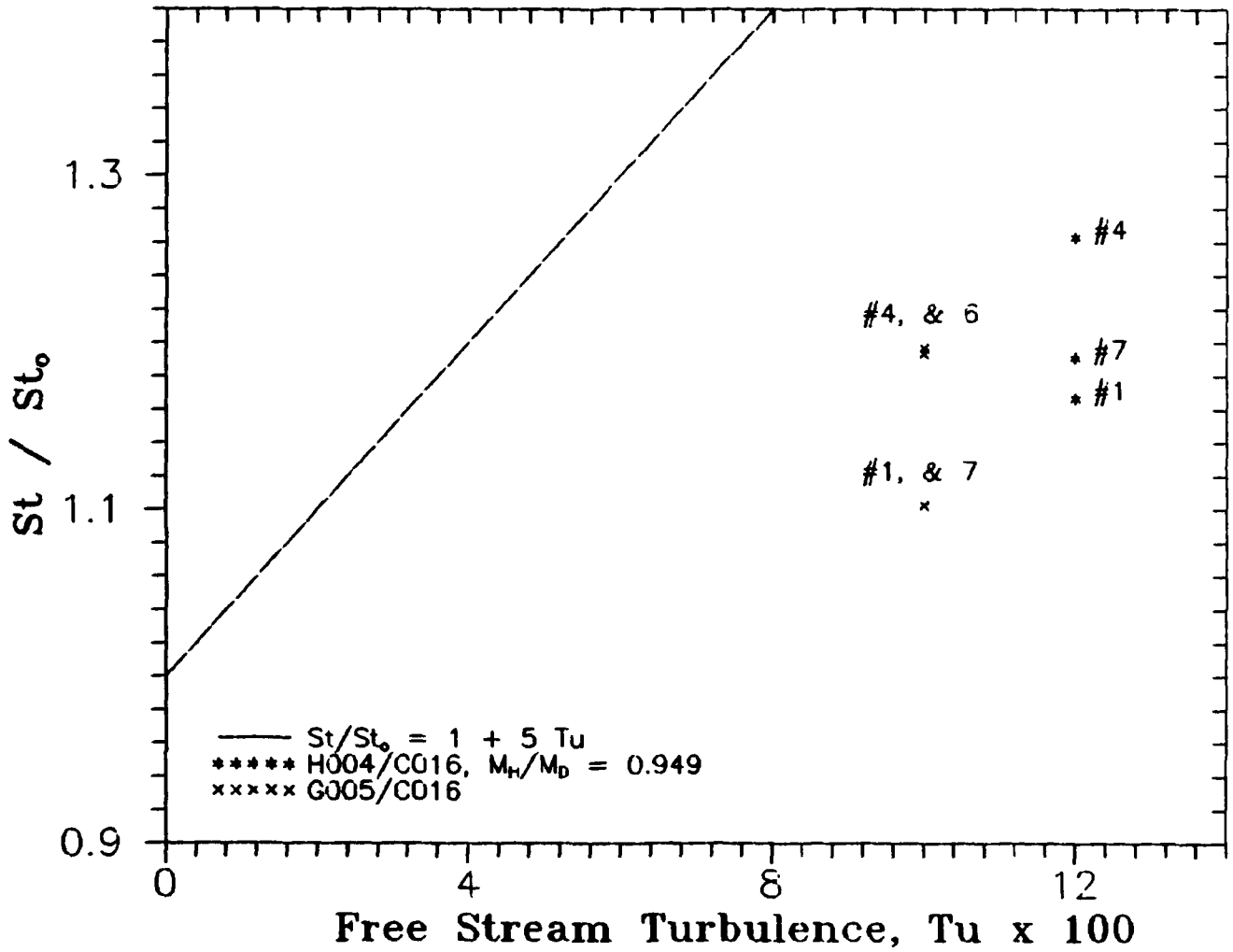

Figure 45 : Free Stream Turbulence Effects, H004

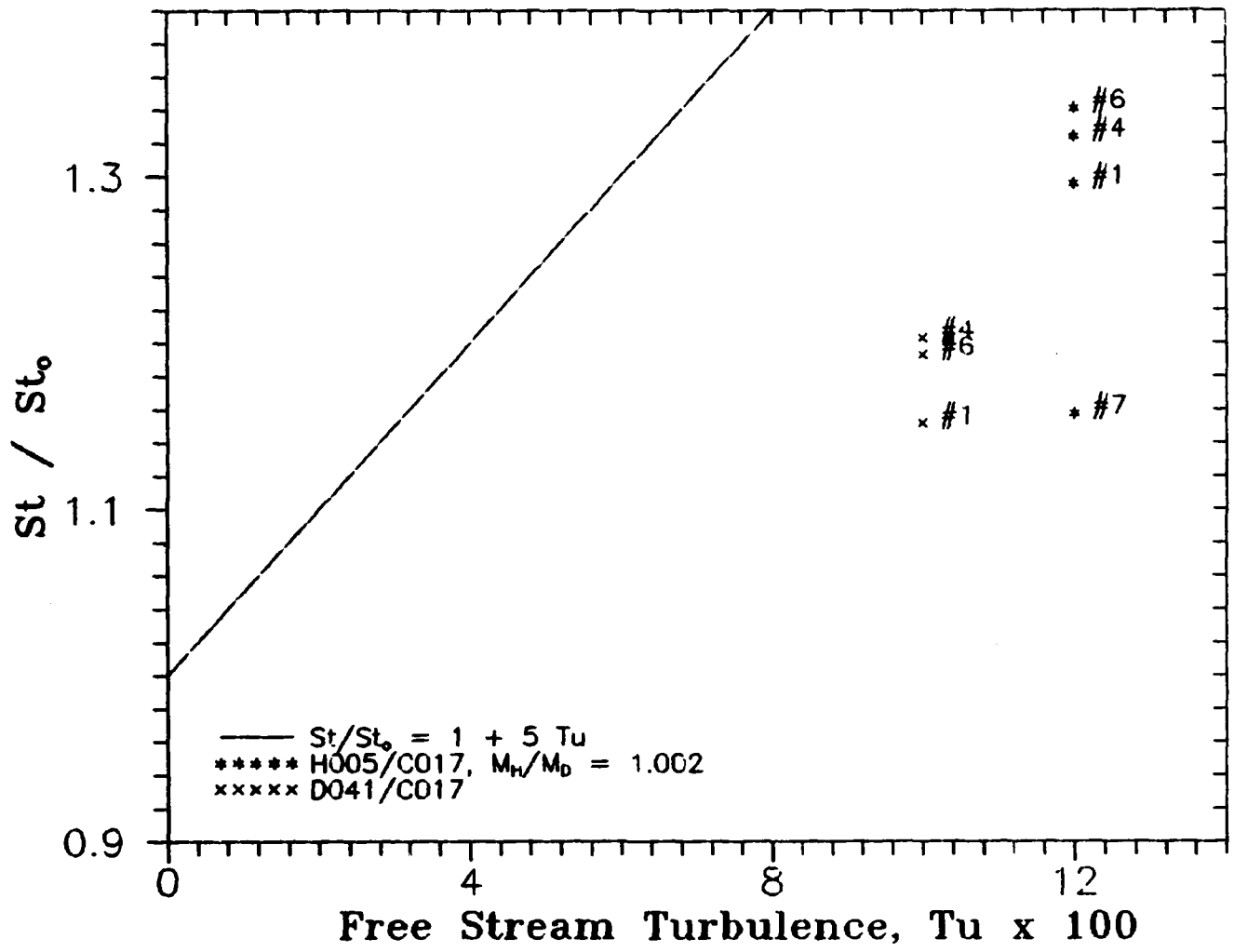

Figure 46 : Free Stream Turbulence Effects,H005

approximately 10 to 20 percent. Figures 43 and 46 seem to indicate that the gage location with the highest ratio, #4, is shifting downstream, to #6, as the turbulence increases. The ratios for gages 4 and 6 in Figures 44 and 45 are the same for the background turbulence level, so the shift is not evident. But the shift does seem to indicate that the increased turbulence level decreases the amount of turbulence decay locally. Since the data used in the figures essentially have the same values of M, and the amount of data available at high shock Mach numbers is limited, any influence that M might have is not known. Figures 43 to 46 also indicate that the liberties taken with this correlation were entirely out of order. Since Simonich and Bradshaw found good agreement with Equation (22), and the ratios of Stanton numbers, as computed here, do not agree it must be due to the ratio being calculated with St and St_o at the same turbulence level. So a few graphs were made to test the effect of plotting the ratio of Stanton numbers between data run series H00x (12 percent Tu) and data runs without free stream turbulence generation (10 percent Tu), versus the change in turbulence intensity between the two data runs. So, the value for St is now the Stanton number from the H00x series, and the value for St_o is now the Stanton number from a corresponding data run with the background free stream turbulence.

The gage location was used in this examination to

determine if an increase in the local turbulence level affected the local Stanton number ratio. Figures 47 through 50 show these plots and indicate that the data now lies above the correlation of Equation (22). However, since these Figures plot the Stanton number ratio at each gage location, the influence of the parameter that provides the greatest influence in plain film cooled heat transfer, the blowing ratio, M, is not clear.

So the "correlation" as it is, was looked at differently. By considering the ratio of Stanton numbers in the same manner as was used in Figures 47 to 50, and computing Stanton number ratios only for data runs with similar blowing parameters the "correlation" provided very good agreement with measured results.

The "correlation" provided by this ratio of Stanton numbers was calculated and plotted against the change in turbulence, 2 percent, the same as Figures 47 to 50. Figures 51 through 54 show the results of these calculations.

These plots indicate that the "correlation" used in this manner does provide a reasonable prediction for the increase in the heat flux that free stream turbulence causes in film cooled heat transfer. In fact, only the data grouped into Figure 51 shows a significant deviation from the correlation, which underpredicts the heat transfer. In Figure 52 the data are grouped right around the prediction

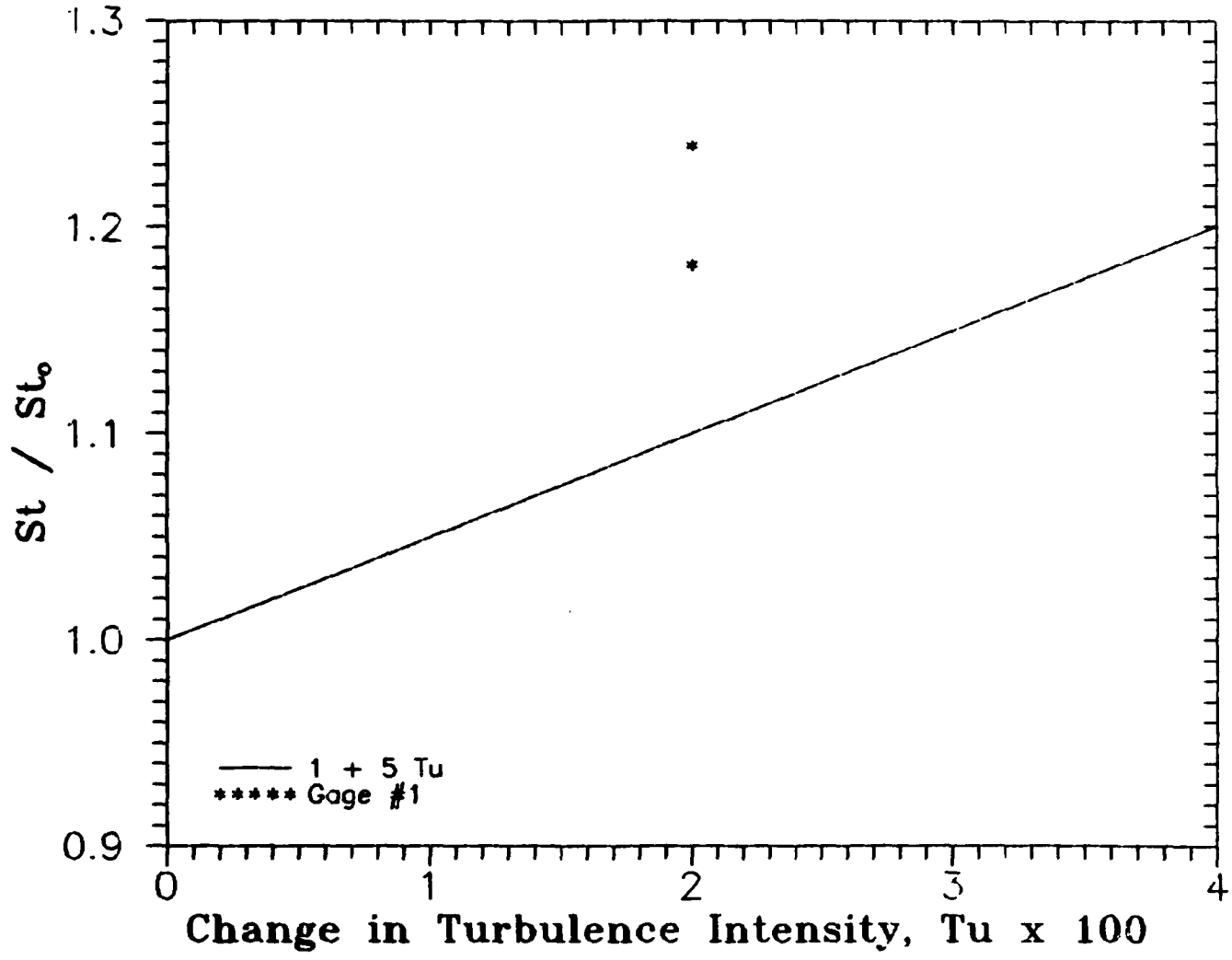

Figure 47 : Free Stream Turbulence Effects, g No 1

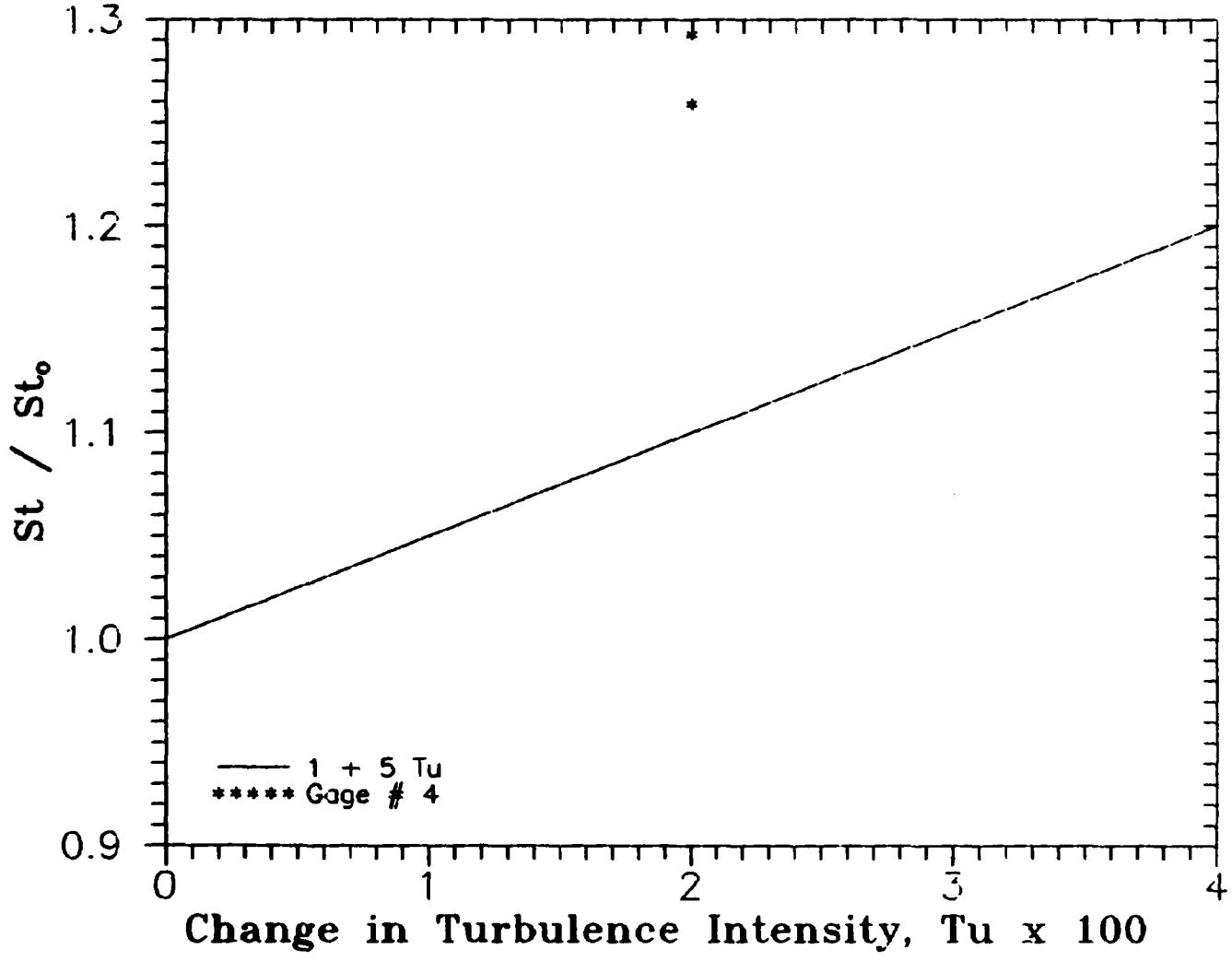

Figure 48 : Free Stream Turbulence Effects, g No 4

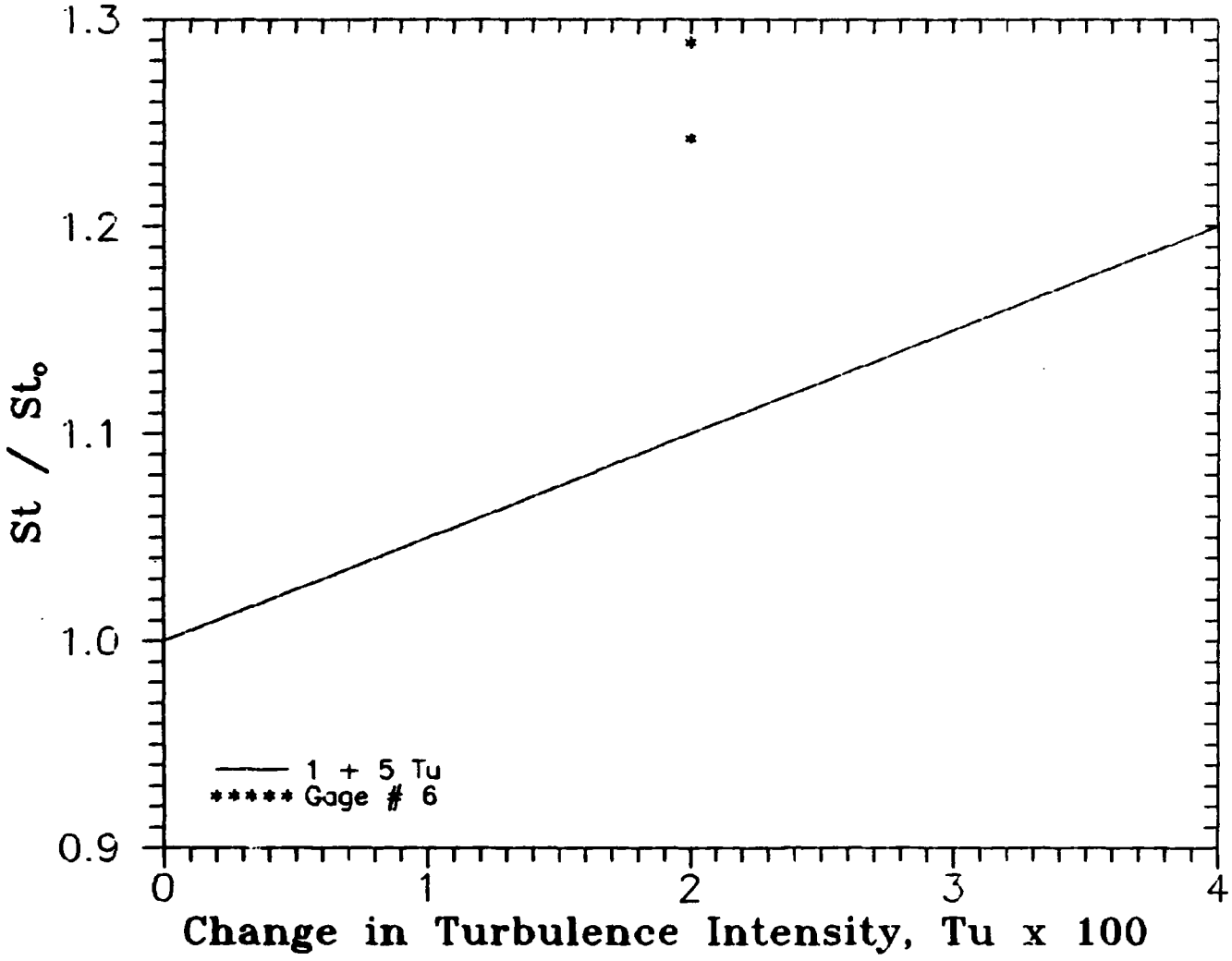

Figure 49 : Free Stream Turbulence Effects, g No 6

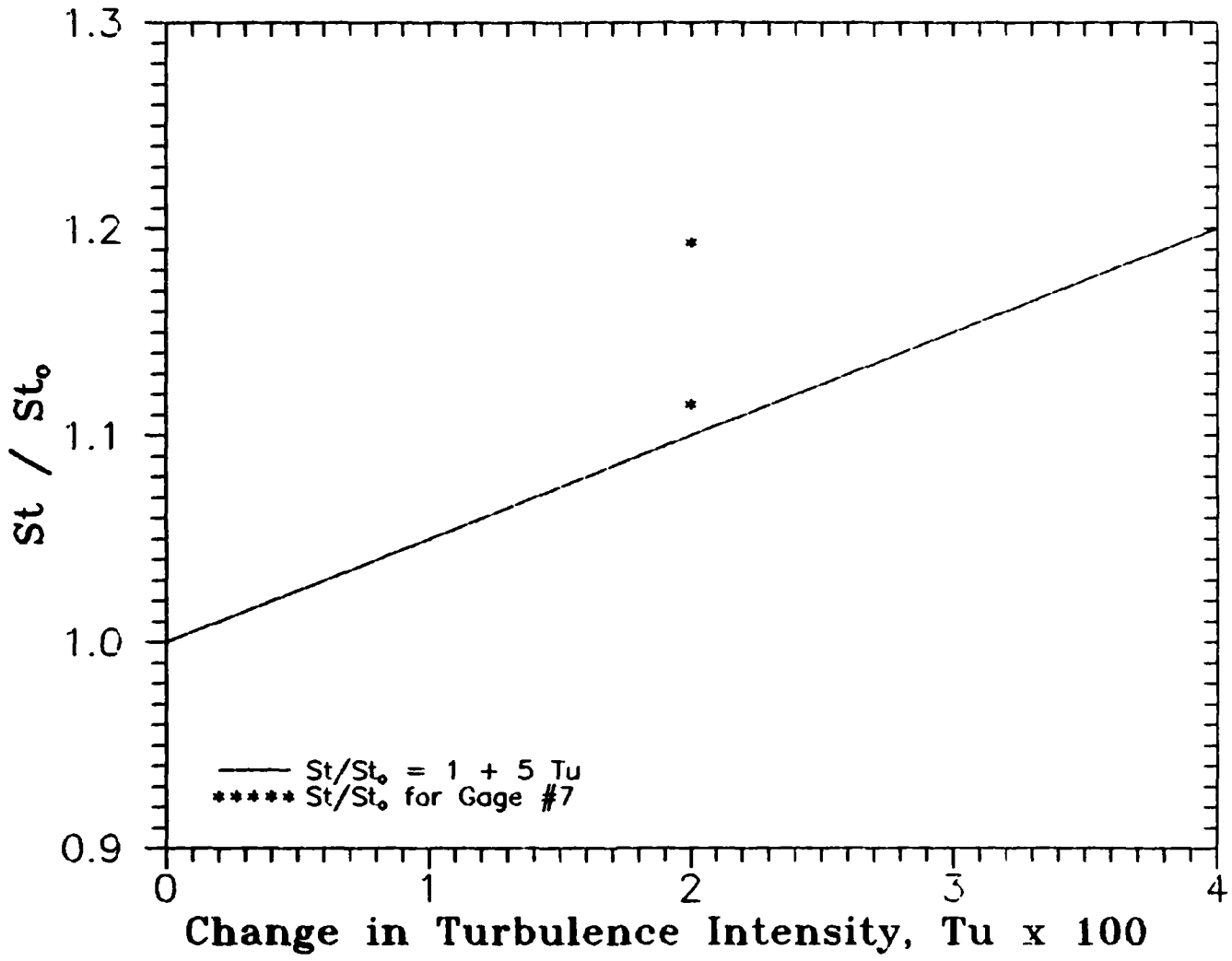

Figure 50 : Free Stream Turbulence Effects, g No 7

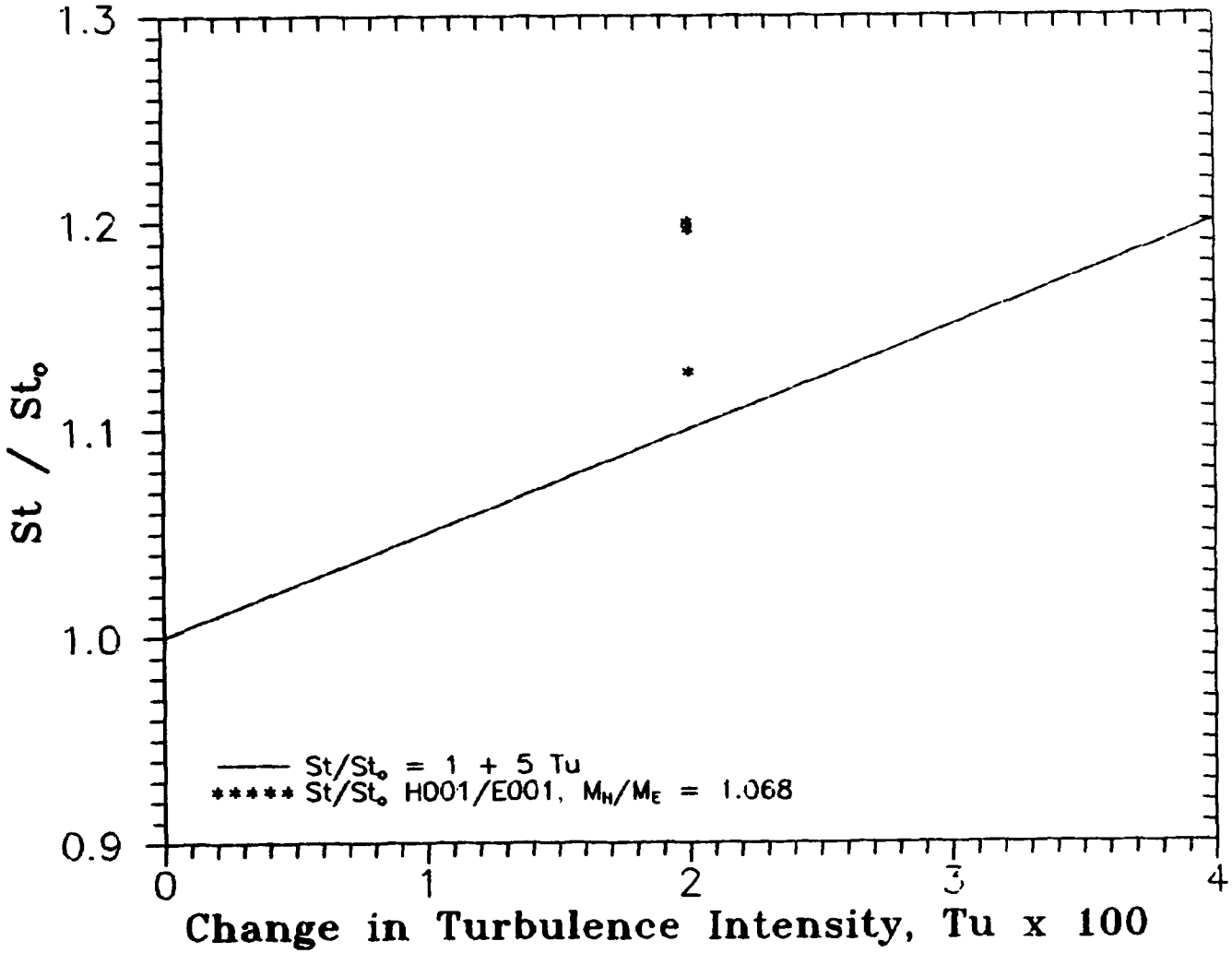

Figure 51 : Free Stream Turbulence Effects, H1E

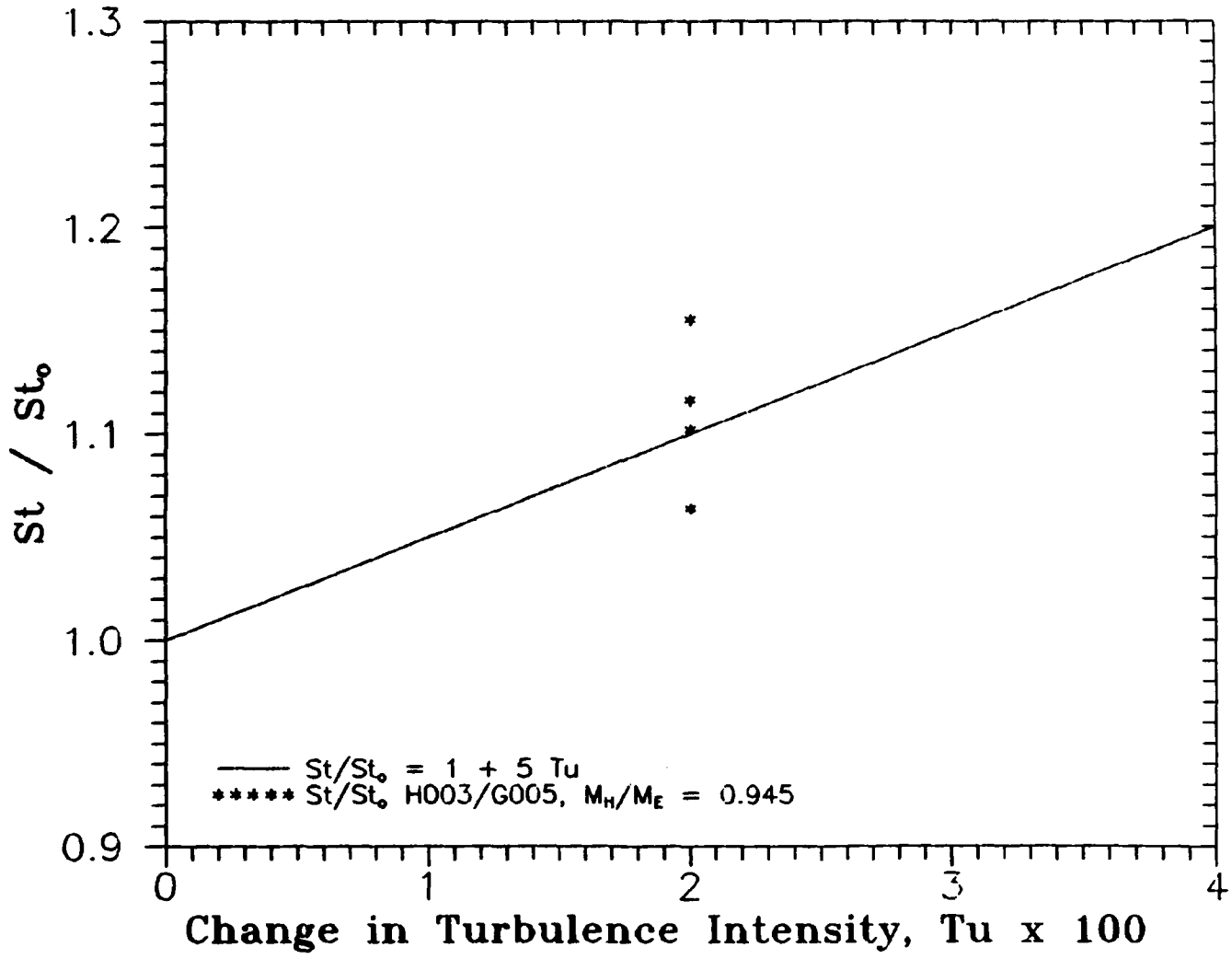

Figure 52 : Free Stream Turbulence Effects, H3G5

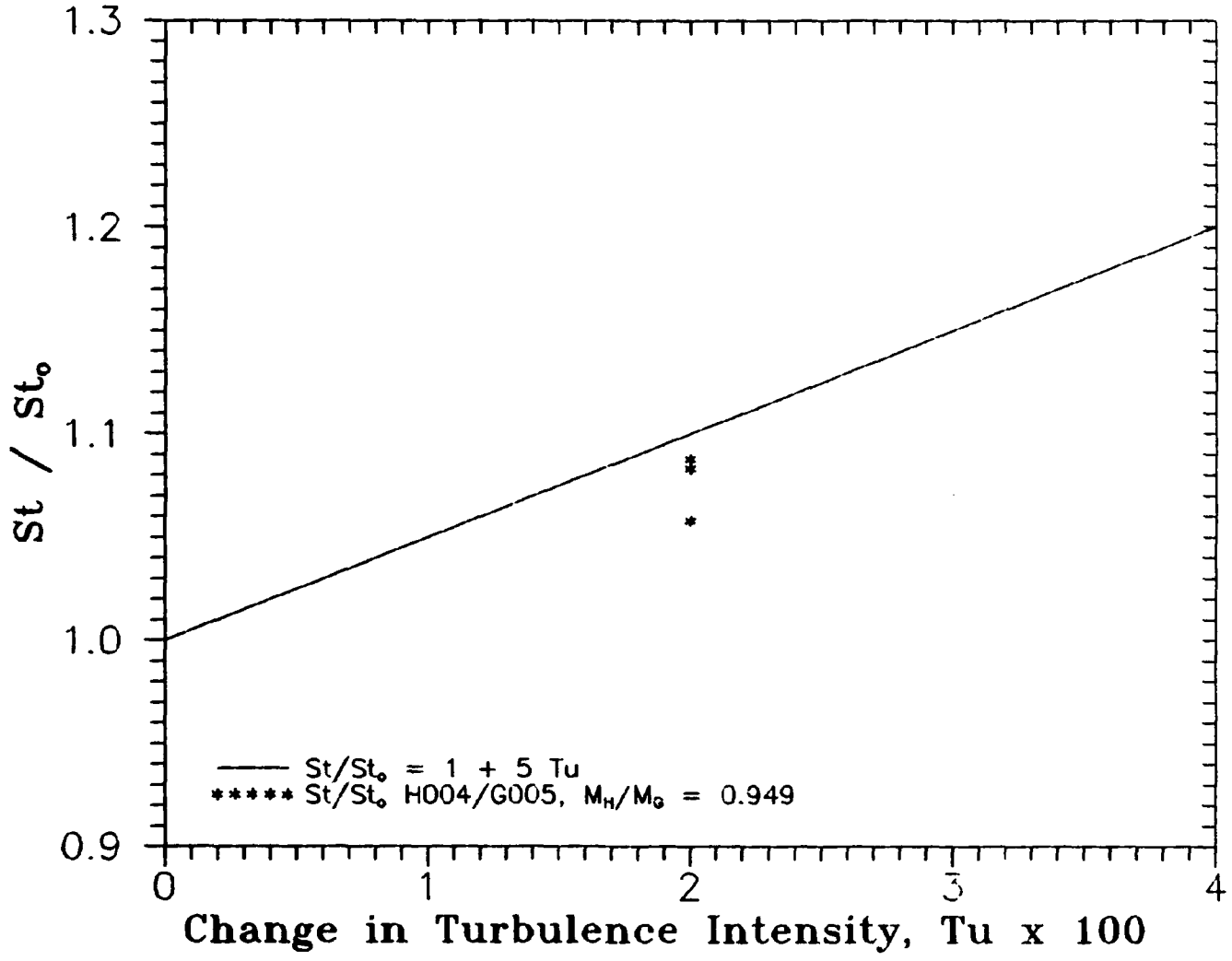

Figure 53 : Free Stream Turbulence Effects, H4G5

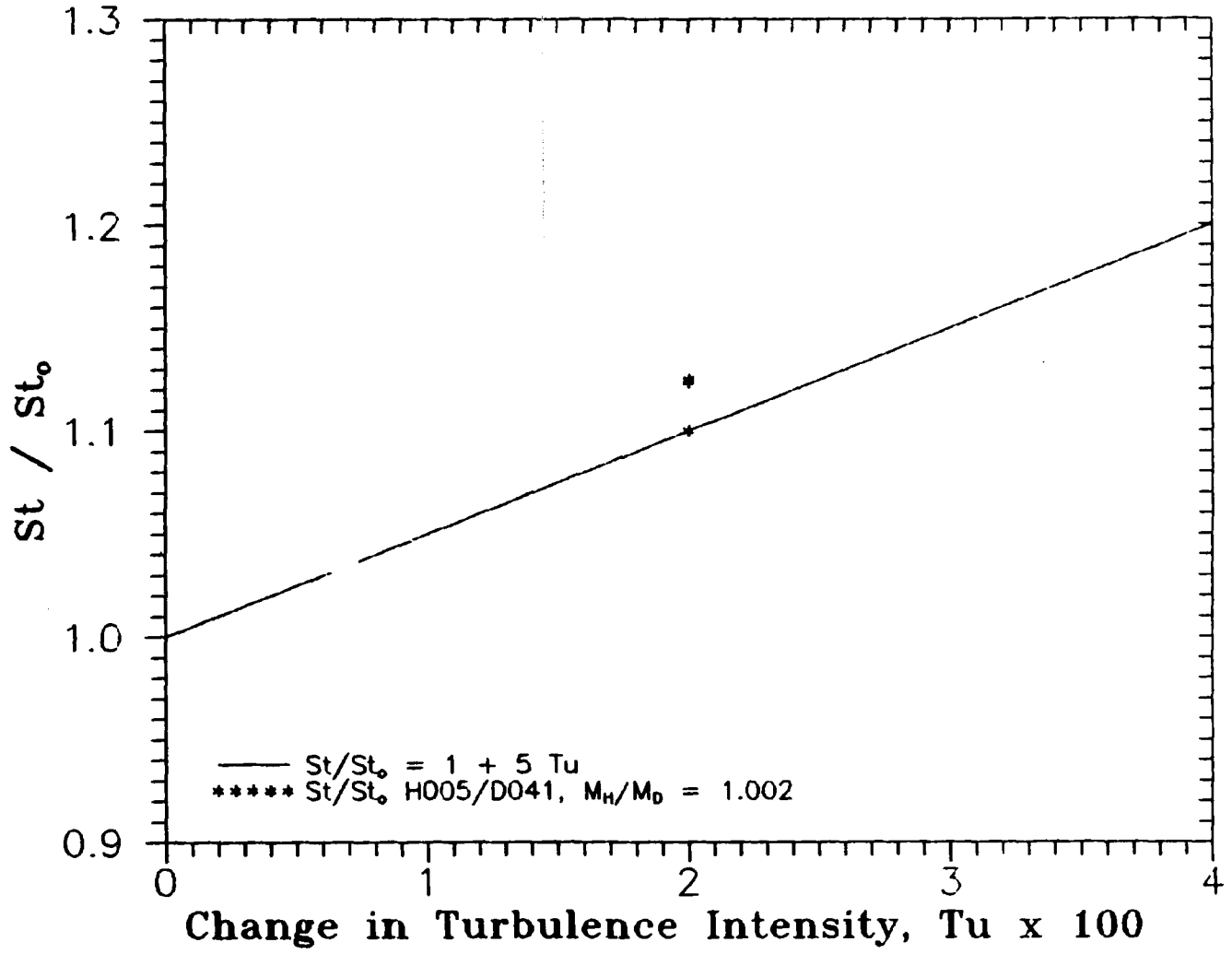

Figure 54 : Free Stream Turbulence Effects, H5D

showing good agreement. Figure 53 also shows good agreement, but the correlation slightly overpredicts the data. However, the prediction provided by the "correlation" in Figure 53 is still much closer to the actual values than Figure 51. Figure 54 shows excellent agreement between the data and the correlation, for all the data points. The data shown in Figure 51 could be attributed to the influence previously described as shock reflections, or perhaps calculation error, and called an anomaly, since all the other data points correlate well with this prediction. Goldstein reports that studies made on the influence of free stream turbulence on film cooling effectiveness show that it significantly reduces the performance (Goldstein, 1971:356). This comparison confirms that the free stream turbulence increases the ratio of the heat transfer coefficients significantly. Also, the prediction provided by equation (22), and as modified here, shows very good agreement with the measured ratios of heat transfer coefficients. The prediction can therefore be used to correlate similar film cooling flows with results that vary by ± 10 percent from the prediction with a high degree of confidence. This percentile includes the data of Figure 51. It should again be noted that many of the data points used in these graphs assumed that the free stream turbulence level along the plate was the same as the level measured by the hot wire upstream, and did not

account for turbulence decay. So this correlation may not prove correct if the local Tu, at each heat flux gage is measured and found to differ, on the other hand the correlation might even produce a higher confidence level.

Since there were not any correlations found that specifically addressed free stream turbulence effects on film cooled heat transfer, the correlation of Equation (22) was modified. Even though the ratios of Stanton numbers computed in the manner previously described is not consistent with the intended use of Equation (22), when plotted against the change in free stream turbulence, a very good prediction of the effects of Tu on film cooling can be obtained.

The final part of this study verified some of the previous data. One of the turbulence generator inserts, shown in Figures 7 and 8, was found to be loose, so they were all tightened up and taped over. The J00x series of runs (a set of data to verify previous calculations) was then made to determine the rate of heat transfer after this repair. The mean rate of the heat transfer was found to be slightly lower. This reduction did not significantly change the correlations previously made, so the plots discussed in the text were not revised. The Mach number of the shock was relatively high in the J00x series, M = 1.31, so the effect would be even less pronounced as the shock Mach number decreased. Rockwell made some background

turbulence level measurements at the J series test conditions and found that the level was still approximately 10 percent (Rockwell, 1989). Figure 55 contains a plot of the Stanton number versus the Reynolds number, for the H and J series of data. The J series does serve to illustrate the difference in the heat transfer coefficient brought about by the increased turbulence of the H series. It also indicates the inability of the theoretical calculations to accurately describe high Tu levels, just as the predictions of equations (2-18) were previously shown to be unable to properly predict the effects of shock reflections. In the J00x series the shock Mach number is so high, that the inability to faithfully predict the measured heat flux to a flat plate behind an incident shock could also attributed to the shock Mach number dependence of the theoretical equations.

Finally, the measured values of P_2 were compared to the values derived by Equation (2) for the highest shock speeds encountered in this study, $M_s = 1.32$, and found to be within ± 2 percent. A similar calculation at the low end of the scale, $M_s = 1.15$, agreed exactly. The verification of T_2 was not so simple. A 0.0005 inch Omega K-type thin foil thermocouple was adapted for measurements in the shock tube. The response time of the instrument was not high enough, so the data was extrapolated out to five time constants. The extrapolation indicated that the

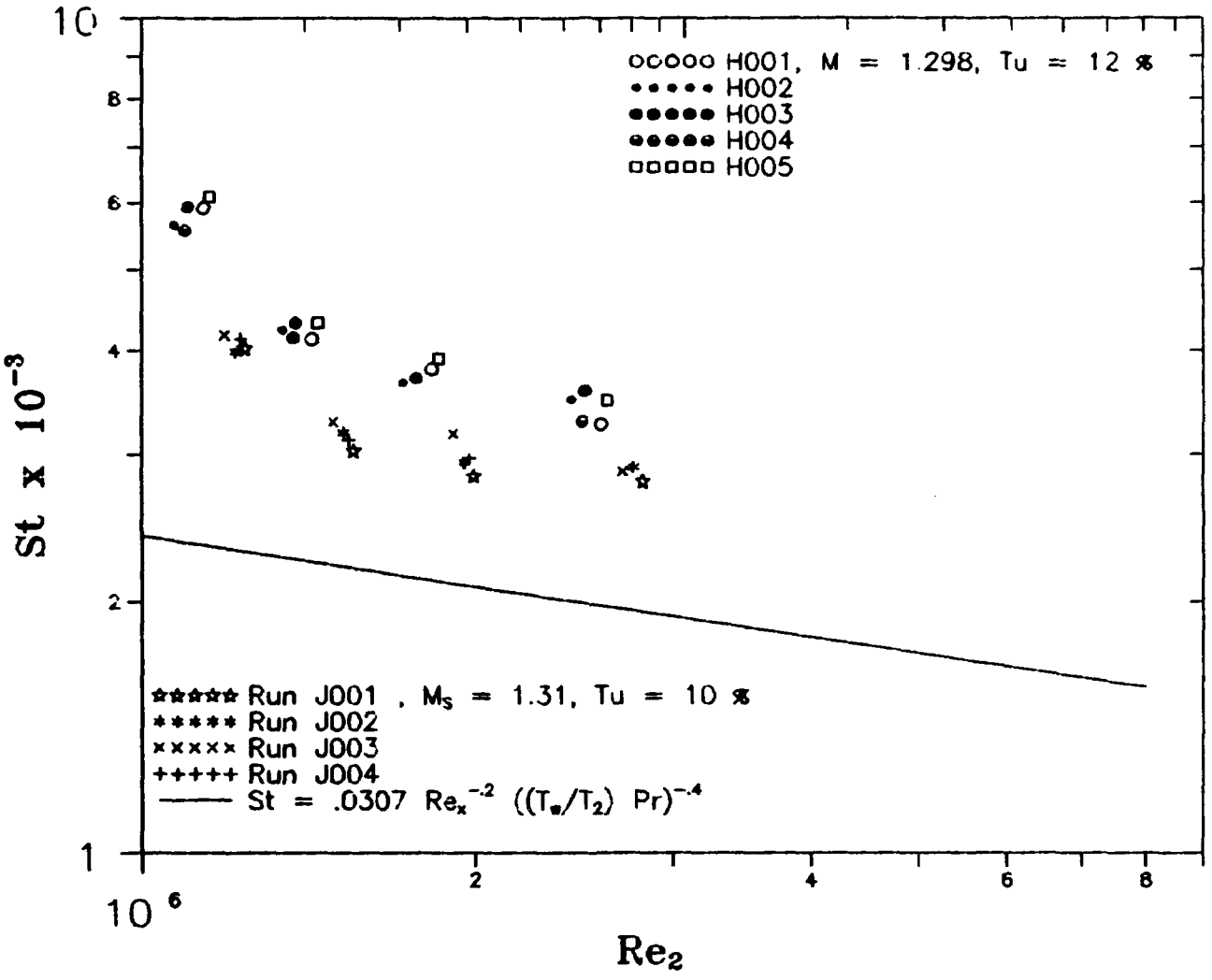

Figure 55 : Effect of Tu on Stanton Number Distribution

temperature as predicted by equation (3) was consistently overpredicting the actual temperature by 3 percent. Three similar measurement attempts with a 0.0005 inch E-type thermocouple wire resulted in the incident shock breaking the bead upon contact.

VI. Conclusions

Careful consideration of the results produced by this investigation leads to the following conclusions:

1. There is a shock reflection occurring in the shock tube and it affects the results of the theoretical predictions, as does the high level of free stream turbulence. In this way the effects of the reflected shock and free stream turbulence are minimized.

2. The program developed for use in this study accurately calculates the actual heat flux to a flat plate behind an incident shock, as well as the theoretical predictions for this heat flux.

3. The use of the program provides a relatively complete graphical history of the plate surface temperature, which can be used to determine a mean value of the heat transfer free of the influence of unwanted flow conditions.

4. The limited range of flow conditions used in this study indicate that these mean values can be used to calculate ratios of heat transfer coefficients. The ratios can then be used to provide an accurate basis for comparison to predictions and correlations. The study shows that the ratio of heat transfer coefficients for the film cooled case is highly dependent on the blowing

parameter, even for the relatively high blowing ratios used in this study.

5. The effect of free stream turbulence on the ratios of heat transfer coefficients for the film cooled and uncooled case was just as theory would predict for the very limited range of data examined. An increase in free stream turbulence increased the ratio. The ratio of Stanton numbers calculated in the manner described in Chapter 5, and plotted against the change in Tu can be can be used as a prediction with an accuracy of ± 10 percent, for the film cooled case.

VII. Recommendations

The results of this study can be used as a tool in developing a better understanding of the film cooling process and its influence on heat transfer. Future work in the following areas would provide valuable information:

1. Replace the rounded leading edge plate used in this study with an elliptical leading edge, other studies indicate good results with this geometry (Goldstein, 1971).
2. Obtain additional heat flux gages and fully instrument the plate in the same configuration used in this study. Some of the most interesting flow phenomena occur at the gage locations that were unavailable.
3. Obtain a plate that is identical to the plate used in the film cooling studies, fully instrumented, and free of film cooling holes. This will eliminate any roughness effects that the taped holes might introduce into the baseline data.
4. Store the raw data from the DL1200 on a magnetic tape reel, in a format that is compatible with the VMS series of machines. This will save considerable time when transferring files to and from the mainframe. And since the shock tube workstation now has a 386 computer, multi-tasking is possible. So the data can be uploaded/downloaded in the background while processing

other work.

5. Expand the film cooling studies to include multiple, staggered row injection. This will provide a more complete picture of the film cooling effects.

6. Measure the free stream turbulence level at various positions along the plate to determine the true local values.

7. Automate the film cooling system flow solenoid, because the degree of error when judging the right time, can be severe.

Appendix A

Instrument Calibrations

The procedure used to calibrate the gages was previously detailed in Chapter IV. The results of this calibration are shown in Figure 56. The equations listed for each gage are the same used to convert voltages to temperatures in the computer program.

The values used for the constant property substrate of the gages were obtained from Figure 57, at an average value for ρ, and at a room temperature of 288 $^{\circ}$K from a table of thermophysical properties (Touloukian, et al, 1970).

The pressure transducers were calibrated using a Mansfield Green Pneumatic dead weight tester, Model HK-500, S/N 79672. The pressure calibration curves were used to verify the flow pressures. Figure 58 shows the calibration data plots.

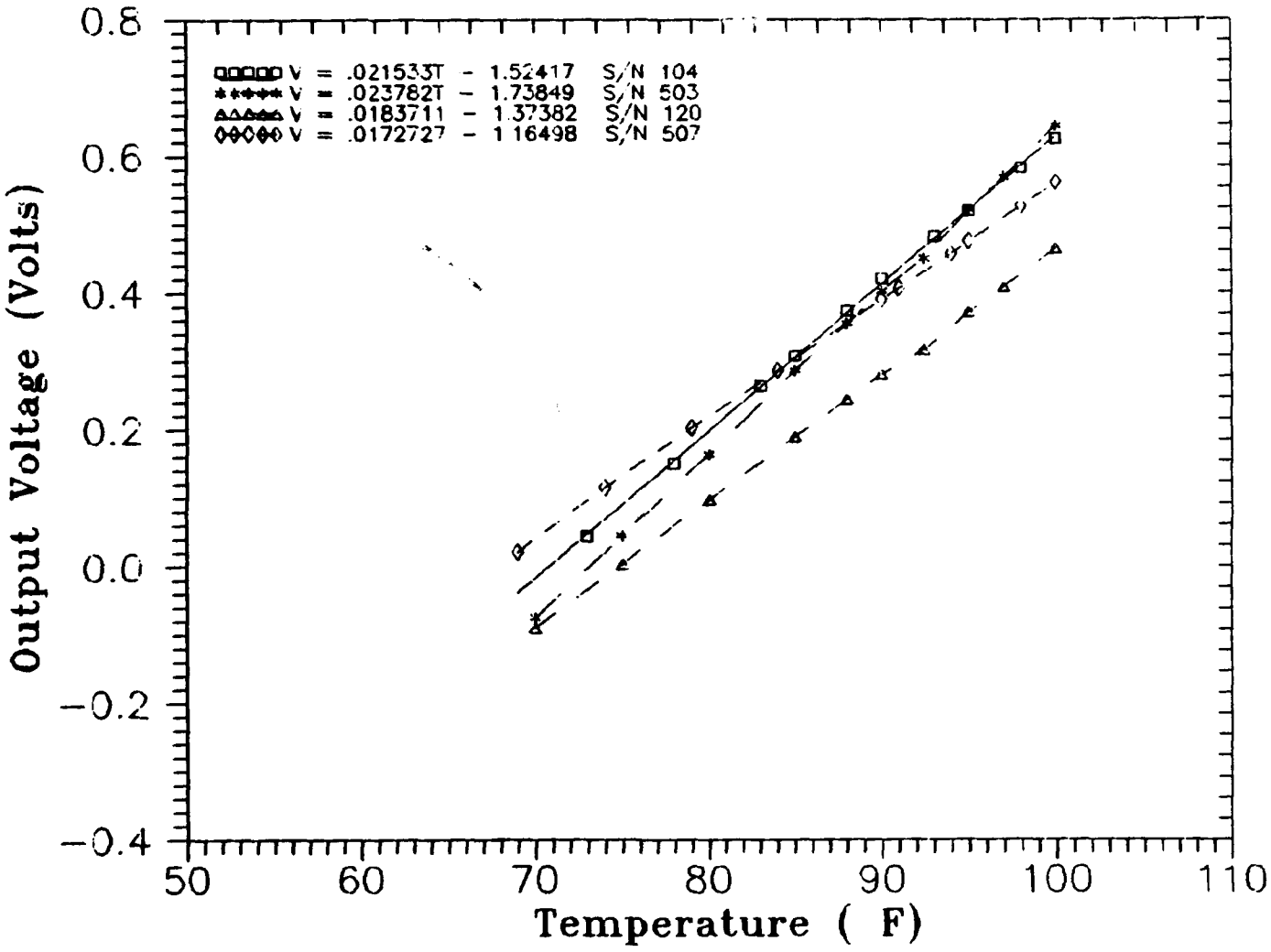

Figure 56 : Calibration Curve for Gages

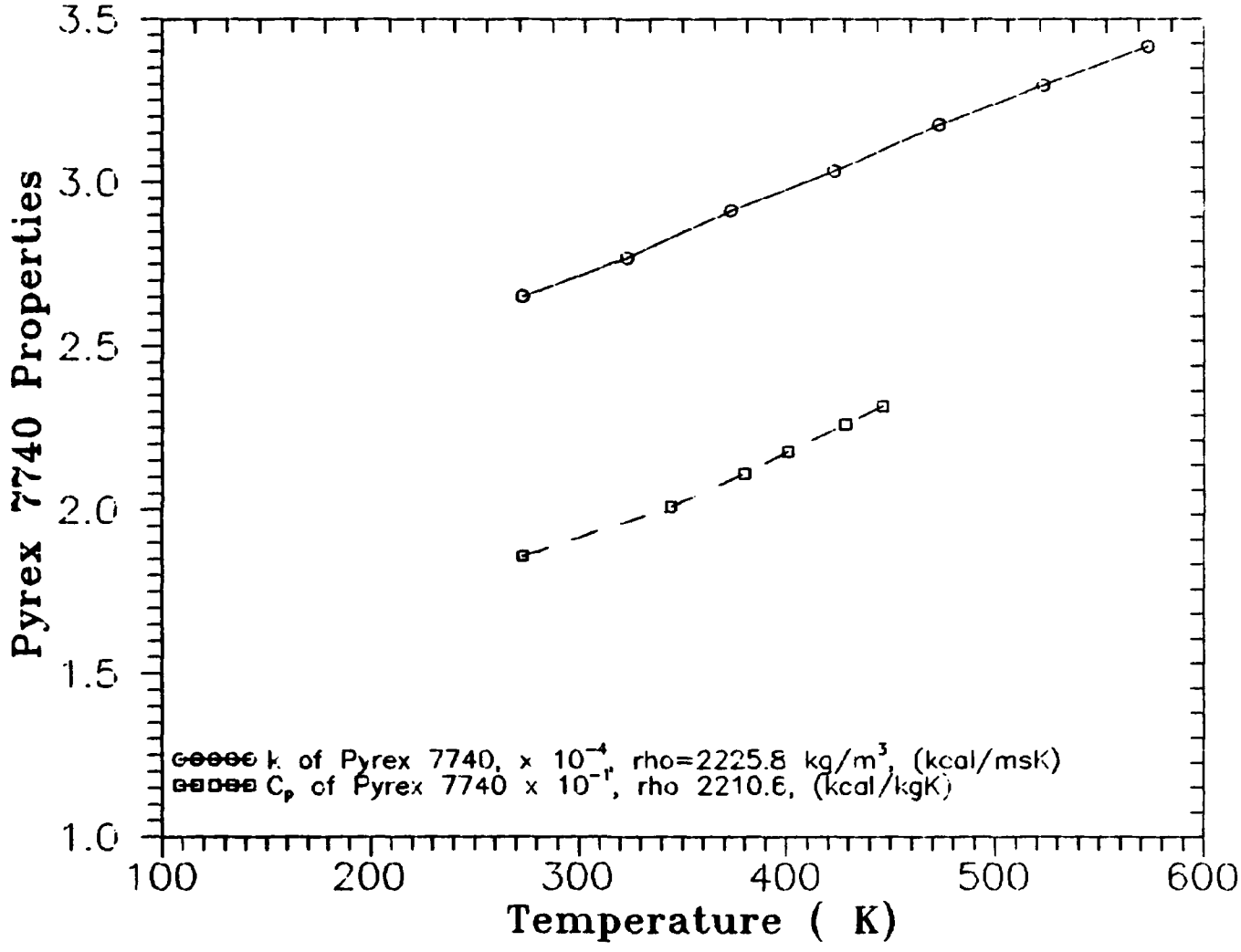

Figure 57 : Pyrex 7740 Substrate Properties

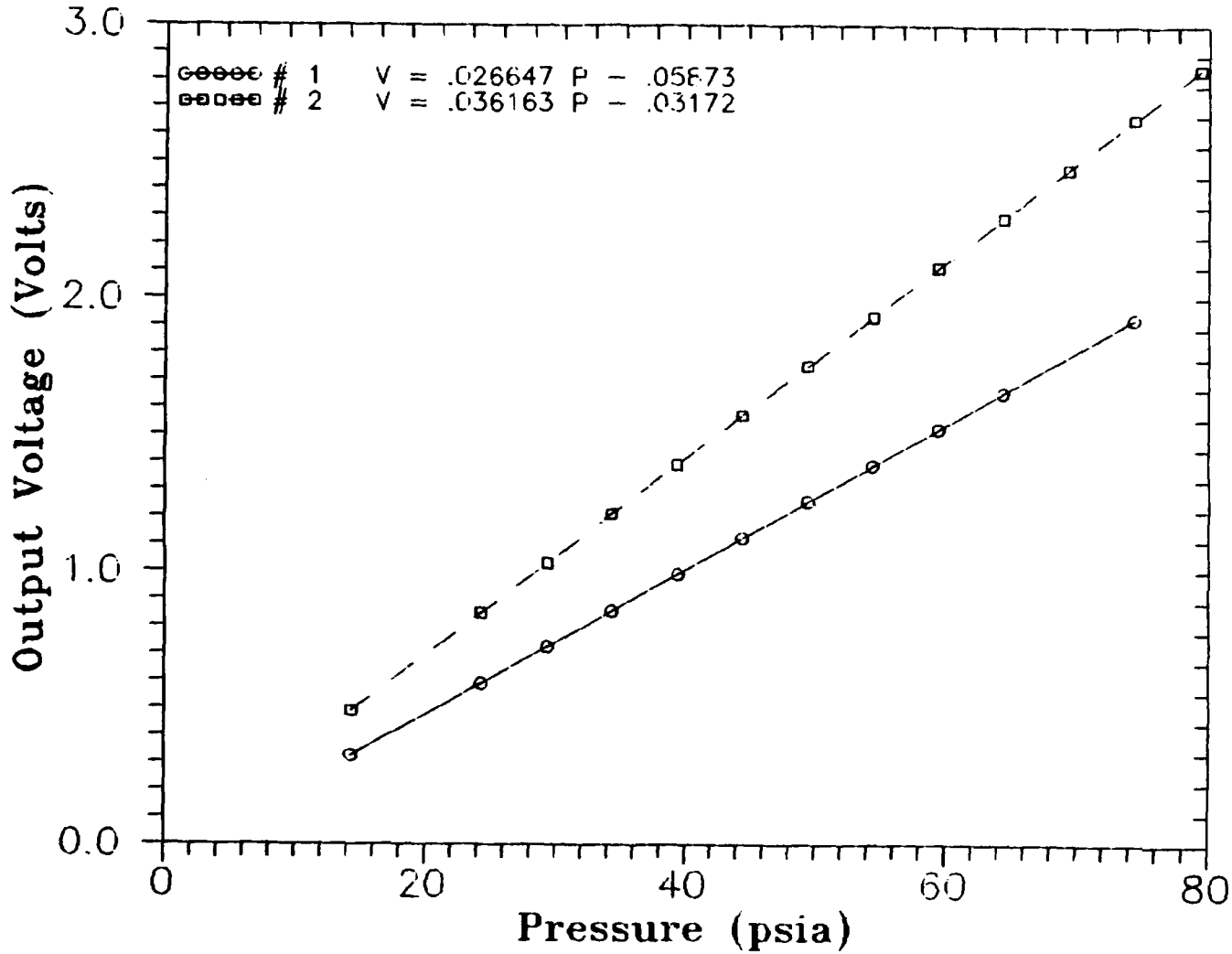

Figure 58 : Calibration Curve for Pressure Transducers One and Two

Appendix B

Computer Programs

Program AVHEAT.FOR was used to calculate the measured and theoretical heat transfer using equations (2-25). The pressure dependent terms in the theoretical equations, μ, ρ, Pr, and even C_p were evaluated by interpolating between one and ten atmospheres, at the temperature in question. This procedure produced consistently accurate results for the temperature and pressure ranges of this study.

The transfer time for a fully loaded DL1200 output file to the VMS computer, at 9600 Baud, is approximately eight minutes. The elapsed CPU time is approximately 2.5 minutes. The download time approximately five minutes. Program RMS.FOR was then used to compute the mean and rms values of the heat flux, which were then used in program STANT.FOR to calculate the values of h, Nu, and St corresponding to the mean heat flux. AVHEAT.FOR is on listed first, followed by program RMS.FOR, then program STANT.FOR on 143. The last program listed, QMAKE.BAS a Quickbasic 4.5 program, is a program used to produce separate files for the actual, and theoretical heat transfer which are then used to produce plots of the heat flux.

```
*     AVHEAT.FOR     PROGRAM BY SCOTT A. JURGELEWICZ
*************************************************************************
*     THIS PROGRAM CALCULATES A MOVING AVERAGE FOR THE TIME DEPENDENT TEMP
*     CHANGE (VOLTAGE) OUTPUT OF (MEDTHERM) HEAT FLUX GAGES. {NOTE THAT A TWO
*     COLUMN FILE (TIME,VOLTAGE) MUST EXIST (ASKED FOR IN PROGRAM), CONTAINING
*     THE NECESSARY INFO. THIS IS BEST PERFORMED ON AN OUTPUT FROM A DL1200.}
*     IT THEN PERFORMS THE REQUIRED HEAT TRANSFER CALCULATIONS USING THE
*     NUMERICAL METHOD RECOMMENDED BY Dr HITCHCOCK, AND THE MEASURED TEMPS.
*     FOR COMPARISON, IT ALSO CALCULATES THE THEORETICAL HEAT TRANSFER RATES
*     OF THE STEADY, AND UNSTEADY, SOLUTIONS DEVELOPED BY MIRELS (SEE THESIS).
*************************************************************************
*     ~~THE FOLLOWING VARIABLES ARE USED TO CALCULATE THE ACTUAL HEAT XFER, Q~~
*************************************************************************
*     STARTG= START OF THE USEFUL MEASUREMENT TIME (WHEN SHOCK PASSES)   (msec)
*     ENDING= END OF USEFUL MEASUREMENT TIME (WHEN REFLECTED SHOCK PASSES)  "
*     GAGE= GAGE NUMBER UNDER CONSIDERATION (FROM LEADING TO TRAILING EDGE, 1-7)
*     COUNT= NUMBER OF DATA PAIRS IN THE USEFUL PERIOD
*     COUNTOUT= END TIME OF THE USEFUL (AVERAGED) PERIOD (0 to countout) (msec)
*     TIME= TIME AT WHICH A VOLTAGE READING WAS TAKEN
*     VOL= VOLTAGE READING AT THAT TIME
*     T= THE TEMPERATURE EQUIVALENT FOR THE VOLTAGE OUTPUT (VOL) OF THE GAGE
*     TAU(I)= INTEGRATION VARIABLE REPRESENTATION OF TIME
*     TAUN=      "          "          "          "  "   AT Nth DATA POINT
*     TEMP(I)= TIME DEPENDENT REPRESENTATION OF THE TEMP WITH TAU(I)      (F)
*     SUM= SUMMING PARAMETER
*     STOP= A VARIABLE USED TO PROPERLY LOOP THE MOVING AVERAGE SUMMATION
*     QSUM= SUMMING PARAMETER
*     TAVG= THE MOVING AVERAGE VALUE OF TEMP(I), OR A "SMOOTHED" POINT
*     C= THE CONSTANT PROPERTIES FOR THE PYREX 7740 SUBSTRATE OF THE GAGE
*     Q= THE HEAT TRANSFER FROM THE FLUID TO THE PLATE              (kcal/m^2 s)
*     FIRST= THE NAME OF THE INPUT FILE
```

```
*     LAST= THE NAME OF THE OUTPUT FILE (theo. sol. are STEADY, UNSTDL & T)
*     INITIALT= THE INITIAL TIME OF THE USEFUL PERIOD                (msec)
*************************************************************************

*************************************************************************
*     ~~~~~~~~THE FOLLOWING SUBROUTINES AND FUNCTIONS ARE CALLED~~~~~~~~~~~~~~~
*     PRANDTL= CALCULATES THE PRANDTL NUMBER, PR, GIVEN A TEMPERATURE
*     SPHEAT=        "       "  SPECIFIC HEAT, CP,     "    "        "
*     VIS=           "       "  KINEMATIC VISCOSITY, V,        "
*     GX=            "       "  GAGE DISTANCE FROM LEADING EDGE
*     REYNO=         "       "  REYNOLDS NO. OF THE FLOW
*     CONDUC=        "       "  THE THERMAL CONDUCTIVITY, K
*     FRICCOF=       "       "  THE FRICTION COEFFICIENT, CF
*     TRANSF=        "       "  THE TEMPERATURE EQUIVALENT FOR THE VOLTAGE
*               OUTPUT OF THE THIN FILM GAGES
*
*     NOTE :     ALL THE ABOVE FUNCTIONS ARE MODELED WITH A POLYNOMIAL CURVE
*                FIT FROM TABULATED DATA (AGAIN, REFER TO THESIS). EXCEPT FOR
*                GX AND TRANSF, WHICH ARE PHYSICAL QUANTITIES.
*************************************************************************

*     DECLARE THE VARIABLES USED IN THE ACTUAL Q CALCS.....

      CHARACTER FIRST*12,LAST*12,INFO*12,QUES*12,G*7,RUN*4,PLOTR*12
      INTEGER GAGE,COUNT,COUNTOUT,I,J,L,N,STEP,STOP,START,CHECK
      REAL STARTG(8),ENDING(8),TIME,VOL,T,C,Q,SUM,QSUM,INITIALT,Z,FT
      REAL TAU(4096),TEMP(4096),TAVG(4096),TOP,BOT,TAUN,FR
      REAL TIMEVOL(4096,0:8),RESULTS(4096,13),DIFF,TEMPO,VOLDIFF,REY,FV

*     DECLARE THE SUBROUTINES USED IN THE Q CALCS.....
```

```
      REAL PRANDTL,SPHEAT,VIS,GX,REYNO,CONDUC,FRICCOF,TRANSF
      EXTERNAL PRANDTL,SPHEAT,VIS,GX,REYNO,CONDUC,FRICCOF,TRANSF

*     DECLARE THE VARIABLES USED IN THE THEORETICAL Q CALCS.....

      CHARACTER STEADY*12,UNSTDL*12,UNSTDT*12,PLOTT*12
      REAL T1,P1,PR,U2,M,T2,V,X,R,K,H,QTHEO,TREF,SRECOVERY,TAWS,MT
      REAL NUX,NUXL,NUXT,QL,QT,USHOCK,ALPH,M2,CF,LAMBDA,TAWU,URECOVERY
      REAL CP1,CP2,CP,P2,P4,MU2,SAVET1,SAVEP1,SAVEP4,FRACPR,MTHEO

*     HERE THE NECESSARY FILES ARE OPENED.....
*          13= ACTUAL DATA FROM GAGE (VOLTAGE OUTPUT vs TIME)
*          16= TIME, HEAT TRANSFER (Q) DATA FOR THE MEASURED HEAT FLUX
*          17=   " ,        "              FOR STEADY, TURBULENT SOLUTION
*          18=   " ,        "              FOR UNSTEADY, LAMINAR SOLUTION
*          19=   " ,        "               "       "   , TURBULENT SOLUTION
*          20= INFORMATION FILE FOR THE RUN BEING CONSIDERED

*     NOW, THE NAMES OF THE FILES ARE ESTABLISHED. THE OUTPUT FILES ARE NAMED
*     WITH A SUFFIX ADDED TO THE NAME OF THE INPUT DATA FILENAME : -M=ACTUAL Q:
*     -S=STEADY THEO Q; -UL=UNSTEADY THEO Q; -UT=UNSTEADY THEO Q; -INF=INFO...

      WRITE (*,*) 'ENTER THE NAME OF THE INPUT FILE '
      WRITE (*,*) 'WITH THE EXTENSION .DAT ! (i.e., file.dat)'
      READ (*,1) FIRST
1     FORMAT (A12)
2     FORMAT (F5.3)

      OPEN (13,FILE=FIRST,STATUS='UNKNOWN')
      READ (13,*) ((TIMEVOL(I,J),J=0,8),I=1,4095)
```

```
*     NOW, THE "USEFUL" TIME PERIOD IS DEFINED (FROM SHOCK PASSAGE TO
*     REFLECTION, OR RAREFACTION ARRIVAL).............................

      WRITE (*,*) ' '
      WRITE (*,*) 'NOTE : WHEN PROMPTED FOR TIME INPUTS, ALL ENTRIES'
      WRITE (*,*) '       MUST BE REAL NUMBERS ! (i.e. 1.0, 2.33, etc)'
      WRITE (*,*) ' '
      DO 3 L=1,7
       IF (L .EQ. 2 .OR. L .EQ. 3 .OR. L .EQ. 5)GOTO 3
       WRITE (*,*) 'ENTER THE STARTING TIME FOR THE TIME PERIOD YOU'
       WRITE (*,*) 'WISH TO ANALYZE, FROM t=0, IN msec !.'
       WRITE (*,*) 'i.e. THE TIME THAT THE SHOCK PASSED GAGE # ',L
       READ (*,2) STARTG(L)
       WRITE (*,*) ' '
       WRITE (*,*) 'NOW ENTER THE ENDING TEST TIME FOR THE RUN (msec !)'
       READ (*,2) ENDING(L)
3     CONTINUE

      WRITE (*,*) ' '
      WRITE (*,*) 'ENTER THE ATMOSPHERIC TEMPERATURE (in deg C)'
      READ (*,*) SAVET1
      WRITE (*,*) ' '
      WRITE (*,*) 'ENTER THE ATMOSPHERIC PRESSURE (in inches of Hg)'
      READ (*,*) SAVEP1
      WRITE (*,*) ' '
      WRITE (*,*) 'ENTER THE SHOCK TUBE DRIVER PRESSURE (also in Hg)'
      READ (*,*) P4
      WRITE (*,*) ' '
      WRITE (*,*) 'ENTER THE MEASURED MACH NUMBER OF THE SHOCK'
```

```
READ (*,*) M
WRITE (*,*) ' '
WRITE (*,*) 'NOW ENTER THE THEORETICAL SHOCK MACH NUMBER'
READ (*,*) MTHEO

INFO=FIRST(1:4)//'INFO'
OPEN (20,FILE=INFO,STATUS='NEW')
RUN=FIRST(1:4)
WRITE (20,*) 'INFO FOR RUN : ',RUN

T1=SAVET1+273.15
USHOCK=SQRT(1.402*287*T1)*M
MT=M
MU2=(USHOCK/M)*.8326395*(MT*MT-1)
G='1234567'
DO 5 L=1,7
 IF (L .EQ. 2 .OR. L .EQ. 3 .OR. L .EQ. 5)GOTO 5
 GAGE=L
 LAST=FIRST(1:4)//'M'
 STEADY=FIRST(1:4)//'S'
 UNSTDL=FIRST(1:4)//'UL'
 UNSTDT=FIRST(1:4)//'UT'
 QUES=FIRST(1:4)//'Q'//G(L:L)
 PLOTR=FIRST(1:4)//'PR'//G(L:L)
 PLOTT=FIRST(1:4)//'PT'//G(L:L)

 OPEN (16,FILE=LAST,STATUS='NEW')
 OPEN (17,FILE=STEADY,STATUS='NEW')
 OPEN (18,FILE=UNSTDL,STATUS='NEW')
 OPEN (19,FILE=UNSTDT,STATUS='NEW')
```

```
      OPEN (21,FILE=QUES,STATUS='NEW')
      OPEN (22,FILE=PLOTR,STATUS='NEW')
      OPEN (23,FILE=PLOTT,STATUS='NEW')

*     NOW GO AND PERFORM THE VOLTAGE TO TEMP TRANSFER CALCULATIONS.....

      COUNT=0
      DO 10 I=1,4095
        IF (L .EQ. 7)GAGE=8
        TAU(I)=0.0
        TEMP(I)=0.0
        TAVG(I)=0.0
        DO 6 J=1,13
           RESULTS(I,J)=0.0
6       CONTINUE

*       TO PROPERLY PERFORM THE Q CALCULATIONS, THE INITIAL PLATE TEMP
*       MUST BE CALCULATED (THE TEMP JUST BEFORE THE SHOCK PASSAGE).....
        Z=TIMEVOL(I,0)
        IF (Z .GT. (STARTG(L)-.004) .AND. Z .LT. STARTG(L))THEN
            DIFF=0.0
            TEMPO=1.8*SAVET1+32
            CALL TRANSF(L,TIMEVOL(I,GAGE),TEMPO,DIFF,T,VOL)
            VOLDIFF=TIMEVOL(I,GAGE)-VOL
            DIFF=-VOLDIFF
            TEMPO=0.0
            CALL TRANSF(L,TIMEVOL(I,GAGE),TEMPO,DIFF,T,VOL)
            INITIALT=T
        ENDIF

*       THE FOLLOWING STATEMENT ALLOWS ONLY THOSE DATA POINTS IN THE USEFUL
```

```
*       PERIOD TO BE CONSIDERED.....................................

        IF (Z .GE. STARTG(L) .AND. Z .LE. ENDING(L))THEN
            CALL TRANSF(L,TIMEVOL(I,GAGE),TEMPO,DIFF,T,VOL)
            TAU(I)=TIMEVOL(I,0)
            TEMP(I)=T
            COUNT=1+COUNT

*           COUNT ESTABLISHES THE NUMBER OF DATA PAIRS IN THE SET.....

        ENDIF
        IF (TAU(I) .GT. 0.0 .AND. TAU(I-1) .EQ. 0.0)START=I
10  CONTINUE

    WRITE (*,*) 'THE # OF DATA PAIRS FOR GAGE # ',L,'  IS :',COUNT

*   AND COMPUTE THE MOVING AVERAGE. HOWEVER, THE AVERAGING PROCESS WILL LIMIT
*   THE HEAT TRANSFER DETERMINATION AT THE ENDS OF THE USEFUL PERIOD BY AN
*   AMOUNT (N-1)/2..............................................

    N=25
    COUNTOUT=COUNT+START-(N-1)/2-1

*   NOTE THAT N MERELY ESTABLISHES A NUMBER THAT IS USED TO "SMOOTH OUT"
*   THE RAW DATA (RATHER THAN AVERAGE SEVERAL RUNS), AND SHOULD BE CHANGED
*   TO THE SMALLEST NUMBER POSSIBLE. SO THE NOISE IS ELIMINATED, BUT NOT THE
*   INFORMATION AVAILABLE IN THE DATA.....................................

    STOP=0
    TAVG(START)=TEMP(START)
```

```
      DO 30 I=(START+1),COUNTOUT
        SUM=0
        IF (STOP .EQ. 0)STOP=1
        DO 40 J=I,(STOP+I)
           SUM=TEMP(J)+SUM
40      CONTINUE
        DO 50 J=(I-1),(I-STOP),-1
           SUM=TEMP(J)+SUM
50      CONTINUE
        TAVG(I)=SUM/(STOP*2.+1)
        IF (STOP .LT. ((N-1)/2))STOP=STOP+1
30    CONTINUE

*     AND THE START OF THE USEFUL WINDOW IS REDEFINED AS t=0.................
      FR=3386.5307*SAVEP1*(1.+1.1673605*(MT*MT-1.))
      FV=MU2/M
      FT=T1*(1.+.139351*(1.402*MT*MT-1./(MT*MT)-.402))
      CALL VIS (FT,(FR/101325.),V)
      CALL GX (L,X)
      FREEREY=(MU2/M)*X/V
      DO 55 I=START,COUNTOUT
        TAU(I)=TAU(I)-STARTG(L)
        RESULTS(I,1)=TAU(I)
        RESULTS(1,7)=(I*.002)-STARTG(L)
        RESULTS(I,10)=FT-TAVG(I)
55    CONTINUE

*     NOW THE SUM BUCKET IS SET TO ZERO TO CALC THE HEAT TRANSFER,
*     Q, AS THE SUMMATION OF THE POINTS.....................................

      C=0.3745541
```

```
      DO 60 I=(START+1).COUNTOUT
        TAUN=TAU(I)*.001
        QSUM=0
        DO 70 J=(START+1),I
           TOP=TAVG(J)-TAVG(J-1)
           BOT=SQRT(TAUN-TAU(J)*.001)+SQRT(TAUN-TAU(J-1)*.001)
           QSUM=TOP/BOT+QSUM
70      CONTINUE
        Q=C*(((TAVG(START)-INITIALT)/(2.*SQRT(TAUN)))+QSUM)
        RESULTS(I,2)=Q
        RESULTS(I,11)=Q/RESULTS(I,10)
        CALL SPHEAT (FT,(FR/101325.),CP)
        RESULTS(I,13)=(RESULTS(I,11)*287.*FT)/(FR*(MU2/M)*CP)
        CALL CONDUC (FT,K)
        CALL GX(L,X)
        RESULTS(I,12)=RESULTS(I,11)*X/K

60    CONTINUE

*************************************************************************
*     NOW THE THEORETICAL SOLUTIONS ARE COMPUTED FOR EACH CASE, FIRST THE
*     STEADY TURBULENT SOLUTION, THEN THE UNSTEADY LAMINAR AND TURBULENT
*     SOLUTIONS, RESPECTIVELY. THE SOLUTIONS USED HERE ARE THOSE DEVELOPED
*     BY MIRELS (WHERE 0.6 < PR < 1.0), AND ARE DETAILED IN THE THESIS.
*************************************************************************
*     THE FOLLOWING NOMENCLATURE IS USED IN THIS PORTION OF THE PROGRAM :
*     ~~~~~~~~~~~~~~~~~ FOR THE UNSTEADY PORTION ~~~~~~~~~~~~~~~~~~~~~~~~
*     USHOCK= VELOCITY OF THE SHOCK                                 (m/s)
*     ALPH= EMPIRICAL COEFFICIENT USED IN THE SOLUTION
*     M2= MACH NUMBER OF THE AIR BEHIND THE SHOCK
```

```
*     RECOVERY= RECOVERY NUMBER FOR THE AIR BEHIND THE SHOCK
*     TAW= ADIABATIC WALL TEMP                                          (K)
*     V= KINEMATIC VISCOSITY                                            (m^2/s)
*     X= GAGE DISTANCE                                                  (m)
*     R= REYNOLDS NUMBER OF THE FLOW BEHIND THE SHOCK
*     CF= FRICTION COEFFICIENT  FOR THE FLOW BEHIND THE SHOCK
*     LAMDA= SAME AS ALPH
*     PR= PRANDTL NUMBER
*     K= THERMAL CONDUCTIVITY                                           (kcal/m s K)
*     NUX= NUSSELT NUMBER FOR THE STEADY SOLUTION
*         NUXL= NUSSELT NUMBER FOR THE UNSTEADY, LAMINAR SOLUTION
*         NUXT=   "       "     "   "     "    , TURBULENT SOLUTION
*     H= HEAT TRANSFER COEFFICIENT                                      (kcal/m^2 s K)
*     Q= HEAT TRANSFER FLUX                                             (kcal/m^2 s)
*         QTHEO= FOR THE STEADY SOLUTION                                    "
*         QL= FOR THE UNSTEADY, LAMINAR SOLUTION                            "
*         QT= FOR THE UNSTEADY, TURBULENT SOLUTION                          "
*     ~~~~~~~~~~~~~~~~~~~~~~~~~ AND THE STEADY SOLUTION ~~~~~~~~~~~~~~~~~~~~~~
*     T1= TEMPERATURE OF THE SHOCK TUBES DRIVEN SECTION  (ATMOSPHERIC)  (K)
*     P1= PRESSURE     "   "    "     "     "       "          "        (Pa)
*     P2=    "         "   "  FLOW AFTER THE SHOCK PASSAGE                "
*     P4=    "         "   "  SHOCK TUBES DRIVER SECTION                  "
*     U2= THE FREE STREAM VELOCITY BEHIND THE SHOCK                      (m/s)
*     CP= SPECIFIC HEAT                                                 (kcal/kg)
*     TREF= REFERENCE TEMPERATURE FOR PROPERTY EVALUATIONS                (K)
*************************************************************************
*     REDEFINE P1, CALC P2, T2, THEN FIND THE STEADY SOLUTION.............

      P1=3386.5307*SAVEP1
      P2=P1*(1.+1.1673605*(MT*MT-1.))
```

```
      FRACPR=P2/101325.
      T2=T1*(1.+.139351*(1.402*MT*MT-1./(MT*MT)-.402))
      CALL PRANDTL ((T1+T2)*.5,FRACPR,PR)
      SRECOVERY=PR**(1./3.)
      CALL SPHEAT (T1,FRACPR,CP1)
      CALL SPHEAT (T2,FRACPR,CP2)
      CP=(CP1+CP2)*.5
      TAWS=T2+SRECOVERY*MU2*MU2/(MT*MT*8368.*CP)

      DO 100 I=(START+NINT(COUNT*.2)),COUNTOUT
        TREF=(T2+TAVG(I))/2.+.22*(TAWS-T2)
        CALL VIS (TREF,FRACPR,V)
        CALL GX (L,X)
        CALL REYNO ((MU2/MT),X,V,R)
        RESULTS(I,8)=R
        CALL PRANDTL(TREF,FRACPR,PR)
        NUX=.0287*R**.8*PR**.6
        CALL CONDUC (TREF,K)
        H=NUX*K/X
        QTHEO=H*(TAWS-TAVG(I))
        WRITE (17,*) TAU(I),QTHEO
        RESULTS(I,3)=QTHEO
100   CONTINUE

C     NOW THE THEORETICAL UNSTEADY LAMINAR , AND TURBULENT, SOLUTIONS

      ALPH=.39-.02/(1.-(MU2/(MT*USHOCK)))
      M2=(MU2/MT)/SQRT(1.402*287.*T2)

      DO 200 I=START+1,COUNTOUT
        CALL VIS (TAVG(I),FRACPR,V)
```

```
      TIME=TAU(I)/1000.
      IF (TIME .EQ. 0.0)TIME=.0000001
      X=TIME*(MU2/MT)
      CALL REYNO ((MU2/MT),X,V,R)
      RESULTS(I,9)=R
      CALL FRICCOF ((MU2/MT),USHOCK,R,CF)
      LAMBDA=.35+.15/(1.-((MU2/MT)/USHOCK))
      CALL PRANDTL (TAVG(I),FRACPR,PR)
      CALL CONDUC (TAVG(I),K)

*     RECALL THE UNSTEADY SOLUTION REQUIRES A DIFFERENT RECOVERY FACTOR.....

      URECOVERY=PR**ALPH
      TAWU=T2*(1.+.201*M2*M2*URECOVERY)
*     NOW THE LAMINAR Q.............................
      IF (TAU(I) .LE. (NINT(COUNT*.3)*.002))THEN
          NUXL=.5*CF*R*PR**LAMBDA
          H=NUXL*K/X
          QL=H*(TAWU-TAVG(I))
          WRITE (18,*) TAU(I),QL
          RESULTS(I,4)=QL
      ENDIF
*     AND THE TURBULENT Q...........................
      IF (TAU(I) .GE. (NINT(COUNT*.1)*.002))THEN
         NUXT=.0287*R**.8*PR**.6
         H=NUXT*K/X
         QT=H*(TAWU-TAVG(I))
         WRITE (19,*) TAU(I),QT
         RESULTS(I,5)=QT
      ENDIF
```

```
200   CONTINUE

      WRITE (20,*) '*********************************************'
      WRITE (20,*) 'GAGE START (msec) END (msec) '
      WRITE (20,202) L,STARTG(L),ENDING(L)
202   FORMAT (X,I2.X,2(5X,F5.3))

      REWIND 13
      CLOSE (16,STATUS='DELETE')
      CLOSE (17,STATUS='DELETE')
      CLOSE (18,STATUS='DELETE')
      CLOSE (19,STATUS='DELETE')
      WRITE (21,*) '     TAU        Q(meas)       Q(steady)  Q(uns,lam)
     :   Q(uns,turb)'
      WRITE (21,203) ((RESULTS(I,J),J=1,5),I=START,COUNTOUT)
203   FORMAT (X,5(2X,F10.5))
      WRITE (22,*) 'THE FREE STREAM Re IS :',FREEREY
      WRITE (22,*) '   TAU           REX           RET    '
      WRITE (23,*) ' DT(K)           h             Nu          St'
      WRITE (22,1001) ((RESULTS(I,J),J=7,9),I=START,COUNTOUT,50)
      WRITE (23,1002) ((RESULTS(I,J),J=10,13),I=START,COUNTOUT,50)
1001  FORMAT (3(1X,E11.4))
1002  FORMAT (4(1X,E11.4))
1000  CONTINUE
   5  CONTINUE
      P1=SAVEP1
      P2=P2*(29.92/101325.)
201   FORMAT (5(X,F7.2),2X,F5.3,4X,F7.2,5X,F7.3,3X,F7.2)
      WRITE (20,*) '*********************************************'
      WRITE (20,*) '   P1      P2       P4       T1       T2      M(act)
```

```
:   Vel(Shock)    M(theo)    U2'
    WRITE (20,201) P1,P2,P4,T1,T2,M,USHOCK,MTHEO,(MU2/MT)
    WRITE (20,*) 'NOTE : P's = in Hg, T's = deg K, AND U2's =  m/s'
    REWIND 20
    REWIND 21
    REWIND 22
    REWIND 23

    END

*   HERE THE VARIOUS FUNCTIONS DEFINED ABOVE ARE CALCULATED

    REAL FUNCTION PRANDTL (TT,FRAC,PP)
    DOUBLEPRECISION TT,PP,FRAC,VISC1,VISC2,VISC,SP1,SP2,SP,CON,RHO
    VISC1=8.62532E-4*TT*TT+.438264*TT-52.2114
    VISC2=8.60678E-5*TT*TT+.04398*TT-5.13936
    VISC=(VISC1+.9*(VISC2-VISC1)*(FRAC-1.))*1.E-7
    SP1=2.58335E-10*TT**3-3.17503E-7*TT*TT+.000164668*TT+.2112
    SP2=1.6667E-10*TT**3-1.65004E-7*TT*TT+7.78354E-5*TT+.2288
    SP=SP1+.9*(SP2-SP1)*(FRAC-1.)
    CON=(1.68609E-8*TT**3-2.69637E-5*TT*TT+.0291598*TT-.54418)*1.E-6
    RHO=(FRAC*101325.)/(287.2*TT)
    PP=(VISC*RHO*SP)/CON
    END

    REAL FUNCTION SPHEAT (TT,FRACT,CC)
    DOUBLEPRECISION TT,FRACT,CC1,CC2,CC
    CC1=2.58335E-10*TT**3-3.17503E-7*TT*TT+.000164668*TT+.2112
    CC2=1.6667E-10*TT**3-1.65004E-7*TT*TT+7.78354E-5*TT+.2288
    CC=CC1+.9*(CC2-CC1)*(FRACT-1.)
```

```
      END

      REAL FUNCTION VIS (TT,FRACTN,VV)
      DOUBLEPRECISION TT,VV1,VV2,VV,FRACTN
      VV1=8.62532E-4*TT*TT+.438264*TT-52.2114
      VV2=8.60678E-5*TT*TT+.04398*TT-5.13936
      VV=(VV1+.9*(VV2-VV1)*(FRACTN-1.))*1.E-7
      END

      REAL FUNCTION REYNO (UAMB,XX,VV,RR)
      REAL UAMB,XX,VV,RR
      RR=UAMB*XX/VV
      END

      REAL FUNCTION FRICCOF (UAMB,US,RR,CCF)
      REAL UAMB,US,RR,CCF
      CCF=(1.128/SQRT(RR))*(1.-.346*UAMB/US)
      END

      REAL FUNCTION CONDUC (TT,KK)
      DOUBLEPRECISION TT,KK
      KK=(1.68609E-8*TT**3-2.69637E-5*TT*TT+.0291598*TT-.54418)*1.E-6
      END

      REAL FUNCTION GX (GG,XX)
      INTEGER GG
      REAL XX
      IF (GG .EQ. 1)XX=.0567531
      IF (GG .EQ. 2)XX=.0611187
      IF (GG .EQ. 3)XX=.0658812
      IF (GG .EQ. 4)XX=.0710406
```

```
      IF (GG .EQ. 5)XX=.0813594
      IF (GG .EQ. 6)XX=.0912812
      IF (GG .EQ. 7)XX=.1293812
      END

      REAL FUNCTION TRANSF (GG,VOLT,TEMPDIFF,DEL,TEM,VOLTO)
      INTEGER GG
      REAL A,B,VOLT,TEM,DEL,TEMPDIFF,VOLTO
      IF (GG .EQ. 1)THEN
         A=1.52417
         B=.0215334
      ENDIF
      IF (GG .EQ. 2)THEN
         A=1.73235
         B=.0248611
      ENDIF
      IF (GG .EQ. 4)THEN
         A=1.73849
         B=.0237824
      ENDIF
*     IF (GG .EQ. 3)  ]  POSITIONS 3 & 5 DON'T HAVE WORKING GAGES INSTALLED,
*     IF (GG .EQ. 5)  ]  SO MODIFY AS NEEDED
      IF (GG .EQ. 6)THEN
         A=1.37382
         B=.0183711
      ENDIF
      IF (GG .EQ. 7)THEN
         A=1.16498
         B=.0172727
      ENDIF
```

```
IF (TEMPDIFF .GT. 0.0)THEN
   VOLTO=B*TEMPDIFF-A
  ELSE
   VOLTO=0.0
ENDIF
TEM=(5./9.)*(((VOLT+A+DEL)/B)+459.67)
END
```

```
PROGRAM RMS



INTEGER I,COUNT
REAL QMEAN,QSUM,Q2,QRMS,Q2SUM,T,START,END



OPEN (13,FILE='QQ.DAT',STATUS='OLD')



WRITE (*,*) 'ENTER START TIME DESIRED FOR CALCULATION OF Qrms &
: Qmean : '
READ (*,*) START
WRITE (*,*) 'AND THE ENDING TIME : '
READ (*,*) END



TEMP=END/.002
STOP=NINT(TEMP)
COUNT=0
QSUM=0.0
Q2SUM=0.0
DO 10 I=1,1301
   READ (13,*) T,Q
   IF (T .GE. START .AND. T .LE. END)THEN
       QSUM=Q+QSUM
       Q2SUM=Q*Q+Q2SUM
       COUNT=1+COUNT
   ENDIF
```

```
10   CONTINUE
     QMEAN=QSUM/(COUNT*1.)
     QRMS=SQRT(Q2SUM/(COUNT*1.))
     WRITE (*,*) 'QRMS = ',QRMS
     WRITE (*,*) 'QMEAN =',QMEAN
     END
```

```
      PROGRAM STANT




      INTEGER I.COUNT
      REAL Q,T,H,NU,ST,DELT,DELH,DELNU,DELST



      OPEN (13,FILE='ST',STATUS='OLD')



      WRITE (*,*) 'ENTER THE MEAN Q :'
      READ (*,*) Q

      DO 10 I=1,25
         READ (13,*) T,H,NU,ST
         IF (I .GE. 6 .AND. I .LE. 23)THEN
            DELT=DELT+T
            DELH=DELH+H
            DELNU=DELNU+NU
            DELST=DELST+ST
            COUNT=COUNT+1
         ENDIF
10    CONTINUE
      T=DELT/(COUNT*1.)
      H=Q/T
      NU=DELNU/(COUNT*1.)
      ST=DELST/(COUNT*1.)
      WRITE (*,*) ' DT      H     NU     ST'
      WRITE (*,20) T,H,NU,ST
20    FORMAT (4(1X,E12.4))
      END
```

```
0 DEFINT I-Q
5 ON ERROR GOTO 100
30 DIM DAT(1 TO 3000, 1 TO 5)
35 '$DYNAMIC
0 OPEN "QQ.DAT" FOR INPUT AS #1
50 OPEN "Q.DAT" FOR OUTPUT AS #2
60 OPEN "QST.DAT" FOR OUTPUT AS #3
0 OPEN "QUL.DAT" FOR OUTPUT AS #4
0 OPEN "QUT.DAT" FOR OUTPUT AS #5
91 I = 1
3 DO WHILE NOT EOF(1)
4   IF LOC(1) >= LOF(1) THEN GOTO 100
95   INPUT #1, DAT(I, 1), DAT(I, 2), DAT(I, 3), DAT(I, 4), DAT(I, 5)
97   I = I + 1
9 LOOP
00 L = I
110 M = 0
20 N = 0
30 O = 0
140 P = 0
50 Q = 0
60 FOR I = 1 TO L
170   IF DAT(I, 3) > 0! THEN
180       IF DAT(I - 1, 3) = 0! THEN P = I
90        M = M + 1
200   END IF
210   IF DAT(I, 4) > 0! THEN
20        N = N + 1
30    END IF
240   IF DAT(I, 5) > 0! THEN
50        IF DAT(I - 1, 5) = 0! THEN Q = I
55        O = O + 1
260   END IF
270 NEXT I
80 FOR I = 1 TO L - 1
290    WRITE #2, DAT(I, 1), DAT(I, 2), DAT(I, 3), DAT(I, 4), DAT(I, 5)
310 NEXT I
15 M = M + P - 1
20 FOR I = P TO M
340     WRITE #3, DAT(I, 1), DAT(I, 2), DAT(I, 3), DAT(I, 4), DAT(I, 5)
60 NEXT I
70 FOR I = 1 TO N
390   WRITE #4, DAT(I, 1), DAT(I, 2), DAT(I, 3), DAT(I, 4), DAT(I, 5)
410 NEXT I
15 O = O + Q - 1
20 FOR I = Q TO O
430  WRITE #5, DAT(I, 1), DAT(I, 2), DAT(I, 3), DAT(I, 4), DAT(I, 5)
40 NEXT I
50 END
```

BIBLIOGRAPHY

Ammari, H.D., et al. "The Effect of Density Ratio on the Heat Transfer Coefficient from a Film Cooled Flat Plate", ASME Gas Turbine and Aeroengine Congress and Exposition, Toronto, Canada, June 4-8, 1989.

Arpaci, Vedat. Conduction Heat Transfer. New York: Addison Wesley, 1966.

Blair, M.F. "Inluence of Free-Stream Turbulence on Turbulent Boundary Layer Heat Transfer and Mean Profile Development, Part II - Analysis of Results.", Journal of Heat Transfer, 105: 41 - 47, November 30, 1983.

Blasius, H. "Grenzschichten in Flussigkeiten mit kleiner Reibung." Z. Math Physics, 56 1-37, 1908. English Translation in NACA TM 1256, 1956.

Bogdan, Leonard and Joseph E. Garberoglio. Transient Heat Transfer Measurement with Thin-Film Resistance Thermometers - Fabrication and Application Technology. Technical Report AFAPL-TR67-72. Cornell Aeronautical Laboratory Inc., June 1967.

Chapman, Alan J. and William F. Walker. Introductory Gas Dynamics. New York: Holt, Rinehart and Wilson, Inc., 1971.

Cook, W.J. and E.J. Felderman. "Reduction of Data from Thin-Film Heat-Transfer Gages: A Concise Numerical Technique.", AIAA Journal. March, 1966.

Davis, W.R. and L. Bernstein. "Heat Transfer and Transition to Turbulence in the Shock-Induced Boundary Layer on a Semi-Infinite Flat Plate.", Journal of Fluid Mechanics, Volume 36: Part 1. 1969.

Dillon, R.E. and H.T. Nagamatsu. "Heat Transfer and Transition Mechanisim on a Shock-Tube Wall.", AIAA Journal, 22: No. 11, November, 1984.

Dunn, Michael G. Heat Flux and Pressure Measurements and Comparison with Prediction for a Low Aspect Ratio Turbine Stage. Technical Report AFWAL-TR-85-2044. Calspan Advanced Technology Center, Buffalo, NY. July 1985.

Dunn, Michael G. and Frank J. Stoddard. Studies of Heat Transfer to Gas Turbine Components. Technical Report AFAPL-TR-77-66. Calspan Corporation, Buffalo, NY. October, 1977.

Eckert, Ernst G. and Richard J. Goldstein. Measurements in Heat Transfer to Gas Turbine Components. (Second Edition). Washington: Hemisphere Publishing Corporation, 1976.

Felderman, E.J. "Heat Transfer and Shear Stress in the Shock-Induced Unsteady Boundary Layer on a Flat Plate.", AIAA Journal 6: No. 3, 1968.

Gaydon, A.G. and I.R.Hurle. The Shock Tube in High-Temperature Chemical Physics. New York: Reinhold Publishing Corporation, 1963.

Glass, I.I. "Shock Tubes, Part 1: Theory and Performance of Simple Shock Tubes.", UTIA Review No. 12. Toronto, Canada: Institute of Aerophysics, University of Toronto, 1958.

Goldstein, Richard J., et al. Advances in Heat Transfer. New York: Academic Press, 1971.

Hitchcock, James. Personal Notes, Unsteady Surface Temperature, Semi-Infinite Solid, Transient Heat Flux Gage. School of Engineering, Air Force Institute of Technology (AU), Wright Patterson AFB, OH, July 1985.

Jones, T.V. and D.L. Schultz. "Film Cooling Studies in Subsonic and Supersonic Flows Using a Shock Tunnel.", Shock Tube Research, Proceedings of the Eigth International Shock Tube Symposium, Imperial College, London, England, 5-8 July 1971.

Kays, W.M. and M.E. Crawford. Convection Heat and Mass Transfer. New York: McGraw-Hill Book Company, 1980.

King, Paul I. and L.G. Oldfield. An Examination of Curve Smoothing Using Digital Filter Theory. USAFA-TR-85-2, 1985.

Kakaç, Sadik, et al. Handbook of Single-Phase Convective Heat Transfer. New York: John Wiley and Sons, 1987.

Medtherm Corporation. Design and Manufacture of Medical and Thermal Instruments, Catalog, Huntsville, Alabama, 1985.

Mirels, J. "Boundary Layer Behind Shock of Thin Expansion Wave Moving into a Stationary Fluid.", NACA TN 3712, 1956.

Novak, Capt Joseph T. Investigation of Heat Transfer to a Flat Plate in a Shock Tube. Thesis, AFIT/GA/AA/87D-5, School of Engineering, Air Force Institute of Technology (AU), Wright Patterson AFB, OH, 1987.

Rockwell, Capt R. Transient Heat Flux Measurements on a Flat Plate in Turbulent Flow Using an Electrical Analog. MS Thesis, School of Engineering, Air Force Institute of (AU), Wright-Patterson AFB, OH, 1989.

Schlichting, Herman. Boundary-Layer Theory (Seventh Edition). New York: McGraw-Hill Book Company, 1979.

Shapiro, Ascher H. The Dynamics and Thermodynamics of Compressible Fluid Flow, Vol. 2. New York: The Ronald Press Company, 1954.

Simonich, J.C. and P. Bradshaw. "Effect of Free-Stream Turbulence on Heat Transfer Through a Turbulent Boundary Layer." Journal of Heat Transfer, 100: 671-677, November, 1978.

Skinner, George. "Analog Network to Convert Surface Temperature to Heat Flux." ASTIA. 247-277.

Smith, Capt B.J. Investigation of Heat Transfer to a Sharp Flat Plate in a Shock Tube. MS Thesis, AFIT/GAE/ENY/86D-16, School of Engineering, Air Force Institute of Technology (AU), Wright-Patterson AFB, OH, December, 1986.

Schmitz, L.S. Nonlinear Analog Network to Convert Surface Temperature to Heat Flux. Cornell Aeronautical Laboratory, Inc., Cornell University, Buffalo, NY, June, 1963.

Touloukian, Y.S. and E.H. Thermophysical Properties of Matter, The TPRC Data Series, Volume 5, Specific Heat of Nonmetallic Solids. 1230-1233, New York: IFI Plenum, 1970.

Touloukian, Y.S., et al. Thermophysical Properties of Matter, The TPRC Data Series, Volume 2, Thermal Conductivity of Nonmetallic Solids. 922-933, New York: IFI Plenum, 1970.

Zucrow, Maurice J. and Joe D. Hoffman. Gas Dynamics, Volume I. New York: John Wiley and Sons, 1976.

Vita

Scott A. Jurgelewicz [redacted] In May 1979 he graduated from Massassoit Community College with an Associates in Science degree. After enlisting in the Air Force in March 1980 he attended the University of Massachusetts at Amherst under the Airmans Education and Commissioning Program. He received his Bachelor of Science in Mechanical Engineering in May 1984. Upon graduation from Officer Training School he received his commission in September 1984. From October 1984 until April 1988 he was assigned to the 6595th Aerospace Test Group, Vandenberg AFB, California, where he served as chief of Titan space launch facilities. He entered the Master of Science degree program at AFIT in June 1988.

REPORT DOCUMENTATION PAGE

Form Approved
OMB No. 0704-0188

1a. REPORT SECURITY CLASSIFICATION: UNCLASSIFIED	1b. RESTRICTIVE MARKINGS
2a. SECURITY CLASSIFICATION AUTHORITY	3. DISTRIBUTION/AVAILABILITY OF REPORT: Approved for public release; distribution unlimited
2b. DECLASSIFICATION/DOWNGRADING SCHEDULE	
4. PERFORMING ORGANIZATION REPORT NUMBER(S): AFIT/GAE/ENY/89D-17	5. MONITORING ORGANIZATION REPORT NUMBER(S)
6a. NAME OF PERFORMING ORGANIZATION: School of Engineering; 6b. OFFICE SYMBOL (If applicable): AFIT/ENA	7a. NAME OF MONITORING ORGANIZATION
6c. ADDRESS (City, State, and ZIP Code): Air Force Institute of Technology, Wright-Patterson AFB, OH, 45433-6583	7b. ADDRESS (City, State, and ZIP Code)
8a. NAME OF FUNDING/SPONSORING ORGANIZATION: AF Aeropropulsion Lab; 8b. OFFICE SYMBOL (If applicable): AFWAL/POTC	9. PROCUREMENT INSTRUMENT IDENTIFICATION NUMBER
8c. ADDRESS (City, State, and ZIP Code): Wright-Patterson AFB, OH, 45433-6583	10. SOURCE OF FUNDING NUMBERS: PROGRAM ELEMENT NO. / PROJECT NO. / TASK NO. / WORK UNIT ACCESSION NO.

11. TITLE (Include Security Classification)
INVESTIGATION OF HEAT TRANSFER WITH FILM COOLING TO A FLAT PLATE IN A SHOCK TUBE

12. PERSONAL AUTHOR(S)
Scott A. Jurgelewicz, B.S., Capt, USAF

13a. TYPE OF REPORT	13b. TIME COVERED	14. DATE OF REPORT (Year, Month, Day)	15. PAGE COUNT
Thesis	FROM _____ TO _____	1989 December	149

16. SUPPLEMENTARY NOTATION

17. COSATI CODES			18. SUBJECT TERMS (Continue on reverse if necessary and identify by block number)
FIELD	GROUP	SUB-GROUP	Flat Plate, Shock Tube, Heat Transfer, Thermal Boundary Layer, Film Cooling, Turbulence
20	04		

19. ABSTRACT (Continue on reverse if necessary and identify by block number)

Title: INVESTIGATION OF HEAT TRANSFER WITH FILM COOLING TO A FLAT PLATE IN A SHOCK TUBE

Thesis Chairman: Dr. William C. Elrod

Committee Members: Dr. James Hitchcock, Lt. Col. Paul King

20. DISTRIBUTION/AVAILABILITY OF ABSTRACT: ☐ UNCLASSIFIED/UNLIMITED ☒ SAME AS RPT. ☐ DTIC USERS	21. ABSTRACT SECURITY CLASSIFICATION: UNCLASSIFIED
22a. NAME OF RESPONSIBLE INDIVIDUAL: Dr. William C. Elrod	22b. TELEPHONE (Include Area Code): (513) 255-3517 / 22c. OFFICE SYMBOL: AFIT/ENY

DD Form 1473, JUN 86 — Previous editions are obsolete.

ABSTRACT

The heat transfer in the flow induced behind a shock wave moving across a flat plate with a rounded leading edge was studied experimentally. The collected data was reduced using a numerical technique coded in Fortran. This heat transfer data is then compared to empirical solutions also produced by the code. Film cooling effects on the heat transfer are compared to heat transfer without cooling for the same geometry and flow conditions. These results are then compared to theory. The influence of free stream turbulence on heat transfer is also examined and compared to previous investigations.